# Impact Assessment of Large-scale Penetration of Permanent Magnet Synchronous Generators on Power Quality


**Prepared by:**

**Ntlahla Ntsadu**

**NTSNTL001**

Department of Electrical Engineering
University of Cape Town

**Prepared for:**

**Prof KA Folly**

**and**

**Prof MA Khan**

Department of electrical engineering
University of Cape Town

**3 April 2017**

Submitted to the Department of Electrical Engineering at the University of Cape Town in partial fulfilment of the academic requirements for a Master of Science degree in Electrical Engineering

**Key Words:** Power quality, PMSG based WECSs, Modelling and Transient stability

# Declaration

1. I know that plagiarism is wrong. Plagiarism is to use another's work and pretend that it is one's own.
2. I have used the IEEE convention for citation and referencing. Each contribution to, and quotation in, this final year project report from the work(s) of other people, has been attributed and has been cited and referenced.
3. This final year project report is my own work.
4. I have not allowed, and will not allow, anyone to copy my work with the intention of passing it off as their own work or part thereof

5. I know the meaning of plagiarism and declare that all the work in the document, save for that which is properly acknowledged, is my own. This thesis/dissertation has been submitted to the Turnitin module (or equivalent similarity and originality checking software) and I confirm that my supervisor has seen my report and any concerns revealed by such have been resolved with my supervisor.

Name: **Ntlahla Ntsadu**

Signature: Signed by candidate
Signature Removed

**Date:** 3 April 2017

# Terms of Reference

The University of Cape Town (UCT) and the University of Tunis EL Manar (UTM) have joined forces to study the impact of large scale permanent magnet synchronous generators (PMGMs) and doubly-fed induction generators (DFIGs) wind energy conversion systems on power quality of the grid. This project is as a result of collaboration between Advance Machines and Energy Systems (AMES) research group of the University of Cape Town (UCT) and Electrical Systems laboratory (LSE) research group at the University of Tunis El Manar (UTM). The AMES research group studies the PMSG technology in South Africa while the LSE research group studies DFIG in Tunisia. The main objectives of this report therefore are to:

- Conduct a literature scan of power quality (PQ) issues with regards to grid integration of PMSGs
- Develop models and methodologies for assessing the impact of PMGs integration to the grid
- Model the PMSG wind energy conversion system in MATLAB Simulink
- Use DIgital SImuLation and Electrical NeTwork calculation program (DIgSILENT) to simulate PQ conditions in a simple network which is typical representation of the South African grid
- Study the stability problems that permanent magnet synchronous generator based wind turbines introduce to the grid

# Abbreviations

**AMES** = Advance Machines and Energy Systems research group

**DFIG** = Doubly-fed induction generator

**DSL** = DIgSILENT simulation language

**GW** = Giga watts

**HVRT** = High voltage ride through

**LSE =** Electrical Systems laboratory research group

**LVRT** = Low voltage ride through

**MPPT** = Maximum power point tracking

**MS** = Machine side

**MW** =Mega watts

**PCC** = Point of common coupling

**PLL** = Phase-locked loop

**PMSG** = Permanent magnet synchronous generator

**PQ =** Power quality

**REIPPPP** = Renewable Energy Independent Power Producer Procurement Program

**RL** = Resistor inductor

**RPP** = Renewable power plant

**SCIG** = Squirrel cage induction generator

**SMPM** = Surface mount permanent magnet

**STATCOM** = Static compensator

**SVC** = Static var compensator

**SVPWM** = Space vector pulse width modulation

**THD** = Total harmonic distortion

**TWh** = Tera Watts hours

**WECS** = Wind energy conversion system

**WRIG** = Wound rotor induction generator

# Acknowledgements

My gratitude and appreciation goes to all the people who have assisted me in carrying out this project. Their criticisms and friendly advices were the cornerstones to the success of this project.

**University of Cape Town**

- I would like to thank my supervisor Professor KA Folly. His criticism and advice is appreciated.
- I would also like to thank my co-supervisor Professor MA Khan for both academic and financial support. Professor MA Khan assisted me with acquiring funding for this project.
- I would like to thank the national research foundation (NRF) for funding this project.


**Family and colleagues**

- I would a like to thank my colleagues form the AMES research group for their involvement with this project.
- I would like to thank my family, especially my mother for giving me the moral support.

# Abstract

Wind power generation has gained a large share in the renewable energy market over the past few years. This study investigates the impact of large scale penetration of permanent magnet synchronous generator (PMSG) based wind turbines on power quality of the grid. PMSGs are attractive due to the absence of a gearbox in the drive-train, which results in lower maintenance costs and higher reliability. Moreover, the advancements in power electronics have facilitated PMSGs to generate optimal power at varying wind speed conditions. This is achieved through the use of maximum power point tracking algorithms. The drawbacks of PMSG based wind energy systems are that they inject harmonics into the network and cause flicker as well as other power quality issues. Despite these disadvantages, the grid code requires that PMSGs stay connected to the grid even under grid disturbances. This is because the reactive power control capability of PMSG based wind energy systems can actually assist with voltage support. It will be shown in this study that disconnecting large scale PMSGs based wind turbines during grid disturbances has a detrimental effect on transient stability of the grid. This study will show that PMSG based wind energy systems improve transient stability and assist in voltage support through reactive power control. Moreover, the impacts of large scale PMSG based wind turbines on power quality of the grid can be reduced by various means, which are also addressed in the study.

The increase in wind power production has led to the development of renewable power plant (RPP) grid code. RPPs are thus regulated in terms of the amount of power quality problems they introduce to the grid. The grid code requires that RPPs with power ratings greater than 20MVA remain connected to the grid as long as there is wind available so as to assist under power system disturbances. It will be shown in this study that the network behaves better when the PMSG wind turbines remain connected under low events.

The grid code requires that RPPs with power ratings greater than 20MVA produce 33% of rated active power as reactive power in order to support voltage. There are three common modes of reactive power control. These are constant reactive power, voltage and power factor control.

The power quality issues caused by PMSG wind turbines which are studied here are harmonics, voltage dips, voltage flicker and voltage rise. Due to the advancements in power electronics, PMSG based wind energy conversion systems (WECSs) can operate under varying wind speed conditions while still producing optimal active power.

The main source of flicker in PMSG based WECSs is the fluctuating wind speed, tower shadow and wind shear effect. Flicker is measured by two indices which are the short and long term flicker severity indices. Ramp rates are imposed on WECS so as to limit the rate at which wind power production changes. By limiting the amount of active power changing rates, flicker can be reduced. A way to reducing the impact of wind shear and tower shadow effect is to increase the moment of inertia of the wind turbine blades and turbine shaft by using materials with higher mass density.
Flicker can also be reduced by installing a voltage regulating device at the point of common coupling (PCC). A much cheaper alternative is to use active power control on the machine side control of a PMSG based WECS.

PMSG based WECSs improve the transient stability of the grid if they remain connected to the network under low voltage events.

# Table of Contents

1 Introduction ..... 1
1.1 Background of the study ..... 1
1.2 Objectives of this study ..... 1
1.2.1 Problems to be investigated ..... 2
1.2.2 Purpose of the study ..... 2
1.3 Scope and limitations ..... 2
1.4 Plan of development ..... 2
2 WECS Overview ..... 3
2.1 Types of WECS ..... 3
2.1.1 Squirrel cage induction generator based WECS ..... 3
2.1.2 Limited speed asynchronous generator based WECS ..... 3
2.1.3 Doubly-fed induction machine based WECS ..... 4
2.1.4 Permanent magnet synchronous machines WECS ..... 5
2.2 Principle of wind turbines ..... 5
2.2.1 Maximum power point tracking ..... 6
2.2.2 Operating regions of a WECS ..... 7
2.3 Power electronics for wind systems ..... 7
2.3.1 Power converter ..... 8
2.3.2 Space vector pulse width modulation ..... 8
3 Power Quality Issues ..... 9
3.1 Voltage variations ..... 9
3.2 Voltage swell ..... 10
3.3 Voltage flicker ..... 11
3.4 Transients ..... 14
3.4.1 Switching operations ..... 14
3.4.2 Voltage interruptions and LVRT ..... 14
3.4.3 Voltage sag ..... 15
3.5 WECS harmonics ..... 15
3.6 Voltage unbalance ..... 16
3.7 Grid frequency ..... 16
3.7.1 Active power response ..... 17
3.8 Tower shadow and shear effect ..... 18
3.9 Reactive power control ..... 18
3.9.1 Constant reactive power and power factor control ..... 18
3.9.2 Droop control ..... 19

4 Impact of PMSG on power quality ..... 20
4.1 Impact of PMSGs on flicker ..... 20
4.2 Impact of PMSG on harmonics ..... 20
4.3 Impact of PMSG based WECS on transient stability ..... 21
5 Modelling PMSG based WECS ..... 22
5.1 Reference planes ..... 22
5.2 Wind model ..... 23
5.3 Aerodynamic model turbine ..... 24
5.4 Mechanical model ..... 25
5.5 Electrical model ..... 25
5.5.1 Modelling Inverters ..... 25
5.5.2 Modelling permanent magnet synchronous generator ..... 27
5.5.3 PMSG model in d-q form ..... 28
5.5.4 Grid side models ..... 29
5.5.5 Machine side electrical power ..... 30
5.5.6 Grid side electrical power ..... 30
5.5.7 Electrical torque ..... 31
5.5.8 DC-link ..... 32
5.5.9 The transmission line ..... 32
5.5.10 Filter design ..... 33
6 Control of PMSG based WECS ..... 34
6.1 Machine side control ..... 35
6.1.1 d-axis current control loop ..... 35
6.1.2 Pitch control ..... 35
6.1.3 Angular speed control ..... 36
6.2 Grid side control ..... 36
6.2.1 Reactive power control ..... 36
6.2.2 DC-link voltage control ..... 37
6.2.3 Phase-locked loop ..... 37
7 Model verification ..... 39
7.1 Controller design ..... 39
7.1.1 Machine side controller design ..... 39
7.1.2 Grid side controller design ..... 43
7.2 Final model ..... 47
7.2.1 Machine side model verification ..... 47
7.2.2 Grid side model verification ..... 49

8 Effect of PMSGs on power quality ..... 52
8.1 System overview ..... 52
8.2 Effect of PMSG based WECS on voltage rise ..... 53
8.2.1 Voltage rise and reactive power ..... 53
8.2.2 Voltage rise and transmission line length ..... 54
8.2.3 Voltage rise and X/R ratio ..... 54
8.3 Effect of PMSG based WECS on Flicker ..... 55
8.3.1 Continuous operation flicker ..... 55
8.3.2 Switching operations and flicker ..... 56
8.4 Effect of PMSG on harmonics ..... 58
8.4.1 THD and Penetration ..... 59
8.5 Voltage sag and PMSG LVRT ..... 59
8.5.1 LVRT of PMSG based WECS ..... 60
9 Conclusions ..... 62
9.1 Impact of WECS on power quality ..... 62
9.2 PMSG based WECS control ..... 62
9.3 The effect of PMSG turbine location ..... 62
9.4 Voltage improvement ..... 62
9.5 PMSG based WECSs improve transient stability ..... 62
9.6 Source of flicker ..... 62
9.7 Source of harmonics ..... 63
9.8 Switching operations ..... 63
10 Recommendations ..... 64
10.1 Location of PMSG based WECSs ..... 64
10.2 LVRT of PMSG based WECSs ..... 64
10.3 Flicker reduction ..... 64
10.4 PMSG based WECSs harmonics ..... 64
11 List of References ..... 65
12 Appendices ..... 69
12.1 PMSG control system in MATLAB Simulink ..... 69
12.1.1 Machine side block ..... 69
12.2 Phase-locked loop ..... 72
12.3 MS d-axis current control ..... 72
12.4 Angular speed control ..... 73
12.5 Grid side block ..... 74
12.6 Reactive power control ..... 75

12.7 D-link voltage control ..... 76
12.8 The phase-locked loop block ..... 77
12.9 Flicker model ..... 78
12.10 DSL code ..... 78

# List of Figures

Figure 2.1: SCIG based WECS ..... 3
Figure 2.2: WRIG based WECS ..... 4
Figure 2.3: DFIG based WECS ..... 4
Figure 2.4: PMSG based WECS ..... 5
Figure 2.5: Power coefficient curves ..... 6
Figure 2.6: Operating region of a variable speed WECS ..... 7
Figure 2.7: General block diagram of power electronics for WECS ..... 8
Figure 2.8: Back-to-back converter ..... 8
Figure 3.1: Hierarchy of electrical power quality ..... 9
Figure 3.2: Power quality events as per IEEE 1159 – 1995 ..... 10
Figure 3.3: Grid code reactive power limits for RPP ..... 11
Figure 3.4: Flicker limit curve ..... 12
Figure 3.5: The flicker meter block diagram ..... 13
Figure 3.6: LVRT curve of a wind turbine ..... 15
Figure 3.7: The frequency operating regions for RPPs ..... 16
Figure 3.8: Required active power response to frequency changes for RPPs ..... 17
Figure 3.9: Reactive power control ..... 18
Figure 3.10: Voltage control ..... 19
Figure 5.1: Basic vector combinations ..... 26
Figure 5.2: Cross-sectional view of a PMSG ..... 27
Figure 6.1: The PMSG based WECS and its associated control system ..... 34
Figure 6.2: Id current control loop ..... 35
Figure 6.3: Rotor angular speed controller ..... 36
Figure 6.4: Reactive power controller ..... 37
Figure 6.5: DC-link voltage controller ..... 37
Figure 6.6: Phase-locked Loop controller ..... 38
Figure 7.1: The root locus plot for MS q-axis current control loop ..... 40
Figure 7.2: Unit step response of the MS q-axis current control loop ..... 40
Figure 7.3: Discrete root locus plot of the MS q-axis current control loop ..... 41
Figure 7.4: Discrete unit step response of the MS q-axis current control loop ..... 41
Figure 7.5: Speed control root locus in the s-domain ..... 42
Figure 7.6: Unit step response for angular speed control ..... 42
Figure 7.7: Discrete root locus for speed control ..... 43
Figure 7.8: Unit step response for discrete speed control ..... 43
Figure 7.9: Root locus of reactive power control loop ..... 44
Figure 7.10: Unit step response of reactive power control ..... 44
Figure 7.11: Discrete root locus for reactive power control ..... 45
Figure 7.12: Unit step response for discrete reactive power control ..... 45
Figure 7.13: Root locus plot for DC-link voltage control loop in the s-plain ..... 46
Figure 7.14: Continuous unit step response of DC-link voltage control ..... 46
Figure 7.15: DC-link voltage control loop root locus in the z-plain ..... 46
Figure 7.16: Discrete unit step response for the of DC-link voltage control ..... 47
Figure 7.17: Input wind speed ..... 47
Figure 7.18: PMSG angular speed ..... 48
Figure 7.19: The machine side d-axis current ..... 48

Figure 7.20: The machine side q-axis current ..... 48
Figure 7.21: The mechanical torque ..... 49
Figure 7.22: PMSG electrical torque ..... 49
Figure 7.23: DC-link voltage ..... 50
Figure 7.24: Grid side dq0 currents ..... 50
Figure 7.25: Grid side d-q axis voltages ..... 50
Figure 7.26: PMSG based WECS active power ..... 51
Figure 7.27: Grid side reactive power ..... 51
Figure 8.1: System overview ..... 52
Figure 8.2: Effect of reactive power on voltage rise ..... 53
Figure 8.3: Effect of transmission line length on voltage rise ..... 54
Figure 8.4: Effect of X/R ratio on voltage rise ..... 54
Figure 8.5: Active power due to tower shadow effect ..... 55
Figure 8.6: PCC voltage for case with and without a station controller ..... 56
Figure 8.7: Pst value for case without station controller ..... 56
Figure 8.8: Pst value for case with station controller ..... 56
Figure 8.9: PCC flicker vs grid strength ..... 57
Figure 8.10: PCC flicker vs N10 ..... 57
Figure 8.11: PCC flicker vs N120 ..... 58
Figure 8.12: PCC flicker vs step factor ..... 58
Figure 8.13: THD and penetration ..... 59
Figure 8.14: PCC voltage ..... 60
Figure 8.15: Synchronous machine rotor angle ..... 61
Figure 12.1: The machine side model in MATAB Simulink ..... 69
Figure 12.2: Wind turbine model ..... 70
Figure 12.3: Simulink machine side control system ..... 71
Figure 12.4: PLL block model ..... 72
Figure 12.5: MS d-axis current control ..... 73
Figure 12.6: Angular speed control ..... 74
Figure 12.7: Grid side block in Simulink ..... 74
Figure 12.8: Grid side control system ..... 75
Figure 12.9: Reactive power control loop ..... 76
Figure 12.10: DC-link voltage controller ..... 76
Figure 12.11: The Simulink PLL block ..... 77

# List of Tables

Table 3.1: Short term and long term flicker severity indices IEEE 1453 ..... 13
Table 3.2: Frequency settings ..... 17
Table 8.1: System elements and corresponding quantity ..... 53
Table 8.2: THD model based on NRS 048:4 harmonic limits ..... 59
Table 12.1: The PI controller parameters ..... 69
Table 12.2: Wind turbine parameters ..... 70
Table 12.3: PMSG parameters ..... 71
Table 12.4: IGBT converter parameters ..... 71
Table 12.5: The PLL block parameters ..... 72
Table 12.6: Grid side elements parameters ..... 75
Table 12.7: Grid side PLL parameters ..... 77
Table 12.8: Flicker model for switching operations ..... 78

# 1 Introduction

## 1.1 Background of the study

The increasing electrical power demand in South Africa is met mainly by generation from coal fired power plants. Coal generation contributes up to 77% of the electrical generation of the country [1]. Coal is a non-renewable resource of energy and thus will eventually run out. In addition to depletion, coal combustion contributes to climate change due to the emission of green-house gases such as carbon dioxide. To reduce the reliance on coal, the South African Department of Energy (DoE) plans to increase the renewable energy generation in the energy mix by 17.8GW according to the integrated resource plan of 2010 ( IRP2010) that was published in 2011[2]. The IRP2010 of 2011 provided that the 17.8GW of new generation will be from solar and wind by the year 2030. The solar technologies included in the plan were concentrated solar power (CSP) and photovoltaic power (PV). Wind power was planned to reach 8.4GW while PV and CSP are planned to reach 8.4 GW and 1GW respectively.

Wind power was reduced to 4.36GW in the 2014 revision of the IRP2010 while PV and CSP were increased to 9.77GW and 3.3GW respectively, by the year 2030 [3]. A draft of the integrated resource plan of 2016 (IRP2016) was opened for review by the DoE [4]. The time horizon for the IRP2016 is 2016 to 2050. Wind power and PV are planned to reach 17.5GW and 37.4GW respectively. The CSP solar technology was not included in the IRP2016 draft.

The DoE plans to increase renewables through a tender process known as the Renewable Energy Independent Power Producer Procurement Program (REIPPPP) in which private companies bid for a 20-year contract to connect to the grid and sell power to Eskom (the only power utility in South Africa). Generation from renewables is clean however renewables do not come without problems. The problems that are investigated in this study are power quality as well as transient stability impacts of PMSG based WECSs on the grid.

## 1.2 Objectives of this study

The objectives of this study are to investigate the impact of large scale PMSG based WECSs integration on power quality and transient stability of the grid. This study shows that even though PMSG based WECSs bring power quality problems, they improve the transient stability provided that they stay connected under transient events. The objectives of this study are therefore to:

- Conduct a literature survey of power quality (PQ) and grid-integration issues associated with PMSGs
- Develop an aggregation model and methodology for Permanent Magnet Synchronous Generator
- Use of DIgSILENT to investigate the effect of PMSG on PQ and stability of the grid
- Draw conclusions and make recommendations based on the findings

### *1.2.1 Problems to be investigated*

Electrical power as a product must be sent to the end user in good quality. Good quality is defined by the grid code. The grid code outlines the requirements for use of, and connection to, the grid. Voltage and frequency are the main indicators of power quality and thus many power quality indices and limits are formulated based on voltage and frequency. The power quality issues investigated in the study are listed:

- Harmonics
- Voltage flicker
- Voltage dips
- Transients
- Voltage rise
- Voltage regulation

### *1.2.2 Purpose of the study*

The purpose of this study is to investigate the impact of large scale PMSG based WECSs on power quality of the grid. It is shown in this study that although PMSG based WECSs introduce power quality problems, they improve the transient stability of the grid and assists in voltage control through the generation of reactive power. The power quality problems caused by PMSG based WECSs can be minimised in various ways that will be shown in this study.

The study also aims to show the relative ease of PMSG based WECSs electrical control system introduced by using the Park and Clarke transforms of original equations of electrical model of the PMSG based WECS.

## 1.3 Scope and limitations

The PMSGs are divided into trapezoidal and sinusoidal types. The sinusoidal types are further divided into surface magnets and interior magnet. The modelling of PMSGs will be limited to surface mount PMSGs. The model of the PMSG based WECS was not implemented in the lab but done in the form of a simulation. The mechanical model of PMSG based WECSs is not included in the modelling section and only the electrical model is used. The impacts of PMSG based WECSs on inter-harmonics and voltage unbalance are not included in this study.

## 1.4 Plan of development

**Chapter 1** is the introduction. It covers the background, purpose and the scope of this study.

**Chapter 2** is a review of WECS technologies. The WECS technologies discussed are the PMSG, DFIG, squirrel cage induction generator (SCIG) and wound rotor induction generator (WRIG) based WECS. The WECSs with the highest share in the renewable wind energy market are based on PMSGs and DIFGs. This is because they have advanced power electronics which enhance them to operate at varying wind speeds and high efficiencies. The power electronics also allows for reactive power control which is required for voltage support. The grid code requires renewable technologies connected to the South African grid to have these features hence PMSGs and DFIGs are the most common technologies.

**Chapter 3** is a review of the power quality problems introduced by WECSs. The problems discussed are flicker, harmonics and voltage rise. The grid code requirements for renewable power plants in South Africa are also discussed.

**Chapter 4** discusses the impact of large-scale penetration of PMSG based WECS on the grid. It is found that the PMSG based WECS introduce harmonics to the grid. However, the total harmonic distortion can be reduced by adding a filter. Moreover, the total harmonic distortion decreases with increase in wind speed.

**Chapter 5** is a review of the PMSG based WECS model. An overview of the wind turbine model is presented but more attention is paid to the electrical model. The PMSG based WECS is modelled using aerodynamic, mechanical and electrical principles. The model of concern is the electrical model and forms the core of this research. The electrical models presented are for the PMSG, control systems and space vector pulse width modulation.

**Chapter 6** is a follow up on chapter 5. The control of a PMSG based WECS is greatly simplified by applying the Clarke and Park transforms on the three-phase voltages and currents of PMSG model equations. In this case, simple control algorithms like the proportional integral differential (PID) are used to for compensation. The advantage of using PID controllers is that they are cheaper compared to most algorithms.

**In chapter 7**, the PMSG based WECS model is verified in MATLAB Simulink. The controllers are designed using the root locus method using the SISOTOOL of MATLAB. Controllers were designed in the continuous state and later converted to the discrete state to increase the simulation time in Simulink.

**In Chapter 8,** a simple network which consists of a PMSG based wind farm, a synchronous generator and three loads is used to investigate the impact of large scale PMSG based WECSs grid integration on power quality of the gird. The studies are done in DIgSILENT. The power quality issues investigated include: flicker, harmonics, low voltage ride through capability and voltage rise. The DIgSILENT simulation language (DSL) in power factory is used to assess the impact of PMSG based WECSs on flicker at the point of common coupling.

**Chapter 9** is about the conclusions based on the findings. Wind speed fluctuation, Tower shadow and wind shear effect are the main sources of flicker. Flicker can be reduced by installing a voltage regulating device at the point of common coupling.

**Chapter 10** is about the recommendations based on the findings. It is recommended that the PMSG based wind farms should be connected on strong parts of the grid as this will reduce the impact on power quality. The use of a voltage regulating device at the PCC reduces the impact of PMSG based wind farm on flicker.

# 2 WECS Overview

In this section a literature review on WECSs is conducted. There are four wind technologies studied and each has its own advantages and disadvantages.

## 2.1 Types of WECS

WECSs come in a variety of topologies. Some have turbine blades that spin in a horizontal axis and are called horizontal axis wind turbines while some have blades that spin on vertical axis which are called vertical axis wind turbines. This section takes a closer look at the three blade horizontal axis wind turbine based WECS. Horizontal axis wind turbines are further categorised as fixed speed and variable speed.

### *2.1.1 Squirrel cage induction generator based WECS*

Squirrel cage induction generators (SCIG) based wind systems are constant speed WECSs. They usually have a gear box, a soft starter and a capacitor bank as shown in Figure 2.1. A pitch controller is used to keep the angular speed constant. The gear box is used to step up the low speed of the turbine shaft to high speed generator shaft so as to generate at grid frequency. An induction generator produces inrush currents during connection to the grid. Inrush current is a function of rotary speed, magnetisation of the core and the initial state of charges in the primary winding [9]. Inrush current causes voltage fluctuations and dips which is why SCIGs are fitted with a soft starter to limit the amount of inrush currents during grid synchronisation. An induction generator also requires reactive power to generate active power hence a capacitor bank is used to provide the needed reactive power [10]. The major disadvantage of SCIG based WECSs is that keeping a constant angular speed stresses the mechanical components which increase maintenance costs.

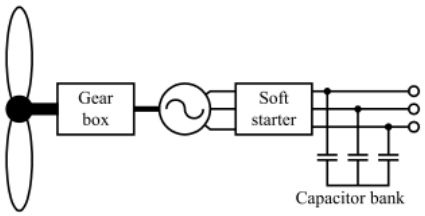


Figure 2.1: SCIG based WECS [10]

### *2.1.2 Limited speed asynchronous generator based WECS*

The limited speed asynchronous generator technology (also known as the wound rotor induction generator (WRIG)) is similar to the SCIG technology. The WRIG based WECS is shown in Figure 2.2. The unique thing about the WRIG based WECS is that instead of keeping the generated frequency constant by using pitch control as the case for SCIG based WECS, electrical torque control is used. Electrical torque control is achieved by controlling

the rotor resistance. The electrical torque is adjusted in proportion to the mechanical torque so as to generate at constant frequency to meet the grid code frequency requirements. Therefore instead of stressing the mechanical components of the turbine as the case for SCIG based WECS, the rotor resistance is used in the case of WRIG based WECS. However, the problem with this approach is that electrical power is lost as heat dissipated in the added rotor resistor. This therefore reduces the efficiency of the WRIG based WECS.

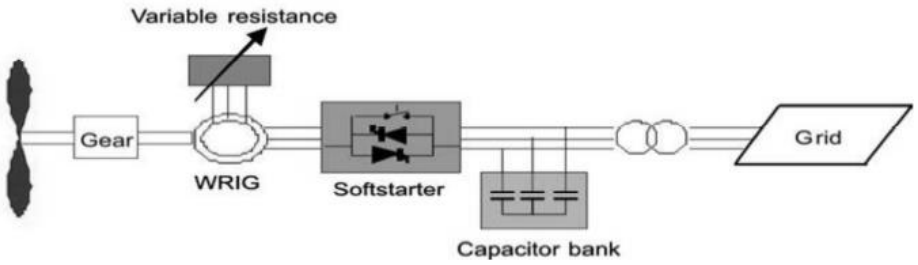


Figure 2.2: WRIG based WECS [10]

### *2.1.3 Doubly-fed induction machine based WECS*

The advancements in power electronics have led to efficient ways of extracting wind power while still meeting the grid code requirements. The doubly-fed induction generator (DFIG) based WECS, as shown in Figure 2.3, is an example of a WECS that uses power electronics to achieve high efficiencies. The DFIG based WECS operates by having its net magnetic flux angular speed controlled by the generator shaft as well as the injected rotor currents. When the generator shaft speed decreases, the injected current frequency is increased so as to produce a magnetic field at grid frequency; when the generator shaft speed increases, the line current frequency is reduced so as to keep the net flux angular speed at grid frequency. To control the frequency of the injected rotor currents, a rectifier-inverter combination coupled by a DC-link is used. The rectifier converts the alternating current (AC) voltage of the grid to direct current (DC) voltage which is smoothened by the DC-link capacitor. The inverter, through the use of controllers, adjusts the injected current frequency to achieve the required magnetic field magnitude and frequency. The power electronics components only have to handle 30% to 35% of the rated turbine electrical power [13]. The machine side control variable is the electrical torque. The grid side control variables are the voltage and power factor. The DFIG based WECS is able to control reactive power sent to the grid which is part of the grid code requirement that a wind farm must be able to control its reactive power.

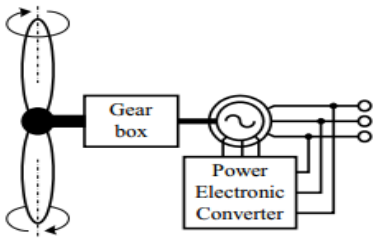


Figure 2.3: DFIG based WECS [11]

### *2.1.4 Permanent magnet synchronous machines WECS*

Another technology that uses power electronics to extract maximum power at higher efficiencies is the permanent magnet synchronous generator based WECS shown in Figure 2.4. As opposed to DFIG based WECS which uses an induction generator, the PMSG based WECS uses a permanent magnet synchronous generator which eliminates the reliance on an external exciter. Synchronous generators are electrically excited while permanent magnet synchronous machines are excited by the permanent magnet. PMSGs have many poles and usually come without a gear box. This reduces maintenance costs. In a PMSG based WECS, the generator stator terminals are connected to a rectifier-inverter combination coupled by a dc-link. The power electronics components must be able to handle 100% of the rated turbine power. The control system of a PMSG is divided into grid side control and machine side control. The machine side control variables are the angular speed, torque and pitch angle. The grid side control variables are the DC-link voltage and reactive power.

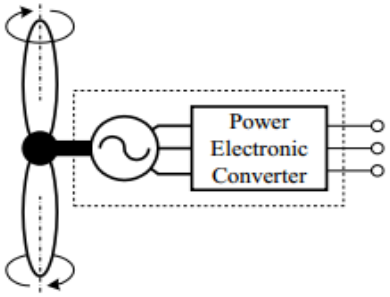


Figure 2.4: PMSG based WECS [11]

## 2.2 Principle of wind turbines

The kinetic energy in the wind can be extracted and converted to electrical energy by using a wind turbine coupled to an electrical generator. The wind kinetic energy is first converted to mechanical power which is just the kinetic energy of the shaft connected to rotor of an electrical generator. The electrical generator then converters the mechanical power into electrical power. The electrical generator comes in different forms such as synchronous and induction machine. There is a limit to the amount of electrical power that can be extracted from the wind. A Betz [5] showed that not more than 59.3% of wind energy can be captured and this is called the Betz limit. Even the available Betz limit cannot be extracted entirely as there are still losses to overcome depending on the efficiencies of the wind system. The design of a wind turbine also influences the amount of wind power that can be extracted from the wind [6]

Equation 2.1 shows the relationships between wind power and wind speed. The wind power ( $P_{Wind}$ ) is proportional to the product of air mass density ( *p* ), blade swap area *( A )* and the cube of the wind speed ( $V_{Wind}^{3}$ )**.** The active power produced by the wind turbine is proportional to the cube of the wind speed and this is why wind systems have a ramp rated limit to limit the proportional changes in the produced active power as a result of the fluctuating wind speed.

Equation 2.2 shows the relationship between wind power and the extracted power by the wind turbine ($P_{wt}$). The limit to the amount of power extracted by the wind turbine is modelled by the power coefficient ($C_p$).

$$P_{wind} = \frac{1}{2} pAV_{wind}^3 \quad (2.1)$$

$$P_{wt} = P_{wind} C_p \quad (2.2)$$

### *2.2.1 Maximum power point tracking*

The advancements in power electronics have made it possible for PMSG based WECSs to achieve maximum power point tracking (MPPT). MPPT is achieved by operating the turbine at the optimal tip-speed-ratio($\gamma$). A tip-speed-ratio is the ratio of the tip speed of a turbine blade to the wind speed. An optimal tip-speed-ratio is the tip-speed-ratio at which the power coefficient $(C_p)$ is maximized. The maximum tip-speed-ratio is unique for each turbine pitch angle ( $\vartheta$ ) as shown in Figure 2.5. For optimising the tip-speed-ratio, the only variable available to control is the angular speed of the turbine. Thus optimal tip-speed-ratio is obtained by controlling the angular speed of the generator rotor. This is because the wind turbine shaft is directly connected to the generator rotor in the PMSG based WECS studied in this study.

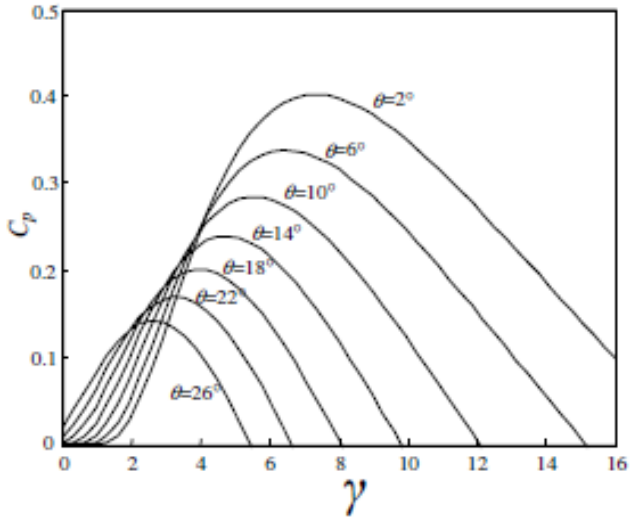


Figure 2.5: Power coefficient curves [7]

### *2.2.2 Operating regions of a WECS*

WECSs are limited in terms of the active power they can produce. A typical WECS has an operating curve like the one shown in Figure 2.2. This curve shows the electrical power output of a WECS as a function of wind speed. There are four regions of interest in this curve and are labelled a, b, c and d. For wind speeds lower than the cut-in speed region a) there is no power output because the torque developed is not enough to overcome frictional torque. MPPT is applied in region b until the wind is such that the WECS has reached its rated power. Exceeding the rated power will damage the WECS (region c). The pitch angle of the blades is kept between 10 and 90 degrees when maximum active power production has been reached [8]. For wind speeds greater than the cut-out speed, the turbine is switched off to prevent mechanical failure (region d).

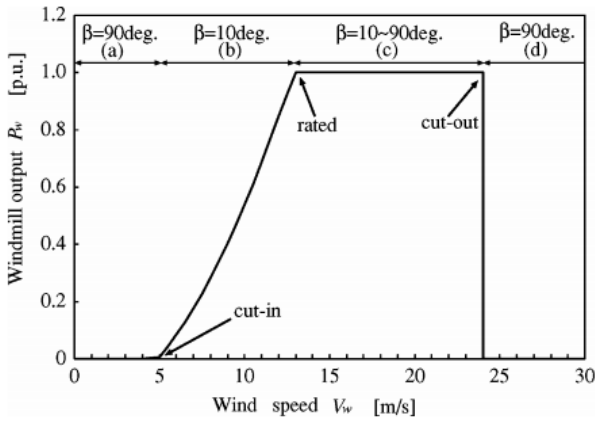


Figure 2.6: Operating region of a variable speed WECS [8]

## 2.3 Power electronics for wind systems

Power electronics enhance PMSG and DFIG wind technologies to achieve maximum power control at higher efficiencies under varying wind speed conditions. The power electronics block is usually in the form shown in Figure 2.7. This is a generic block diagram for the power electronics block of a PMSG and DFIG wind system. Converter 1 and converter 2 are the same and can conduct power in forward and reverse directions [14]. Converter 1 is referred to as machine side converter while converter 2 is referred to as grid side converter. A varying voltage in frequency and in magnitude is fed into the input of the power processor. The power processor converts this to a constant magnitude and frequency voltage. The energy storage device is usually a capacitor or an inductor depending on whether the converter is a current or voltage source. A capacitor is used for voltage source converter while an inductor is used for current source converter.

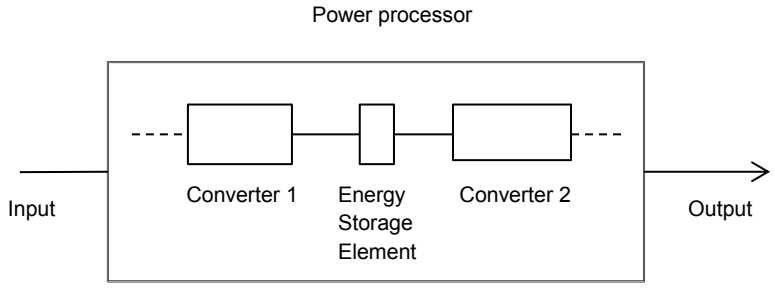


Figure 2.7: General block diagram of power electronics for WECS [14]

### *2.3.1 Power converter*

Power converters come in different forms but the one considered in this study is a two-level three leg converter shown in Figure 2.8. Each leg has two series switches where each switch is in parallel with a diode [14]. The switches are labelled $T_{A+}$, $T_{A-}$, $T_{B+}$, $T_{B-}$, $T_{C+}$ and $T_{C-}$. The corresponding diodes are labelled similar except the later D is used in the place of T. The switches come in different forms. They can be insulated gate bipolar transistors (IGBTs) or any switching alternatives like the gate-turn-off (GTO) thyristors depending on the manufactures preferences. A switching pattern for the switches can be determined using space vector pulse width modulation (SVPWM).

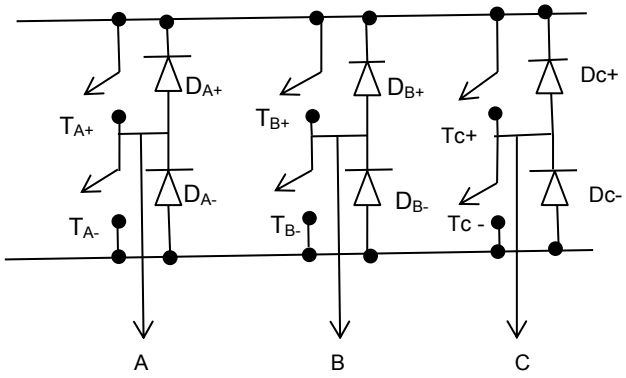


Figure 2.8: Back-to-back converter [14]

### *2.3.2 Space vector pulse width modulation*

Any three-phase balance voltages can be represented as a single phasor rotating at corresponding angular frequency in a two axis plane referred to as the alpha-beta (α-β) plane. The corresponding transformation is called the Clarke transform while its inverse is called the inverse Clarke transform. The α-β representation of the three-phase quantities is very useful as it is used to determine the switching pattern of the power converter in section 2.3.1. Each point on the circle formed by the rotating α-β phasor corresponds to a switching pattern of the top switches of a back-to-back converter [15].

# 3 Power Quality Issues

Voltage and frequency are the main indicators of electrical power quality. This is why many electrical power quality indices are defined in terms of voltage.
The frequency must be must comply with the grid code to prevent malfunction of electrical equipment. Operating the grid at higher frequencies will increase voltage drops across the lines and thus reduce the voltage received by customers. Operating the grid at lower frequencies will reduce the voltage on the secondary of the power transformer as it is directly proportional to the frequency.
The study of power quality is divided into three sections which are voltage, frequency and interruptions as shown in Figure 3.1. Voltage is further divided into four sections: voltage variations, flicker, harmonics and transients.

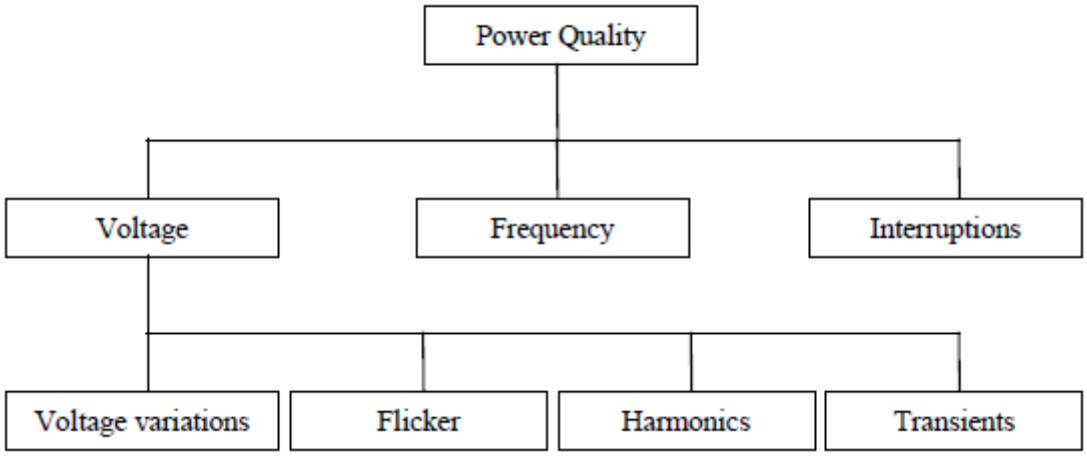


Figure 3.1: Hierarchy of electrical power quality [16]

## 3.1 Voltage variations

The IEEE 1159 – 1995 [17] standard defines voltage variations and transients by means of Figure 3.2. Events where voltage goes above 110% of the rated value are divided into three categories which are transients, swells and overvoltage. Transient events last less than 0.5 cycles, swell events last between 0.5 cycles and 1 minute while overvoltage events last longer than a minute. Events where voltage fall below 90% but above 10% of rated value are divided into two categories which are voltage sag and undervoltage. Voltage sags last longer than 0.5 cycles but less than a minute while undervoltage last longer than a minute. An event where the voltage fall in the range 10% - 90% of nominal value and lasts less than 0.5 cycles is referred to as notch. Events where the voltage is less than 10% of nominal value and lasting longer than 0.5 cycles are divided into three categories which are momentary, temporary and sustained interruptions. Momentary interruptions last between 0.5 cycles but less than 3 seconds, temporary interruptions last between 3 seconds and 1 minute while sustained interruption last longer than 1 minute.

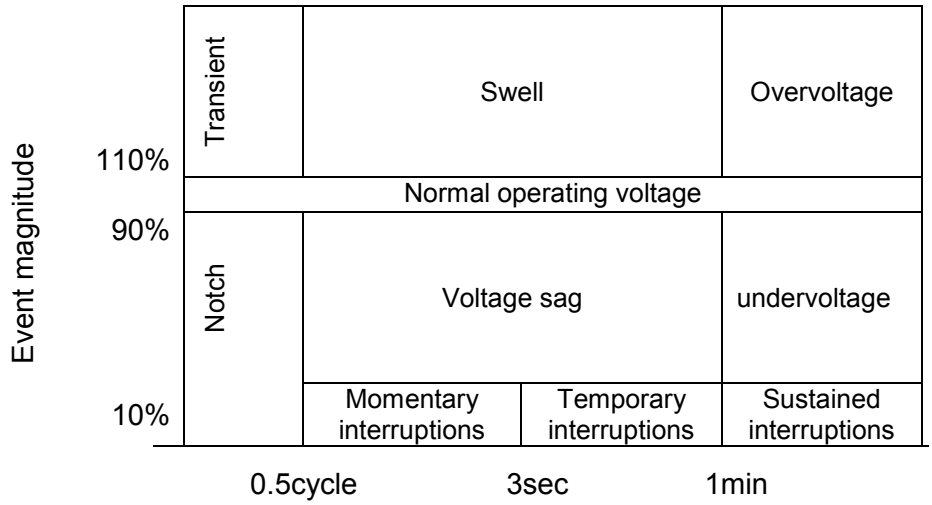


Figure 3.2: Power quality events as per IEEE 1159 – 1995 [17]

## 3.2 Voltage swell

Voltage swells are the events where the voltage rises above 110% of the rated voltage [17] for a time between 0.5 cycles and a minute. Voltage rise is defined as the ratio of the voltage drop across the transmission line to the rated voltage at the point of common coupling. Wind turbines cause voltage rise that is governed by equation 3.1. Voltage rise depends on the maximum apparent power of the wind turbine ( $S_{max}$ ), the angle between voltage and current ( Φ ) as well as the impedance of the grid (resistance ( R ) and reactance ( X )). Voltage rise is caused by increasing the reactive power generated by the wind turbine. This can also be concluded from the voltage rise equation. When the reactive power term is greater than the active power term, the voltage rise is less than zero which implies that the voltage at the PCC is greater than the voltage at the source. The ability of a wind turbine to increase voltage rise at the PCC is used to for voltage support. The grid code requires that wind turbines stay connected to the grid under low voltage conditions. Wind turbines with capacities greater than 20MVA are required to produce reactive power up to 33% of rated active power [18].

$$\Delta u = \frac{S_{max}(R\cos\emptyset - X\sin\emptyset)}{U^2} \qquad (3.1)$$

Where

- $S_{max}$ is the maximum apparent power of the wind turbine
- $\Delta u$ is the voltage rise
- R and X are the resistance and reactance of the transmission line

- Φ is the angle between voltage and the current
- U is the line to line voltage the PCC

The amount of reactive power generated by WECS is controlled by means of three control modes. The modes of reactive power control are constant reactive power, power factor and voltage control. The reactive power limits for wind turbines with capacities greater than 20MWA are shown in Figure 3.3. The sloped and dashed lines are constant power factor lines.

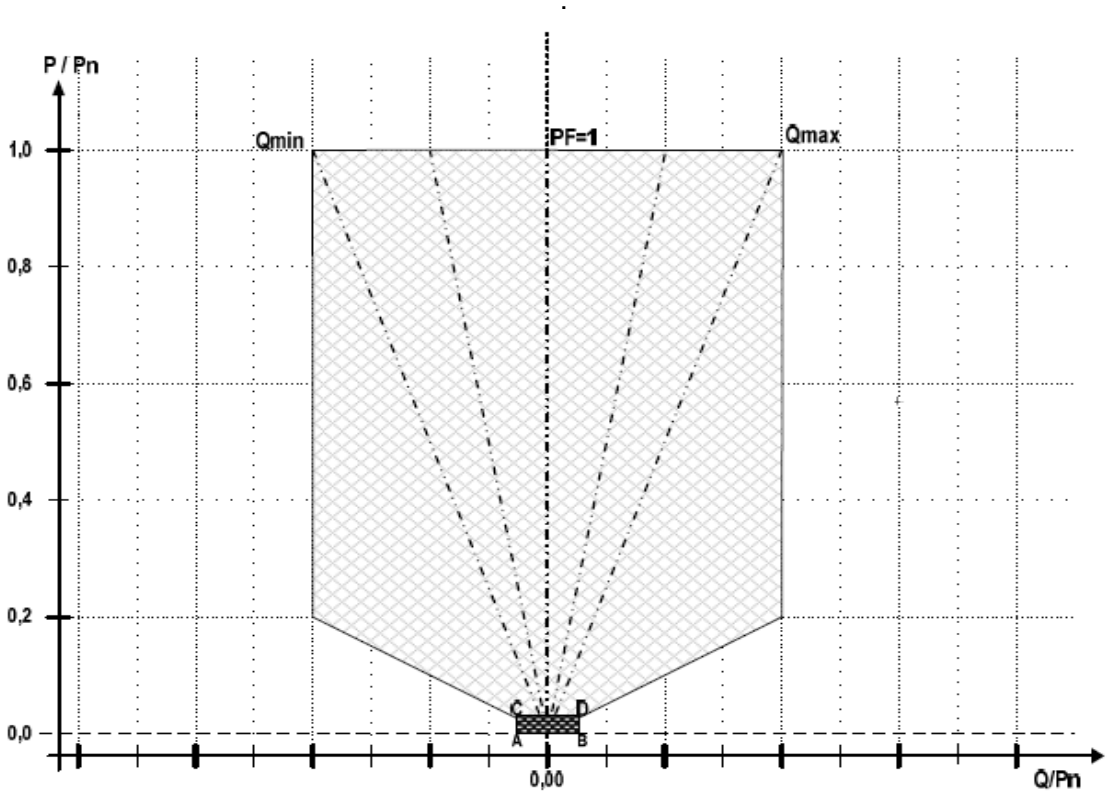


Figure 3.3: Grid code reactive power limits for RPP [18]

Another source of voltage rise is lighting strikes. A wind turbine has to be connected to the electrical network even under high voltage conditions. This is requirement from the grid code. The ability of the wind turbine to remain stable and connected to the grid during high voltage conditions is referred to as the high voltage ride-through (HVRT) capability.

## 3.3 Voltage flicker

Voltage flicker is the event which is defined as fluctuation in the amplitude of the voltage waveform within 10% of nominal voltage [19]. The fluctuating voltage causes light flicker which can annoy certain individuals. The study of flicker is done using an incandescent light bulb because its luminosity is proportional to voltage. Figure 3.4 shows the annoyance threshold curve. This figure is derived using a group of people subjected to a 60 watt

incandescent light bulb with supply voltage of 230 volts root mean square (RMS) at 50 Hz. The amplitude of supply voltage is modulated using a square waveform. The amplitude and frequency of the waveform is varied. The percentage change in voltage at which 50% of the people are annoyed is plotted against the number of voltage variations in one minute. The points above the flicker limit curve annoy people while points below the curve are acceptable. The frequency 8.8 Hz produces the most annoying flicker level even for small changes in voltage amplitude. This is because the human eye is most sensitive to this frequency. The frequency is kept within the band (0.001 to 18Hz) as shown in Figure 3.4 because the human eye is less sensitive to frequency outside this band.

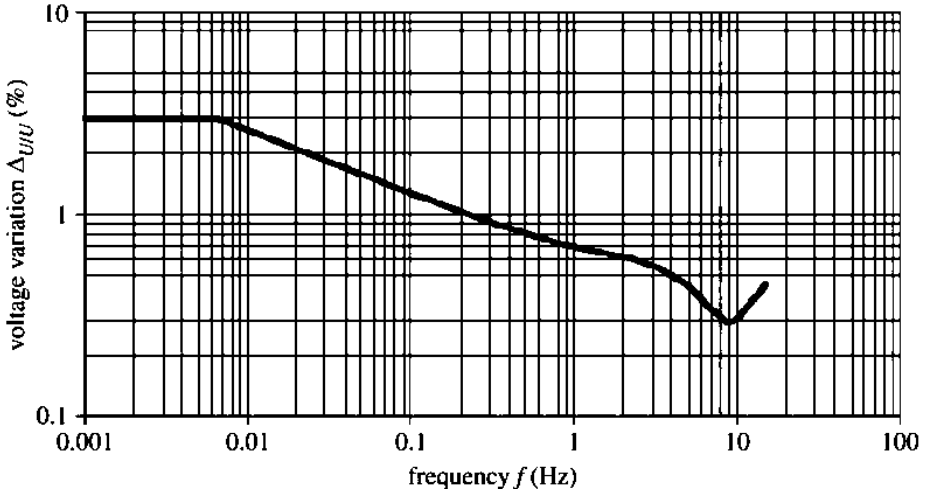


Figure 3.4: Flicker limit curve [20]

### *i. Flicker meter*

A flicker meter is a device derived from signal processing used to measure the degree of annoyance of flicker. A flicker meter takes as input the voltage signal and outputs two indices: short term ( $P_{st}$ ) and long term flicker severity indices ( $P_{lt}$ ) as shown in Figure 3.5. The flicker meter is made up of five modules. The first module is used to scale a signal to get a signal in per units. The second module squares the signal to separate the waveform producing the voltage changes from the mains signal. The human eye and brain is band limited and most sensitive at 8.8Hz in luminosity changes and therefore the third module is a band pass filter which is band limited to frequencies between 0.05 and 35Hz followed by a weighting filter with a peak at 8.8Hz [21]. Module 4 models the way that the human brain responds to fluctuations in illumination using a squaring module and a low pass filter block. The last module statically calculates the long and short-term flicker severity indices.

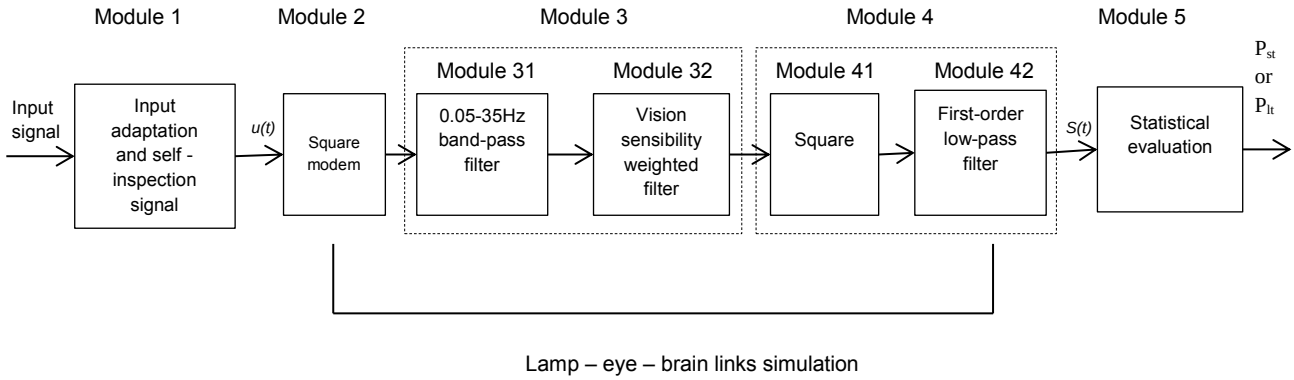


Figure 3.5: The flicker meter block diagram [21]

### *ii. Flicker limits*

The short and long term flicker severity index limit set points are set depending on voltage levels [21] as shown in table 3.1. For low voltages less than 1kV, the short term flicker severity index is limited to 1 while the long term flicker severity index is limited to 0.8. For medium voltages, the short term and long term flicker severity indices are set to 0.9 and 0.7 respectively. For high voltage networks the short and long term flicker severity indices are set to 0.8 and 0.6 respectively.

**Table 3.1: Short term and long term flicker severity indices IEEE 1453 [21]**

| Flicker Index | Low voltage | Medium voltage | High voltage |
|---|---|---|---|
| | $U_N \leq 1$ kV | 1 kV $< U_N \leq$ 35 kV | 35 kV $< U_N \leq$ 220 kV |
| $P_{st}$ | 1.0 | 0.9 | 0.8 |
| $P_{lt}$ | 0.8 | 0.7 | 0.6 |

### *iii. Grid strength*

The impact of large scale integration of WECSs on power quality of the grid depends on the grid strength. The strength of the grid is defined as the ratio of the short circuit level ( $S_k$ ) at the point of common coupling to the wind farm apparent power ( $S_n$). The short term flicker severity index depends on the grid strength [22] as shown by equation 3.2 (for the continuous case). The long term flicker severity index can be calculated from 6 samples of the short term flicker severity index.

$$P_{st} = C_i(\psi_k, v_n)\frac{S_n}{S_k} \qquad (3.2)$$

Where

- $C_i(\Psi_k, v_n)$ is the flicker coefficient,
- $\Psi_k$ is the transmission line impedance angle
- $v_n$ is the annual average wind speed.

## 3.4 Transients

The South African load demand is met by generation that is based on synchronous machines which may lose synchronism due to significant changes of active power. A synchronous generator rotor remains stable and operates at a constant speed if the mechanical power and active power generated matches. The mechanical power is regulated through governor control and is unlikely to change. Electrical power on the other hand changes frequently due to an number of reasons like changing loads. The sudden active power changes introduced by switching off of WECS wind farms on the grid can cause stability problems for synchronous machines.

### *3.4.1 Switching operations*

Switching operations of wind turbines cause voltage transients and may cause flicker. A wind turbine is switched off when there is excessive wind to prevent failure. Also, when there is not enough wind speed to overcome the static torque, the wind turbine will be switched off. Wind turbines can also be switched off due to other reasons like planned outages for maintenance. Other factors that lead to switching off of wind turbines are faults and low voltage events. Switching operations causes flicker. The produced flicker depends on the number of wind turbines as well as the number of switching operations.

### *3.4.2 Voltage interruptions and LVRT*

Voltage interruptions are events in the power system where the root mean square voltage drops below 10% of nominal value for a time longer than 0.5 cycles. The grid code specifies that a RPP with a power rating greater than 20MVA must remain connected on the grid for interruptions lasting less than 0.15 seconds as shown in the low voltage ride through curve of Figure 3.6 [18]. A RPP is required to stay connected to the point of common coupling during the events where the voltage at the PCC fall in the areas A, B and D of Figure 3.6. The RPP is required to assist in voltage set point restoration during the events. The ability of a WECS to remain connected to the network under low voltage conditions is called the low voltage ride through (LVRT) capability of a WECS.
The grid code allows wind turbines to disconnect if the operating conditions fall in region C of the LVRT curve. This is because the low voltage conditions at the PCC can cause tower vibrations which then stress the mechanical components [23].

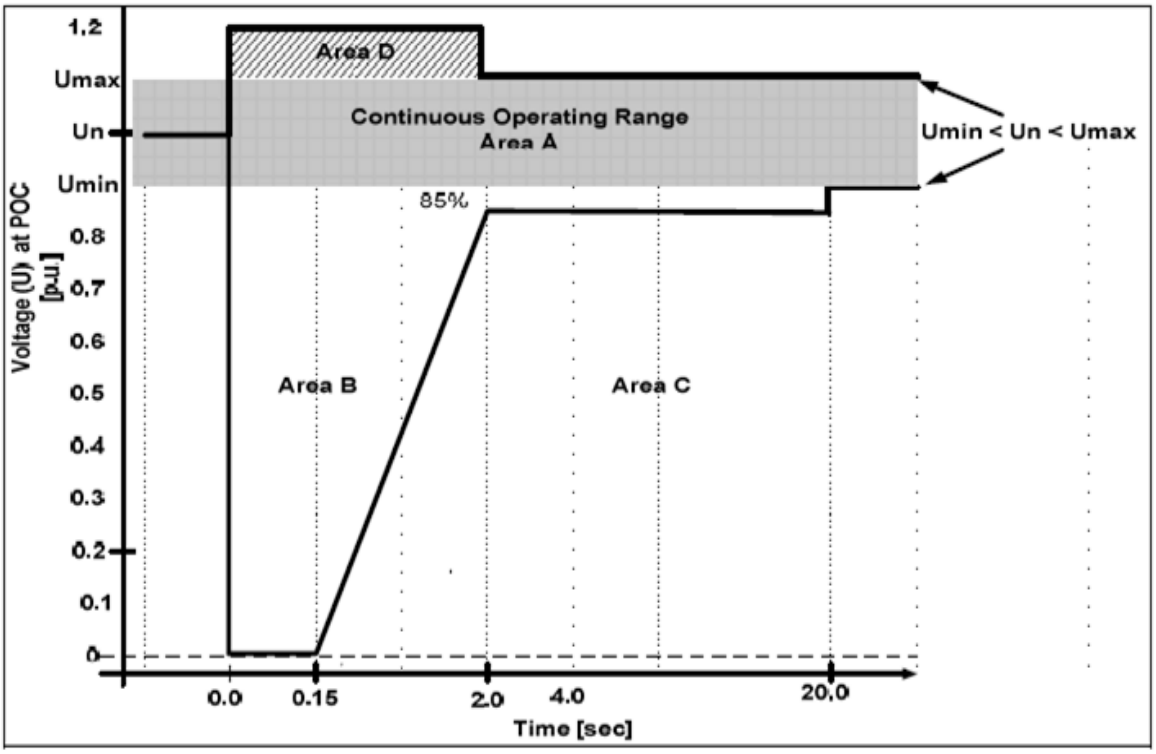


Figure 3.6: LVRT curve of a wind turbine [18]

### *3.4.3 Voltage sag*

Voltage sag events are events where the RMS voltage drops below 90% but remain above 10% of nominal voltage at the PCC for period between 0.5 cycles and 1 minute. Voltage dips are due to different power system disturbances such as faults and induction motor starting without power electronic drives or a soft starter. The acceptable voltage sag is 3% [24].

## 3.5 WECS harmonics

The back-to-back converters of variable speed wind turbines allows them to operate under varying wind speed conditions and allow for maximum power point tracking. However, the converters introduce harmonics into the grid. The level of harmonics can be reduced by filtering. One of the indices for measuring harmonics is the total harmonic distortion (THD). The expression for the THD is given by equation 3.3. Where h is the harmonic number, $V_1$ is the fundamental harmonic and $V_h$ is the $h^{th}$ harmonic. The THD planning level for medium voltage is 6.5% and 3% for a high voltage system [25].

$$V_{THD} = \sqrt{\sum_{h=2}^{40} \frac{V_h^2}{V_1} 100} \qquad (3.3)$$

## 3.6 Voltage unbalance

Voltage unbalance is the condition where the voltage magnitudes differ or phase angles are not 120 degrees apart for three-phase quantities [26]. Any three-phase voltages can be represented as a sum of three sets of voltages namely the zero, positive and negative sequence voltages. The zero sequence set consists of three voltages which are all in phase, the negative sequence consists of three balanced voltages rotating counter clockwise and the positive sequence set consists of three balance voltages rotating counter clockwise. These sets are used to calculate voltage unbalance. Voltage unbalance is calculated using the national equipment manufacturer's association (NEMA) definition, the international electrical and electronics engineers (IEEE) definition and the true definition [27]. NEMA defines voltage unbalance as the ratio of the line quantities maximum deference from the mean to the mean line voltages. The IEEE is similar to the NEMA approach except that the IEEE approach uses phase voltages instead of the line voltages. NEMA and IEEE definitions are a quick way to calculate voltage unbalance. The true definition of voltage unbalance defines voltage unbalance as the ratio of the negative sequence component to the positive sequence component. The voltage unbalance planning level limits are 0.8% for extra high voltage, 1.4% for high voltage and 1.8% for medium voltage [18]. These limits ensure that the low voltage unbalance limit of 3% is not violated.

## 3.7 Grid frequency

The South African grid code [18] stipulates that RPPs with capacities greater than 20MVA should generate at a frequency within the operating region defined in Figure 3.7. The nominal frequency is 50Hz but is allowed vary between 49 to 51 Hz in continuous operating range. The frequency is allowed to drop below 49Hz for periods less than 80 minutes but is limited by the lower limits L1, L2, L3 and L4. Also, the frequency is allowed to exceed 51Hz for a period less than 10 minutes but is limited by the higher limits H1 and H2.

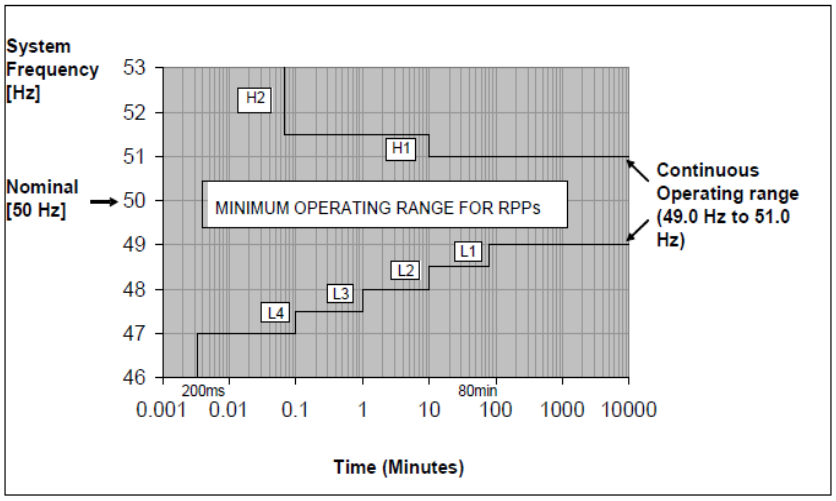


Figure 3.7: The frequency operating regions for RPPs [18]

### *3.7.1 Active power response*

RPPs are required to not only generate at an acceptable frequency but to also react to changes in grid frequency so as to keep it at 50Hz [18]. The grid frequency decreases with increase in active power demand and conversely the grid frequency increases with reduction in active power demand. The grid code requires RPPs to respond to frequency changes by generating active power shown in Figure 3.8. The settings for the frequencies are given in table 3.2. At frequency below f1, the RPP must produce available active power. When the grid frequency drops below f2, the RPP must increase its active power production at a rate equal to droop 1. When the frequency increases above f3, the wind farm must start reducing its active power production at a rate equal to the droop 2. The frequencies and droops are agreed upon connection by the RPP and the service operator (SO).

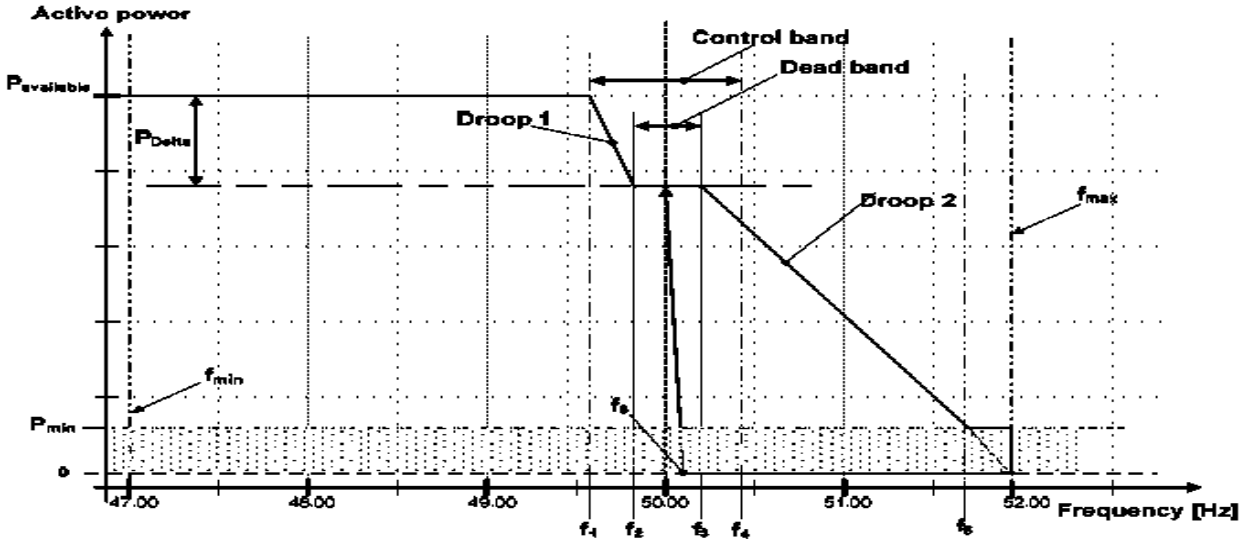


Figure 3.8: Required active power response to frequency changes for RPPs [18]

**Table 3.2: Frequency settings**

| Parameter | Magnitude |
|---|---|
| $f_{min}$ | 47 |
| $f_{max}$ | 52 |
| $f_1$ | As agreed with SO |
| $f_2$ | As agreed with SO |
| $f_3$ | As agreed with SO |
| $f_4$ | 50.5 |
| $f_5$ | 51.5 |
| $f_6$ | 50.2 |

## 3.8 Tower shadow and shear effect

Tower shadow and wind shear effect are the source of power fluctuations in WECSs. When a wind turbine blade passes the tower, the output power is reduced by up to 10% [28]. For a turbine with three blades, this happens three times in one turbine revolution hence the power reduction frequency is three times the angular frequency (3p) of the turbine. Wind shear effect is due to the difference in wind speed magnitude and direction.

Wind speed is not uniform along the height of the wind turbine, it increases with height. The combination of wind shear and tower shadow effect causes power fluctuations. W Hu and *et al.* [29] investigated the impact of large scale integration of PMSG based WECS on small signal stability of the power system. The study was done using a twelve bus two area network. The findings were the wind shear and tower shadow effect increases the power system oscillations when the 3p frequency got closer to the inter-area natural oscillation frequency.

## 3.9 Reactive power control

There are three common voltage control methods applied to WECS. These are constant reactive, power factor and droop control. In constant reactive power control, the reactive power production of a WECS is kept fixed irrespective of active power production. The voltage control methods are now addressed.

### *3.9.1 Constant reactive power and power factor control*

Constant reactive power control acts like a capacitor bank because the reactive power produced remains fixed. The difference is that reactive power produced by a capacitor bank is proportional to the square of the voltage and thus vary with voltage. Constant reactive power control is illustrated by the dotted vertical line in Figure 3.9.

Power factor control on the other hand is where reactive power produced is proportional to the active power thus following a fixed reactive to active power ratio as shown in Figure 3.9.

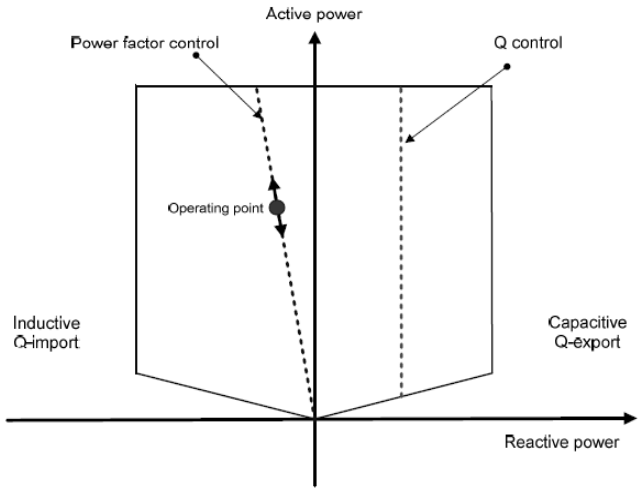


Figure 3.9: Reactive power control [18]

### *3.9.2 Droop control*

Voltage control ensures that the PCC voltage is kept at its nominal value. It produces as much reactive power as required, within limits, to keep the voltage at the set point in the PCC. The voltage is kept within the maximum and minimum limit. The voltage is set to follow the droop as shown in Figure 3.10. The droop is agreed upon between the RPP and the SO. The droop is amount of reactive power required to reach a given voltage set point. Droop 1 is much steeper than droop 2. This implies that more reactive power is needed when the droop setting is droop 2 than when it is droop1 to reach the same voltage set point.

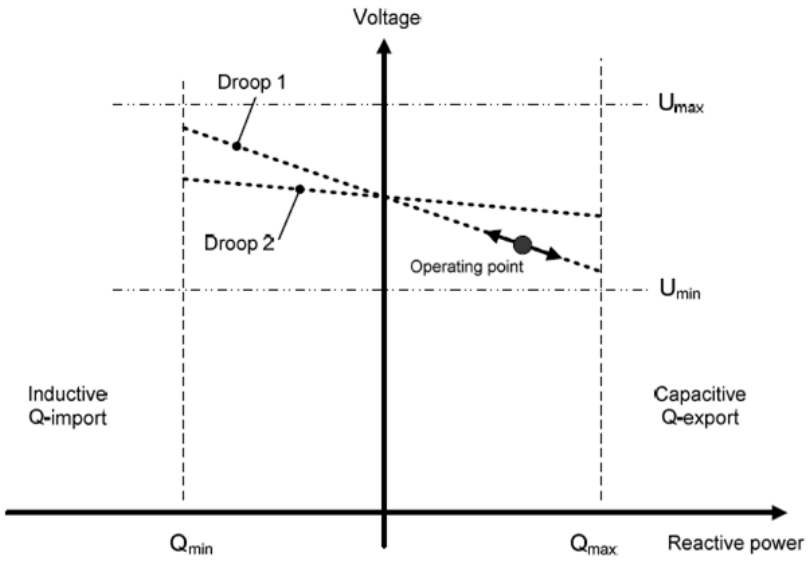


Figure 3.10: Voltage control [18]

# 4 Impact of PMSG on power quality

The study of the impact of permanent magnet based wind energy conversion system on power quality is not recent. There has been intensive research over the years about large scale grid integration of PMSG based WECS impact on power quality [30, 31, and 32]. Some of findings of the research are mentioned in this chapter. These include the effect of PMSGs on voltage flicker, harmonics and transient stability.

## 4.1 Impact of PMSGs on flicker

PMSG based WECS produce flicker as a result of fluctuations in wind speed. These fluctuations in wind speed are translated into voltage fluctuations are the PCC which in turn causes flicker. Other sources of sources of active power fluctuation are the tower shadow and wind shear effect.

Some of the methods of mitigating flicker caused by the PMSG based WECS are to either directly minimise the voltage fluctuations at the PCC or minimise the dips in the input active power. To minimise the voltage fluctuation directly, a voltage regulating device like a static compensator (STATCOM), static var compensator (SVC) or any reactive power compensating devices is used. However, this method increases the cost of the WECS, so it is not attractive. The active power control method on the other hand does not require an additional expensive device. W Hu and *et al.* [30] showed that the flicker due to tower shadow effect can be reduced by controlling the DC-link voltage. Since the dip in active power on machine side produces a voltage dip on the DC-link, active power control keeps the DC-link voltage fixed irrespective of the power dip. This is done by using a flicker mitigation controller (FMC) in series with a band pass filter. The band pass filter is centred on tower shadow frequency and limits the FMC to only react to tower shadow effect. The FMC block changes the DC-link voltage set point in proportion to power dip to keep DC-link voltage fixed and thus minimise flicker.

## 4.2 Impact of PMSG on harmonics

The source of harmonics in a PMSG based WECS is the back-to-back converter. One of the power quality indices used measure harmonics is the THD. It increases with increase in amplitude of the harmonics. The THD can be reduced by filtering. Recent development in power electronics have led to development of multi-level converters. Multi-level converters closely mimic the sinusoidal waveform by introducing intermediate voltage levels. A typical two-level converter uses the maximum voltage as well as minimum voltage to produce the sine wave. However, with multi-level converters the intermediate voltage levels are used. The THD therefore is reduced in the case of a multi-level converter. The disadvantage of multi-level converters is the complexity of the corresponding control system. Moreover, unbalance voltages across the series capacitors of the DC-link cause controller malfunction [31].

The study done by M. Seixas and *et al.* [31] showed that the THD produced by PMSG based WECS can be reduced by using a three-level converter instead of a two-level converter. The

study also showed that the THD depends on the type of a controller used. A fractional proportional integral (PI) controller produced lower THD compared to a classical PI controller. The observation was that the THD reduces with increased wind speed. This implies that the THD decreases with increase in active power production.

## 4.3 Impact of PMSG based WECS on transient stability

PMSG based WECS have to be disconnected during some low voltage events at the PCC. The decreased voltage at the PCC causes voltage increase in the DC-link capacitor [30]. This voltage can damage the switching devices if it is high enough. The severe the voltage dip, the higher the voltage rise on the DC-link capacitor. The reason for the voltage increase is that the sudden voltage dip causes a power imbalance on the DC-link. The turbine power does not match the grid side power during the voltage dip. The power difference is stored in the DC-link capacitor. In order to store the extra power, the DC-link capacitor voltage must rise as the energy stored in a capacitor is proportional to the voltage. In addition to DC-link capacitor voltage rise, voltage dips also causes tower vibrations [23]. The vibrations are the alternative way for the WECS to dissipate the excess power. This stresses the mechanical components of the turbine and may cause turbine failure. For these reasons, independent power producers prefer to disconnect PMSG based WECSs during low voltage events at the PCC. However, disconnecting WECS is a treat to transient stability and thus the grid code requires that requires WECS to remain connected to the grid under some low voltage conditions. So the solution to this problem is to improve low voltage ride through capability of the PMSG based WECSs.

J.F Conroy and R Watson [32] showed that the low voltage ride through capability of a PMSG based WECS can be improved by installing a resistor in parallel with a DC-link capacitor. The resistor (also called a breaking resistor) is in series with a switch so that when the low voltage event occurs at the PCC, the switch is switched on to provide an alternative path for dissipating the excessive power. Another option is to increase the size of the DC-link capacitor so that there is enough room to store the extra power and prevent tower vibrations. The LVRT capability can also be improved by introducing a voltage regulation device at the PCC. However, this solution involves an additional device and has an extra cost implication.

A method for improving LVRT capability which requires no expensive extra electrical equipment is active power control. X.P. Yang and *et al.* [33] showed that the LVRT capability of a PMSG based WECS can be improved by reducing the active power generation during a low voltage event. Thus the turbine and grid side power closely match and there is no need for additional electrical devices. The machine side active power reduction is achieved through pitch control. Increasing the pitch angle of the turbine blades reduces the generated active power.

# 5 Modelling PMSG based WECS

In this chapter an electrical model of the PMSG based WECS is developed. The model of the PMSG based WECS is divided into four sections: these include the aerodynamic, mechanical, electrical and the control system. A complete PMSG based WECS model also includes the wind and the grid model. The electrical control of PMSG based WECS is best simplified by using the Clarke and Park transforms on the three-phase voltages and currents. The corresponding currents and voltages are direct current (DC) and therefore simple controllers like the PI (proportional integral) controllers can be used. PI controllers are easy to tune compared to other methods like the sinusoidal tracker and the hysteresis controllers [34 and 44].

## 5.1 Reference planes

A set of three-phase voltages can be transformed into an alpha-beta representation using the Clarke transform. The result is a rotating vector in the alpha-beta reference frame. The rotating vector is used to determine the switching pattern of the back-to-back converters of the PMSG based WECS. More details about the Clarke transform are provided in section 5.5.1.

There also exists another transformation called the Park transform (equation 5.1) which converts a set of three-phase voltages into three direct current components namely d, q and 0. For a balanced three phase system, the 0 component is equal to zero. The frame used to get the d, q and 0 components rotates at an angular frequency corresponding to the associated system frequency. The frame is referred to as the d-q frame.

$$\begin{bmatrix} V_d \\ V_q \end{bmatrix} = \frac{2}{3}\begin{bmatrix} \cos\emptyset & \cos(\emptyset-\gamma) & \cos(\emptyset+\gamma) \\ -\sin(\emptyset) & -\sin(\emptyset-\gamma) & -\sin(\emptyset+\gamma) \end{bmatrix} x \begin{bmatrix} V_a \\ V_b \\ V_c \end{bmatrix} \quad (5.1)$$

where:

- Vq and Vq are the d and q-axis voltages
- $\gamma$ is a constant which is equal to 120 degrees
- Va, Vb, and Vc are the three-phase voltages
- $\Phi$ angle made by the d-axis component with the horizontal

The inverse of the Park transform exists and is given by equation 5.2. Since the inverse of the park transform exists it is therefore possible to move from the Park transform to the Clarke transform. It is also possible to move from the Clarke transform to the Park transform because the inverse of the Clarke transform also exists. These properties are very useful in the control of the PMSG based WECS. The Park transform (and its inverse) for three-phase voltages has been illustrated here, however, the same matrices can be used for calculating the three-phase currents with V (voltage) replaced by I (current).

$$\begin{bmatrix} V_a \\ V_b \\ V_c \end{bmatrix} = \begin{bmatrix} \cos(\emptyset) & -\sin(\emptyset) \\ \cos(\emptyset - \gamma) & -\sin(\emptyset - \gamma) \\ \cos(\emptyset + \gamma) & -\sin(\emptyset + \gamma) \end{bmatrix} x \begin{bmatrix} V_d \\ V_q \end{bmatrix} \quad (5.2)$$

## 5.2 Wind model

The wind model for a wind turbine can be represented as the sum of three components [26]. The model is given by equation 5.3. The first component ( $V_H$ ) is the wind speed at the hub of the wind turbine. The second component ( $V_{eqws}$ ) is the wind speed component due to wind shear effect. The last component ( $V_{eqts}$ ) models the tower shadow effect.

$$V_{eq} = V_H + V_{eqws} + V_{eqts} \quad (5.3)$$

The wind shear component is given by equation 5.4. It is a function of the wind speed at the hub of the turbine, the turbine blades swept area radius ( R ) and azimuthal angle ( β ). Alpha (α) is the empirical wind shear component.

$$V_{eqws} = V_H[\frac{\alpha(\alpha-1)}{8}\left(\frac{R}{H}\right)^2 + \frac{\alpha(\alpha-1)(\alpha-2)}{60}\left(\frac{R}{H}\right)^3 \cos 3\beta] \quad (5.4)$$

The tower shadow effect component is given by equation 5.5. It is a function of wind speed at the hub height and radius of the blades. $\beta_b$ is the azimuthal angle of each blade, α is the tower radius in meters while x is the distance between the blade origin and the midpoint of the tower height in meters. *m* is the coefficient of the wind turbine.

$$V_{eqts} = \frac{mV_H}{3R^2}\sum_{b=1}^{3}[\frac{a^2}{\sin^2\beta_b}\ln(\frac{R^2\sin^2\beta_b}{x^2}+1) - \frac{2a^2R^2}{R^2\sin^2\beta_b + x^2}] \quad (5.5)$$

## 5.3 Aerodynamic model turbine

The kinetic energy of wind particles can be converted to mechanical energy which is then converted to electrical energy by an electrical generator. The mechanical power of a wind turbine is given by equation 5.6. Where *p* is the air density, $V_w$ is the wind speed and R is the radius of the swept area by the turbine blades. $C_p$ is the turbine power coefficient. Not all kinetic energy can be extracted from the wind. This is referred to as the Betz limit. In practice the extraction capability of a wind turbine varies between 40 – 50% [34]. This is modelled by defining a turbine power coefficient given by equation 5.7 [35].

$$P_{wt} = \frac{1}{2} p V_w^3 \pi R^2 C_p \tag{5.6}$$

$$c_p(\lambda, \beta) = c_1 \left( \frac{c_2}{\lambda_i} - c_3\beta - c_4\beta - c_5 \right) e^{-\frac{c_5}{\lambda_i}} + c_6 \tag{5.7}$$

The power coefficient is a function of the tip-speed-ratio (λ in equation 5.8) and the pitch angle of the turbine blades (β). The parameters $C_1$ to $C_2$ are constants and are unique for different turbines. The parameters $\lambda_i$ is a function of the pitch angle and its expression is given by equation 5.9.

$$\lambda = \frac{\omega_{wt} R}{V_w} \tag{5.8}$$

where:

- $\omega_{wt}$ is turbine shaft angular speed in rad/s
- R is the radius of the turbine blades in meters
- $V_w$ is the wind speed in m/s

$$\frac{1}{\lambda_i} = \frac{1}{\lambda + 0.08\beta} + \frac{0.035}{\beta^3 + 1} \tag{5.9}$$

The graph of the power coefficient ( $C_p$ ) is concave and has one peak. The peak occurs at a specific tip-speed-ratio referred to as the optimal tip-speed-ratio. Thus in order to optimise the extracted power from the wind, the tip-speed-ratio of a wind turbine has to be kept at its optimal value. Referring to equation 5.3.3, one way to achieve this is by controlling the wind turbine shaft angular speed in a way to keep the tip-speed-ratio fixed under varying wind speed conditions.

The torque developed by the wind turbine to the generator shaft for unity gear box ratio is given by equation 5.10. $C_q$ is the quotient of the $C_p$ to the tip-speed-ratio as shown by equation 5.11.

$$T_{wt} = \frac{1}{2} p V_w^2 \pi R^3 C_q \tag{5.10}$$

$$C_q = \frac{C_p}{\lambda} \tag{5.11}$$

## 5.4 Mechanical model

The link between the turbine shaft and the generator shaft is referred to as the drive-train [34]. The drive-train can be modelled as a two mass model: the mass of the turbine shaft and the mass of the generator shaft. The turbine and generator shafts are directly linked in the case of most PMSG. This minimises maintenance costs. The exclusion of a gear box is catered for by the presence of many poles on the generator stator windings. The following equations (5.12 and 5.13) are a link between the turbine shaft and the generator shaft and therefore model the drive-train.

$$J_{wt}\frac{d^2\theta_{wt}}{dt^2} = T_{wt} - K(\theta_{wt} - \theta_m) - D(\frac{d\theta_{wt}}{dt} - \frac{d\theta_m}{dt}) \tag{5.12}$$

$$J_g\frac{d^2\theta_m}{dt^2} = K(\theta_{wt} - \theta_m) + D\left(\frac{d\theta_{wt}}{dt} - \frac{d\theta_m}{dt}\right) + T_e \tag{5.13}$$

where:

- $J_{wt}$ is the wind turbine moment of inertia in kgm$^2$; $J_g$ is the wind turbine moment of inertia in kgm$^2$
- $\theta_{wt}$ is the wind turbine shaft angular position in radians; $\theta_m$ is the angular position of the generator in radians
- t is the time in seconds
- K is the stiffness coefficient of the in Nm/rad; D is the damping coefficient in Nms/rad
- $T_{wt}$ is wind turbine torque in Nm, $T_e$ is generator electrical torque in Nm

## 5.5 Electrical model

The electrical system of a permanent magnet synchronous generator wind energy conversion system consists of a generator, two back-to-back converters and a control system. Other components include the filter and the transformer on the grid side of the system.

### *5.5.1 Modelling Inverters*

The use of back-to-back converters of a PMSG based wind power system allows for operation under varying wind speed conditions. The converters have three lags in the case of a three-phase system. Each lag has two transistors connected in parallel and each

transistor is in parallel with a diode in the case of a two-level converter. Such a converter can conduct power in forward and reverse direction. It can operate as a rectifier as well as an inverter. The two transistors in a lag must not be closed at the same time because a short circuit will be formed. This means that the top transistors of each lag decide the switching combinations. This requires a three bit representation. The switching combinations are shown in Figure 5.1 [36]. The resultant basic vectors are named $V_1$ to $V_6$. These vectors divide the plane into six sectors and they are labelled 1 to 6.

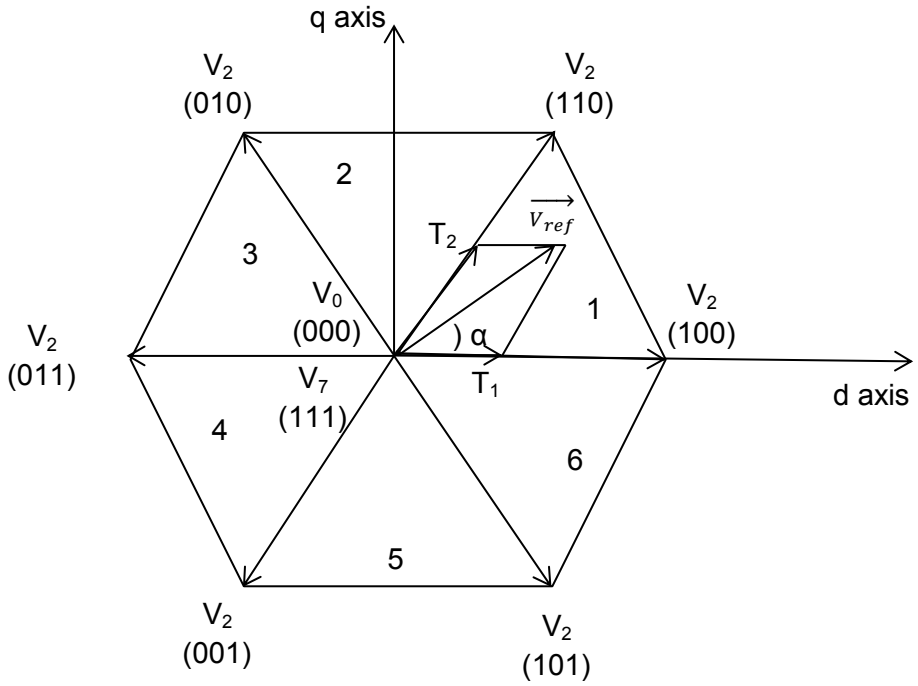


Figure 5.1: Basic vector combinations [36]

Each of the three bits represents the state of the top switches of the converter; the bottom switches are in the opposite states of the top switches. The bit patterns represent a switching combination that will produce a voltage vector in a given sector referred to as the reference vector ( Vref ). The magnitude of the reference vector can be obtained by a given switching combination of the basic vectors applied for particular period of time. For Vref to be in sector 1, the switching combinations (100) and (110) must be used. For Vref to be in sector 2, the switching combinations (010) and (110) must be used and so on. The (000) and (111) switching combinations are used to adjust the magnitude of Vref when used for a time duration of $T_0$ (equation 5.16). The time T1 (equation 5.14) and T2 (equation 5.15) are the switching duration of the basic vectors Vi and Vi+1 (where i is the sector number). T1 and T2 determine the angle alpha (α) in a given sector. A full revolution of the Vref vector will produce three-phase balanced voltages at the output of the inverter. $T_z$ is half of the sample time (equation 5.17).

$$T_1 = T_z \frac{|\vec{V}_{ref}|}{V_{dc}} \frac{\sin(\frac{\pi}{3} - \alpha)}{\sin(\frac{\pi}{3})} \quad (5.14)$$

$$T_2 = T_z \frac{|\vec{V}_{ref}|}{V_{dc}} \frac{\sin(\alpha)}{\sin(\frac{\pi}{3})} \quad (5.15)$$

$$T_0 = T_z - (T_1 + T_2) \quad (5.16)$$

$$T_z = \frac{T_s}{2} \;\&\; T_s = \frac{1}{f_s} \quad (5.17)$$

where:

- 0=<α<=60 degrees,
- Ts is the switching period,
- fs is the switching frequency
- $T_z$ is half the switching period

### *5.5.2 Modelling permanent magnet synchronous generator*

Permanent magnet synchronous machines are a special case of synchronous machines. PMSG have a permanent magnet in the rotor as opposed to the field windings of a typical synchronous machine. Figure 5.2 shows a typical permanent magnet synchronous machine. A and A', B and B', C and C' are the stator windings. $f_a$, $f_b$ and $f_c$ are the magnetomotive force (MMF) phasors produced by the three-phase stator currents [37].

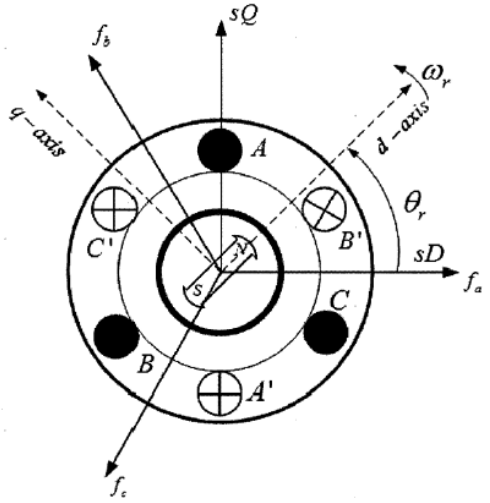


Figure 5.2: Cross-sectional view of a PMSG [37]

A rotating magnetic field from a permanent magnet synchronous generator rotor induces three-stator voltages in the stator windings. The induced voltages are given by equation 5.18 [38]. $v_{as}$, $v_{bs}$, and $v_{cs}$ are the voltages at the terminals of the stator windings while $i_{as}$, $i_{bs}$ and $i_{cs}$ are the stator currents through the a, b and c windings respectively. $R_s$ is the resistance of each winding. $\lambda_{as}$, $\lambda_{bs}$, and $\lambda_{cs}$ are the magnetic flux linkages of the stator windings. The left hand side of equation 5.18 is obtained by applying Kirchhoff's voltage law at the stator terminals where the first term is obtained by applying Ohms law and the second term is obtained by applying Faradays law.

$$\begin{bmatrix} v_{as} \\ v_{bs} \\ v_{cs} \end{bmatrix} = \begin{bmatrix} R_s & 0 & 0 \\ 0 & R_s & 0 \\ 0 & 0 & R_s \end{bmatrix} . \begin{bmatrix} i_{as} \\ i_{bs} \\ i_{cs} \end{bmatrix} + \frac{d}{dt} \begin{bmatrix} \lambda_{as} \\ \lambda_{bs} \\ \lambda_{cs} \end{bmatrix} \tag{5.18}$$

The flux linkages are given by equation 5.19. $L_{as}$, $L_{bs}$ and $L_{cs}$ are the mutual inductances while $L_{aa}$, $L_{bb}$ and $L_{cc}$ are the self-inductances of the windings [2]. $\lambda_r$ is the permanent magnet rotor flux and $\theta_r$ is the angle formed by the rotating d-axis and the horizontal.

$$\begin{bmatrix} \lambda_{as} \\ \lambda_{bs} \\ \lambda_{cs} \end{bmatrix} = \begin{bmatrix} L_{aa} & L_{ab} & L_{ac} \\ L_{ba} & L_{bb} & L_{bc} \\ L_{ca} & L_{ca} & L_{cc} \end{bmatrix} . \begin{bmatrix} i_{as} \\ i_{bs} \\ i_{cs} \end{bmatrix} + \begin{bmatrix} \lambda_r \cos(\theta_r) \\ \lambda_r \cos(\theta_r - \frac{2\pi}{3}) \\ \lambda_r \cos\theta_r + \frac{2\pi}{3} \end{bmatrix} \tag{5.19}$$

### *5.5.3 PMSG model in d-q form*

The control system of the PMSG based WECS is be greatly simplified when a Park transform is applied on equation 5.18. The result is a set of two equations in the d-q reference frame. The d-q frame voltages ($V_{ds}$ and $V_{qs}$) are given by equation 5.20 and 5.21 respectively [37]. These voltages are DC in nature so simple control algorithms like proportional integral (PI) controller can be used in the control system. In the steady state case, the derivative terms are zero and the voltages will only depend on the resistive and the permanent magnet flux component. $V_{ds}$ is a function of q-axis component ($L_q\, i_{qs}$) which is scaled by the electric angular speed $\omega_e$ ; $V_{qs}$ is a function of d-axis component ($L_d\, i_{ds}$) which is also scaled by $\omega_e$. This prohibits the separate control loops of q and d-axis components. However, for small $L_q$ and $L_d$ independent control can be achieved.

$$V_{ds} = R_s i_{ds} + L_d . \frac{di_{ds}}{dt} - \omega_e L_q i_{qs} \tag{5.20}$$

$$V_{qs} = R_s i_{qs} + L_q . \frac{di_{qs}}{dt} + \omega_e L_d i_{ds} + \omega_e \lambda_r \quad (5.21)$$

where:

- V = Voltage
- i = Current
- R = Resistance
- L = Inductance
- $\omega_e$= Electrical angular speed
- $\lambda_r$ = Magnetic flux linkage of the permanent magnets
- s, d and q = Subscripts for stator, d-axis and q-axis

### *5.5.4 Grid side models*

The grid side consists of the grid side converter, a filter and the transmission line as well as a step up transformer. The filter can be in the form of a resistor in series with an inductor (RL filter). In most cases, an inductor alone is sufficient to be a low pass filter. However, since there is no ideal inductor, there is always a resistive component in series with the inductor [39].

The three-phase voltages on the grid side can be converted into corresponding voltages in the d-q reference plane using the Park transform. This greatly simplifies the control loops on the grid side. Equations 5.22 and 5.23 are the d-q frame voltages. $I_{dg}$ and $I_{qg}$ are the grid side d-q frame currents. $V_{dg}$ and $V_{qg}$ are the grid side d-q frame voltages. $R_f$ is the filter resistance, $L_f$ is the filter inductance and $\omega_s$ is the grid side angular frequency. The q-axis voltage depends on the q-axis voltage. This prohibits separate control of the of the d-q voltages. The q-axis voltage is set to zero in equation 5.23 to simplify reactive power control.

$$V_{dg} = R_f i_{dg} + L_f . \frac{di_{dg}}{dt} - \omega_e L_f i_{qg} + v_{dg} \quad (5.22)$$

$$V_{qg} = R_f i_{qg} + L_f . \frac{di_{qg}}{dt} - \omega_e L_f i_{dg} + v_{qg} \quad (5.23)$$

where:

- V = Voltage
- R = Resistance
- i = Current

- L = Inductance
- $\omega_e$ = Electrical angular speed
- g, d, q, f = subscripts for grid, d-axis, q-axis, and filter respectively

### *5.5.5 Machine side electrical power*

For three-phase stator windings, the total electrical power ( $S_{abc}$ ) of the three phases is given by equation 5.24. $V_{as}$, $V_{bs}$ and $V_{cs}$ are the three-phase stator instantaneous voltages at the terminals of the stator windings. $i_{as}$, $i_{bs}$ and $i_{cs}$ are the instantaneous currents through the stator windings.

$$S_{abc} = v_{as}i_{as} + v_{bs}i_{bs} + v_{cs}i_{cs} \quad (5.24)$$

The three-phase instantaneous power expression can be converted to an equivalent expression in the d-q reference frame and the results are shown by equation 5.25. Therefore, the three-phase electrical power is a function of d-q axis stator currents and voltages. The electrical power in the d-q axis thus can be controlled by controlling the d-q currents and voltages.

$$P_{dq} = \frac{3}{2}(v_{ds}i_{ds} + v_{qs}i_{qs}) \quad (5.25)$$

### *5.5.6 Grid side electrical power*

The three-phase instantaneous electrical power on the grid side is given by equation 5.26, Where $V_{ag}$, $V_{bg}$ and $V_{cg}$ are the three-phase grid side instantaneous voltages. $i_{ag}$, $i_{bg}$ and $i_{cg}$ are the three-phase instantaneous currents on the grid side.

$$P_{abc} = v_{ag}i_{ag} + v_{bg}i_{bg} + v_{cg}i_{cg} \quad (5.26)$$

Equation 5.26 can be converted into the d-q reference frame representation [38]. Equations 5.27 and 5.28 are the corresponding grid side active and reactive power respectively. Pg and Qg are the grid side active and reactive power represented in the d-q reference frame respectively. The dg and qg subscripts indicate the grid side voltage ( v ) and current ( i ) in the d-q reference frame respectively.

$$P_g = \frac{3}{2}(v_{dg}i_{dg} + v_{qg}i_{qg}) \quad (5.27.)$$

$$Q_g = \frac{3}{2}(v_{qg}i_{dg} - v_{dg}i_{qg}) \quad (5.28)$$

Setting the q-axis voltage component to zero reduces 5.27 to 5.29 and 5.28 to 5.30. The q-axis voltage component becomes zero when the d-axis component of is aligned with the rotating space vector [37]. The active power sent to the grid can be controlled by controlling the d-axis current while the reactive power sent to the grid can be controlled by controlling the q-axis current. Thus independent control of active and reactive power can be achieved.

$$P_g = \frac{3}{2}(v_d i_d) \quad (5.29)$$

$$Q = -\frac{3}{2}(v_d i_q) \quad (5.30)$$

### *5.5.7 Electrical torque*

A loaded PMSG will produce an electrical torque that opposes the mechanical torque applied to the generator rotor. The expression for electrical torque is equation 5.31 where $T_e$ is the electrical torque, $n_p$ is the number of poles and $\lambda_m$ is the flux linkage due to the permanent magnet [41]. Ld and Lq are the d-q frame inductances respectively.

$$T_e = \frac{3}{2}n_p[\lambda_m i_{qs} + (L_d - L_q)i_{qs}i_{ds}] \quad (5.31)$$

For surface mount permanent magnets (SMPMs) the d-axis inductance is equal to the q-axis inductance. Therefore the equation 5.31 is reduced to equation 5.32. In machine side control the d-axis current is usually set to zero in this case. This aids to limit the machine side current and thus reduce the losses. The electrical torque for SMPM is a function of q-axis current only and therefore it can be controlled by controlling the q-axis current of the stator.

$$T_e = \frac{3}{2}n_p[\lambda_m i_{qs}] \quad (5.32)$$

### 5.5.8 DC-link

The DC-link is used mainly for smoothing the output voltage of the machine side converter. It can be shown that the DC-link is bounded by equation 5.33. *C* is the capacitance, $V_{DC}$ is the voltage across the DC-link capacitor while $P_t$ and $P_g$ are the machine and gird side active power respectively. The machine side active power has to match the grid side active power in order to have a steady state DC voltage ($V_{DC}$) across the DC-link capacitor [42]. This condition must be held in order for the machine side and grid side control system to work. It is important that the DC-link voltage remains fixed to reduce power quality indices such as the flicker severity indices. This is because varying DC-link voltage will produce a varying amplitude output voltage which can increase flicker severity indices.

$$C\frac{dv_{DC}}{dt} = \frac{P_t}{v_{DC}} - \frac{P_g}{v_{DC}} \tag{5.33}$$

### 5.5.9 The transmission line

For the purpose of this study the PMSG based wind turbines are 10km away from the point of common coupling. Thus the short transmission line model is used. The generic matrix [43] for a short transmission lines is:

$$\begin{bmatrix} V_S \\ I_S \end{bmatrix} = \begin{bmatrix} A & B \\ C & D \end{bmatrix} \begin{bmatrix} V_R \\ I_R \end{bmatrix} \tag{5.34}$$

were V represents the voltage and I represents the current. The subscript S represents the sending end quantities while the subscript R represents the receiving end quantities. A, B, C and D are the transmission line parameters and are often referred to as *ABCD* parameters. For short transmission lines (length less than 100km) with series impedance Z, the *ABCD* parameters are given by equations 5.35 to 5.37.

$$A = D = 1 \tag{5.35}$$

$$B = Z \tag{5.36}$$

$$C = 0 \tag{5.37}$$

### *5.5.10 Filter design*

The filter used in this study is an RL filter. The transfer function of the filter ( *H*(s) ) is given by equation 5.38. $R_f$ and $L_f$ are the resistance and inductance of the filter respectively. The cut-off frequency of the filter is set at 60Hz. The resistance of the filter is 1 ohm. Therefore the inductance size is 2.65mH for a cut-off frequency at 60Hz. There is no special reason for choosing these values the filter resistor and inductor. Other values could have been chosen as long as they ensure that the filter will pass only the fundamental harmonic at 50Hz and attenuate other harmonic components.

$$H(s) = \frac{1}{L_f S + R_f} \qquad (5.38)$$

# 6 Control of PMSG based WECS

The control system of a PMSG based WECS is divided into two sub-control systems: the machine and grid side control systems [37]. The generator side control system is divided into angular speed, yaw and pitch control. The grid side control system is divided into DC-link voltage and reactive power control. An overview of the control system of a PMSG based WECS is given in Figure 6.1. The generator side control system involves the measurement of the three-phase voltages ( $V_{abc}$ ) and currents ( $i_{abc}$ ). These are then fed to the Clarke transform blocks ( abc/αβ ). The outputs of the Clarke transform blocks are fed into the Park transform block (abc/dq) and phase measuring device which is usually a phase-locked loop ( PLL ). The output of the Park transform block is fed to the grid side PI controllers. The set point for the rotor angular speed is determined with intention to extract maximum power as discussed in section 5.3. The d-axis current is set to zero. The output of the angular speed and machine side current controllers is fed into the inverse Park transform block ( dq/abc ) followed by a Clarke transform block. The output of the Clarke transform block is fed into the space vector pulse width modulation ( SVPWM ) block which determines the switching combination for the machine side converter.

The grid side control concept is similar to the machine side and thus will not be discussed any further. The difference is that the primary focus of the grid side control system is to control the reactive power as well the voltage across the DC-link capacitor instead of angular speed and d-axis current.

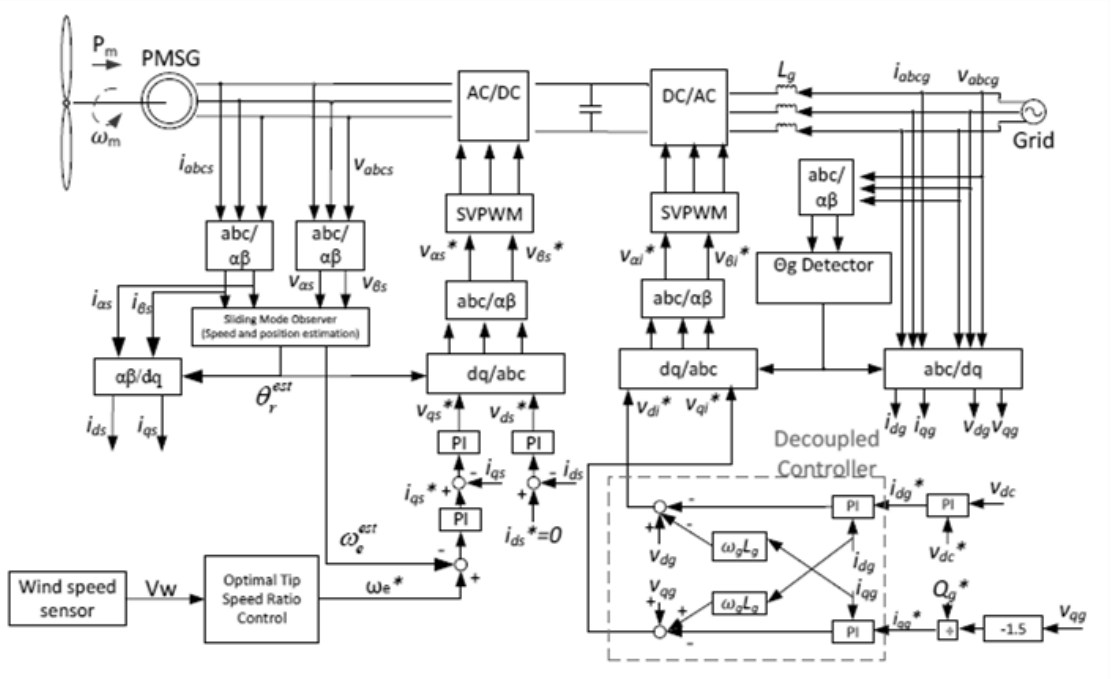


Figure 6.1: The PMSG based WECS and its associated control system [37]

## 6.1 Machine side control

The machine side control system is responsible for maximum power point tracking (MPPT). This section discusses the machine side control concepts and shows the associated control loops. Chapter 5 was about the modelling of the PMSG based WECS. This section is a follow up on chapter 5 where a Fourier transform of the electrical models in chapter 5 was taken to get to the transfer functions used in the control loops in this section.

### *6.1.1 d-axis current control loop*

The d-axis current loop is shown in Figure 6.2. The poles introduced by the control algorithm, inverter and sampling module are neglected. The loop is shown for the d-axis current but is a generic loop for all the d-q axis current control loops. Thus the q-axis current loop is the same as the loop for d-axis current control loop with Id replaced by $I_q$. The D parameter of the PID controller is set to zero so the controller is a PI controller. The PMSG is modelled as a first order transfer function. L is the inductance and R is the resistance of the winding of the PMSG stator.

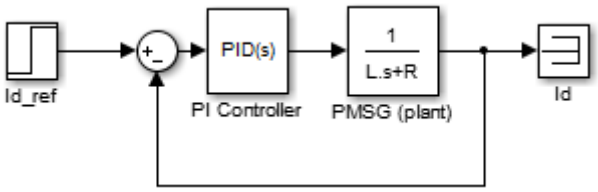


Figure 6.2: Id current control loop

### *6.1.2 Pitch control*

Pitch control enhance a wind turbine to be operated on its operating region to prevent damage. The operating region of a wind turbine was discussed in section 2.1.2. At wind speeds lower than the cut-in speed, the pitch angle is set at 90 degrees so as to bring the turbine to a halt. At wind speeds greater than the cut-in but lower than rated wind speeds, the turbine pitch angle is set between 0 to 24 degrees [34]. A typical range is 0 to 10 degrees as was shown in section 2.1. At this point the maximum power point tracking algorithm is used to extract optimal power from the wind. For wind speed greater than the rated wind speed but less than the cut-out speed, the pitch angle is set between 10 and 90 degrees so as to not exceed the rated power of the turbine. The pitch angle is set at 90 degrees at wind speeds greater than the cut-out speed, this is done so as to bring the wind turbine to a halt and prevent damage.
Pitch control does not form part of the scope of controller design in this study and thus will not be discussed any further.

### *6.1.3 Angular speed control*

The angular speed control allows the wind turbine to extract optimal power. The tip-speed-ratio is the function of the angular speed. When the wind speed varies, the tip-speed-ratio also changes. The tip-speed-ratio can be kept constant by changing the angular speed in proportion to the wind speed. The angular speed is set such that the tip-speed-ratio is optimal, meaning that it is a tip-speed-ration that yields a maximum power coefficient. The block diagram for the angular speed control is shown in Figure 6.3. The poles introduced by the control algorithm, inverter and sampling module are neglected. The D parameter of the PID controller is set to zero so the controller is a PI controller. The input of the PI controller is the error between the reference angular speed ( Wm_ref ) and output angular speed (Wm). The $I_q$ current control closed loop is the represented by the first order transfer function with a time constant $T_q$. The torque equation block is based on the torque equation where npp is the number of pole pairs and F is the permanent magnet flux. The inertia model block models the effect of inertia and J is the moment of inertia of the PMSG rotor. From the output of the torque equation block the mechanical toque (Tm) is subtracted and fed to the inertia block to obtain angular speed.

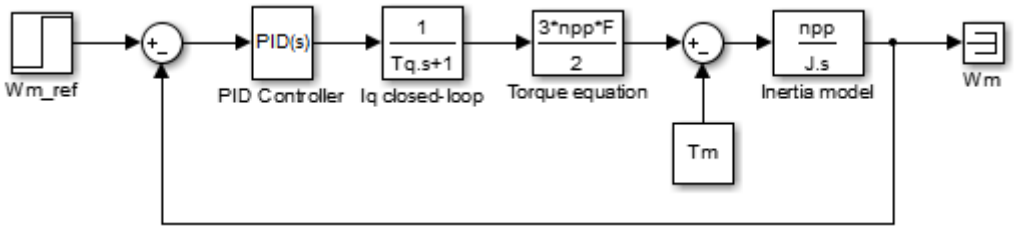


Figure 6.3: Rotor angular speed controller

## 6.2 Grid side control

The grid side control is divided into two kinds: the DC-link voltage control and reactive power control. Both control loops will be addressed in this study starting with reactive power control.

### *6.2.1 Reactive power control*

Reactive power control assist in voltage control at the PCC. Reactive power is controlled by controlling the q-axis current. This is based on the fact that the reactive power is proportional to the $I_q$ current as was shown in section 5.5.6. The closed loop diagram for reactive power control is shown in Figure 6.4. The poles introduced by the control algorithm, inverter and sampling module are neglected. The plant in this case is the filter. The filter is modelled as a first order transfer function where Lf is the inductance and $R_f$ is the resistance of the filter. The output $I_q$ current is subtracted from the reference $I_q$ current (Iq_ref) and the error is fed to the PID controller. The D parameter of the PID controller was set to zero so the controller is a PI controller.

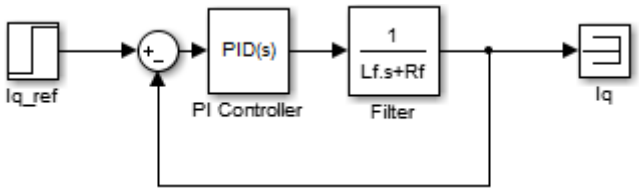


Figure 6.4: Reactive power controller

### *6.2.2 DC-link voltage control*

The DC-Link voltage control is part of the grid side control. The primary purpose of the dc-link voltage control is to keep the voltage across the capacitor constant. The control loop for the DC-link voltage is shown in Figure 6.5. The Id current control close-loop is modelled as the first order transfer function with a time constant Td. The DC-link is modelled as an integrator, where C is the capacitance of the DC-link capacitor. A dc-link voltage set point ( Vdc_ref ) is compared to the Vdc output voltage and the error is fed to the PID controller. The D parameter of the PID controller is set to zero so the controller is a PI controller.

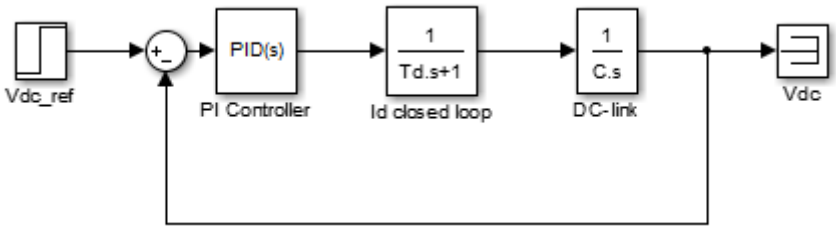


Figure 6.5: DC-link voltage controller

### *6.2.3 Phase-locked loop*

The phase-locked loop (PLL) is used to measure the phase angle. The PLL model in MATLAB Simulink can also measure the frequency of the currents and voltages. The phase angle information is used when applying the Park transform. The control loop for the PLL is shown in Figure 6.6. A Park transform is applied to the three-phase voltages to obtain the d-q components. The q-axis voltage is set to zero. The q-axis voltage is passed through proportional integral controller where it is converted to angular speed and added to the grid angular frequency set point. The sum is then fed to an integrator which converts to phase angle.

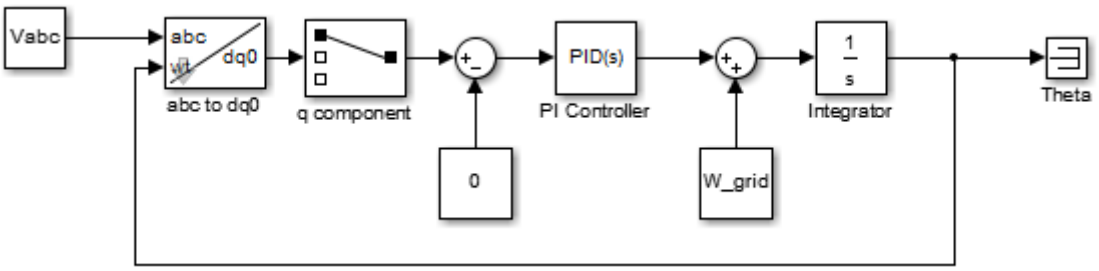


Figure 6.6: Phase-locked Loop controller

# 7 Model verification

The model of permanent magnet synchronous generator based wind energy system discussed in chapters 5 and 6 is now verified in this chapter. The model verification is implemented in MATLAB Simulink. First the controller design is done using the SISOTOOL of MATLAB and then the controllers are implemented in the Simulink model. An overview of the Simulink model is shown in the appendix, section 12.1. It should be noted that all the step inputs have a steady state value of 1.

## 7.1 Controller design

The controllers are designed using the root locus method. This method involves the placement of poles on the second and third quadrant of the s-plain and adjusting the gain of the controller to position the closed loop poles. The controllers are first designed in the s-domain and then converted to the z-domain in this study. This is because the Simulink is very slow in the continuous state and hence it changed to do calculations in the discrete state.

The control objectives were that a closed loop system +/- 1% settling time must be 0.4 seconds and the damping factor must be greater than 0.7. The P and I controller parameters for the machine side and grid side PI controllers are shown in table 12.1 in the appendix. The robustness of the system was tested because the model is only verified in the form of simulations here but will not be implemented in the laboratory.

### *7.1.1 Machine side controller design*

The machine side controller designs are shown in this section. The controllers are designed in the continuous domain and then converted to the discrete domain.

#### *i. Machine side q-axis current control*

Angular speed control has an inner control loop: the q-axis current control loop. The SISOTOOL of MATLAB was used to determine the PI parameters of the machine side q-axis current control loop. The root locus plot of the q-axis control loop is shown in Figure 7.1. The PI controller introduces a pole at the origin to ensure zero error tracking. A zero is then placed at 10.86 on the real axis to 'attract' the pole to the left of the real axis. However, it must not be close to the pole introduced by the PMSG. The gain is set to 5 such that the closed loop poles yields a system with time constant less than 0.4 seconds. The machine side (MS) d-axis control loops is the same as the machine side q-axis current control loop and thus the PI control parameters are the same. The corresponding step response of the machine side q-axis current control loop is shown in Figure 7.2. As can be seen from the figure, the +/- 1% settling time is less than 0.4 seconds and the damping factor is greater than 0.7.

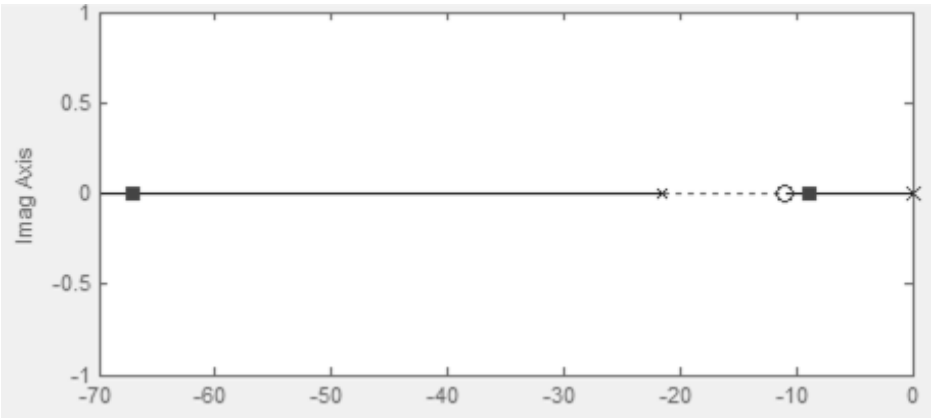


Figure 7.1: The root locus plot for MS q-axis current control loop

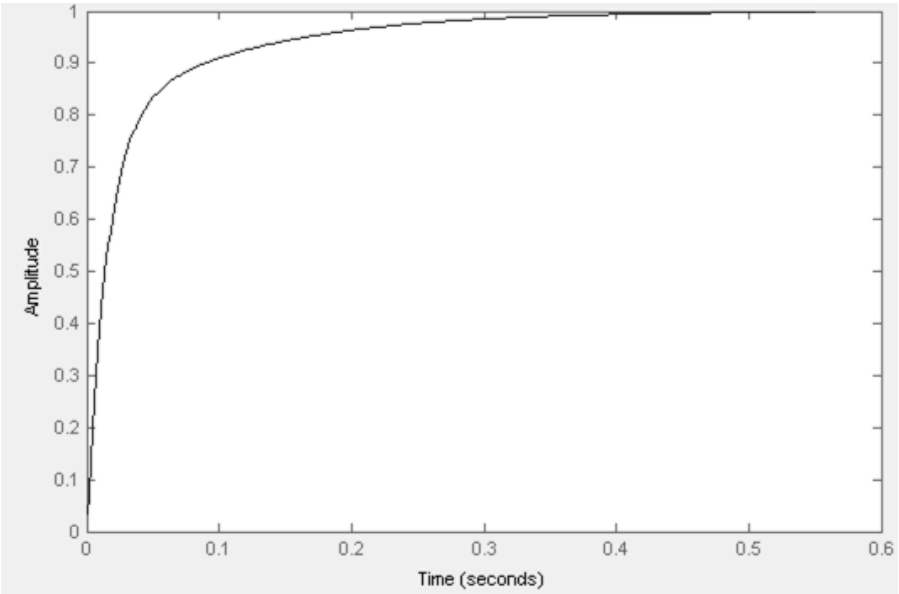


Figure 7.2: Unit step response of the MS q-axis current control loop

The corresponding z-domain root locus pot is shown in Figure 7.3. The discrete step response is shown in Figure 7.4. The system is stable with no oscillatory modes and meets the control objectives.

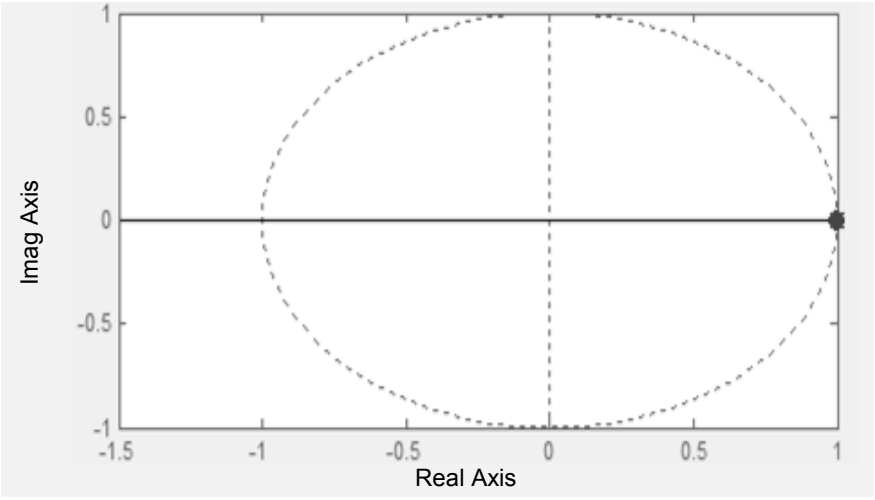


Figure 7.3: Discrete root locus plot of the MS q-axis current control loop

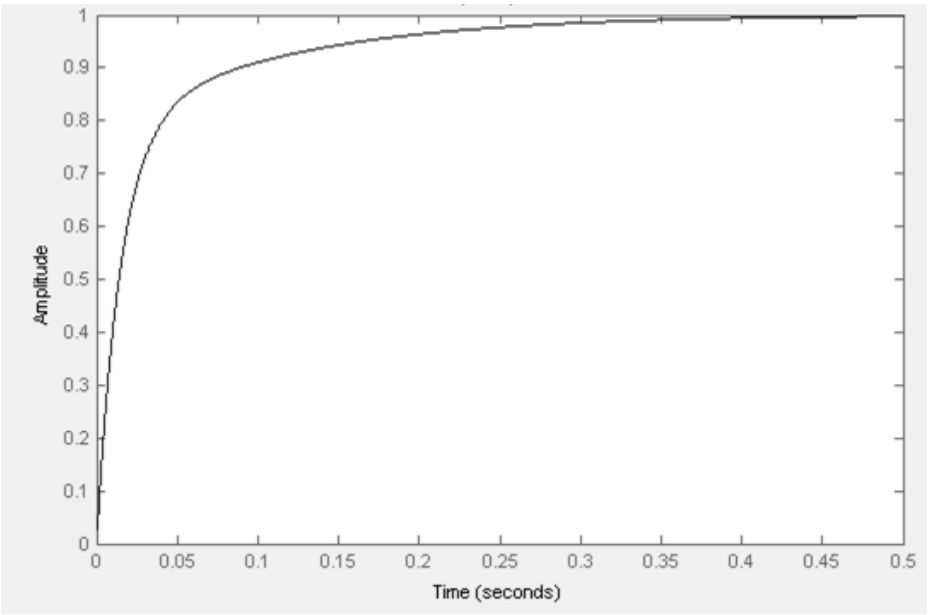


Figure 7.4: Discrete unit step response of the MS q-axis current control loop

### *ii. Angular speed control*

The machine side outer loop control is the angular speed control. The root locus for angular speed control is shown in Figure 7.5. The corresponding unit step response is shown in Figure 7.6. The PI controller introduces a pole at the origin to ensure zero error tracking. A zero is placed at 1 on the real axis to attract the pole. The closed loop gain is set at 23600 to achieve a closed loop system with a +/-1% settling time less than 0.4 seconds and damping factor greater than 0.7. The gain is quite large however can be reduced by using an anti-windup controller. The design of the anti-windup controller does not form part of the scope of this study.

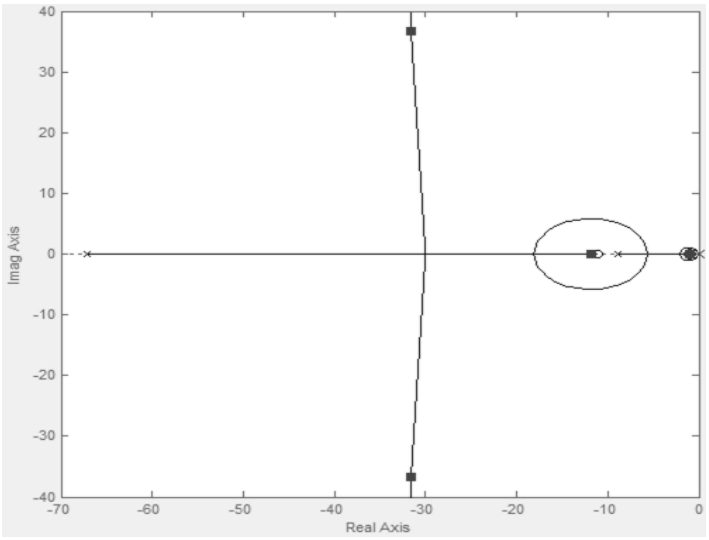


Figure 7.5: Speed control root locus in the s-domain

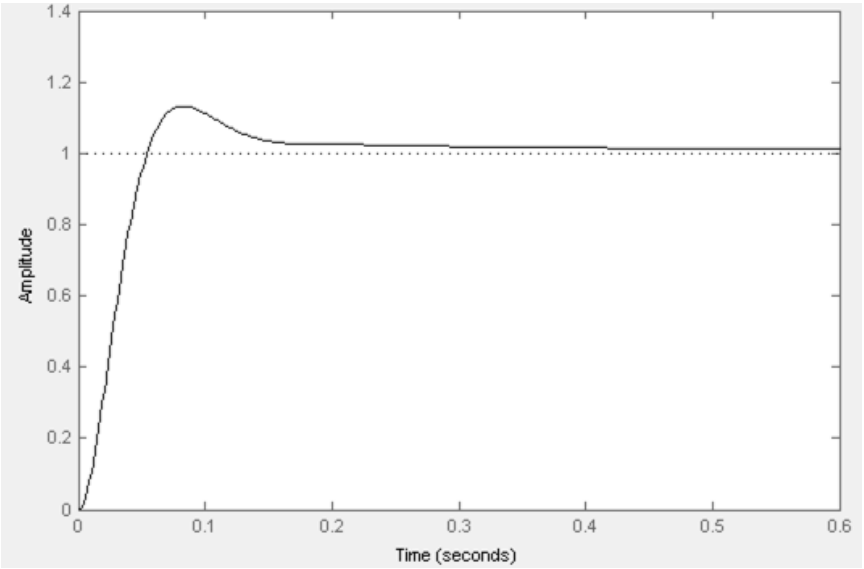


Figure 7.6: Unit step response for angular speed control

Figure 7.7 to 7.8 shows the discrete root locus in the z-plain and the corresponding unit step response. The system is stable with not oscillatory modes.

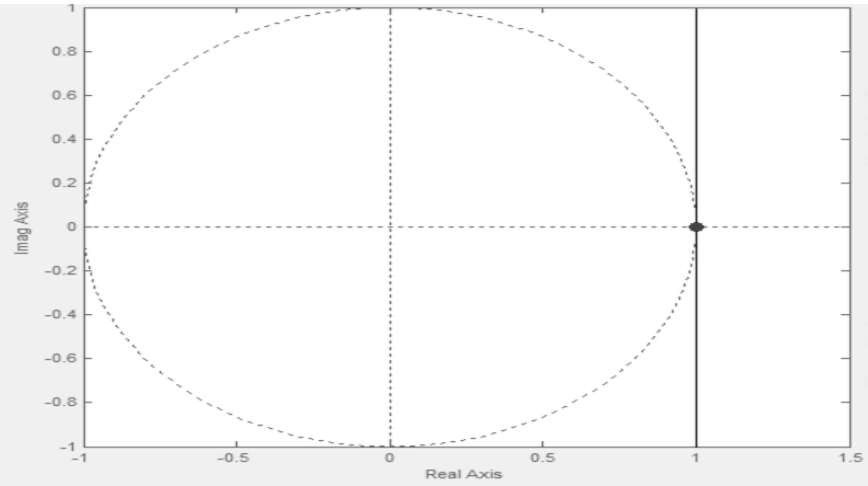


Figure 7.7: Discrete root locus for speed control

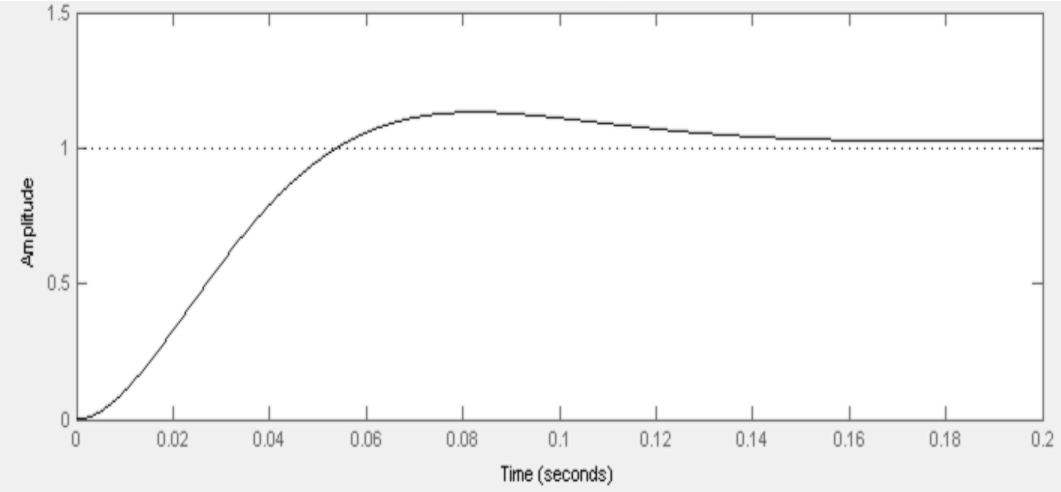


Figure 7.8: Unit step response for discrete speed control

### *7.1.2 Grid side controller design*

The grid side control is divided into two kinds: the DC-link voltage and reactive power control. Both kinds will be addressed in this study starting with reactive power control. The controller parameters are determined using the SISOTOOL of MATLAB. The root locus control design process was followed. The control objective was to achieve a closed loop system +/- 1% settling time of less than 0.4 seconds and a damping factor greater than 0.7.

#### *i. Reactive power control*

Figure 7.9 shows the root locus of the reactive power control open loop system. Figure 7.10 shows the corresponding unit step response. To achieve zero error tracking of set point, the PI q-axis controller introduces a pole at the origin. A zero is placed at 192 on the real-axis of the s-plain to 'attract' the pole at the origin to the left. The gain of the PI controller is set to 685 to ensure that the +/- 1% settling time of the closed loop system is less than 0.4 seconds and the damping factor is greater than 0.7. The gain is quite large however there

are methods to reduce it [39]. However, this does not form part of the scope of this study. Reactive power control is essentially grid side q-axis current control as reactive power is directly proportional to the q-axis current. The q-axis control is the same as the d-axis current control so d-axis current control results and design process will not be shown herein this section.

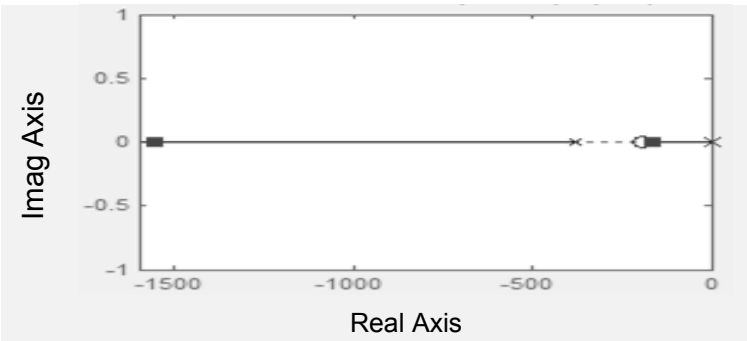


Figure 7.9: Root locus of reactive power control loop

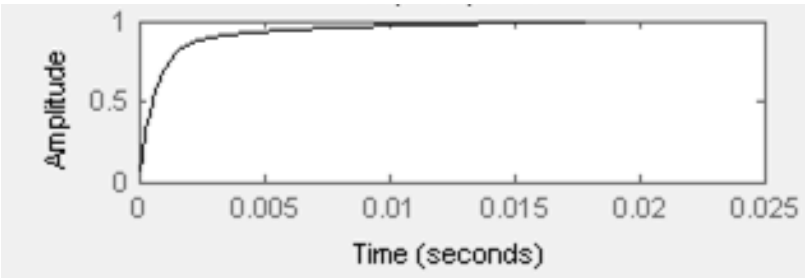


Figure 7.10: Unit step response of reactive power control

Figure 7.11 to 7.12 shows the root locus and the unit step response of the reactive power control loop in the discrete domain. The system is stable and meets the control objectives.

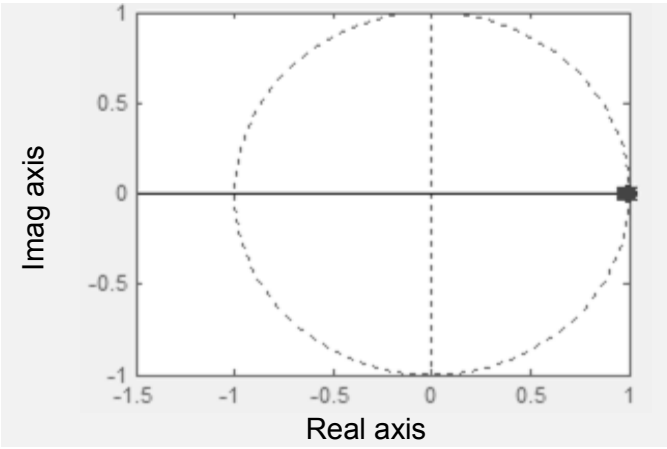


Figure 7.11: Discrete root locus for reactive power control

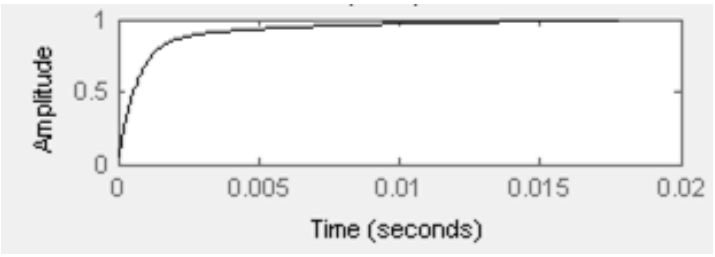


Figure 7.12: Unit step response for discrete reactive power control

### *ii. DC-link voltage control*

The DC-link voltage control loop has an inner control loop which is the grid side d-axis current control. The grid side d-axis current control loop is similar to the grid side reactive power control loop which was discussed in section 7.1.2. The root locus plot for DC-link voltage control is shown in Figure 7.13 and the corresponding unit step response is given by Figure 7.14. The DC-link PI controller introduces a pole at the origin of the s-plain. A zero is placed at 10 on the real axis of the s-plan to 'attract' the closed loop poles to the left of the s-plain such that the controller meets the control objectives.

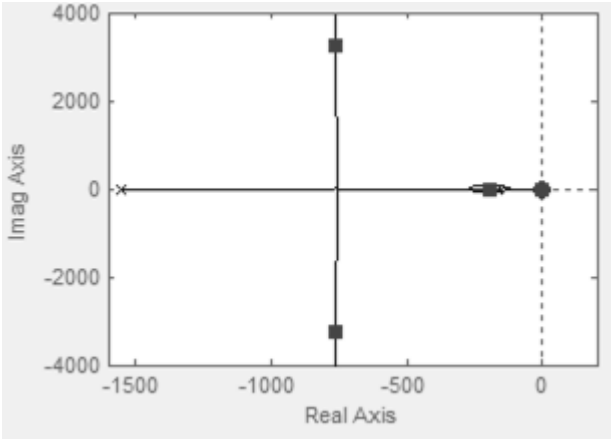


Figure 7.13: Root locus plot for DC-link voltage control loop in the s-plain

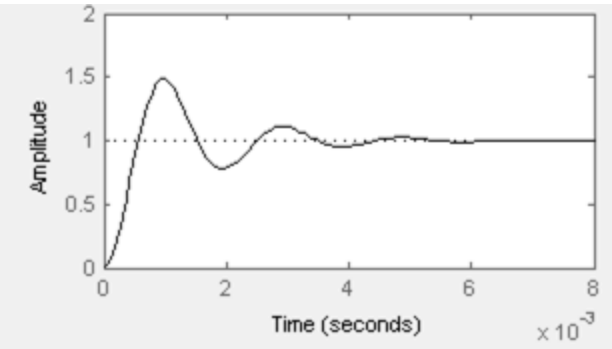


Figure 7.14: Continuous unit step response of DC-link voltage control

Figure 7.15 shows the root locus of the DC-link voltage control for the discrete case. Figure 7.16 shows the unit step response for the discrete case. The system is stable and meets the closed loop control objectives.

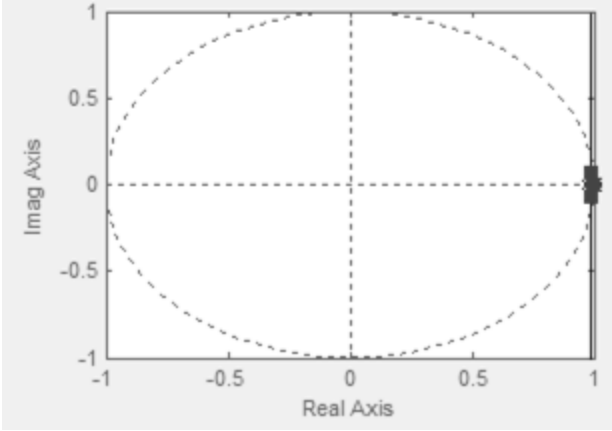


Figure 7.15: DC-link voltage control loop root locus in the z-plain

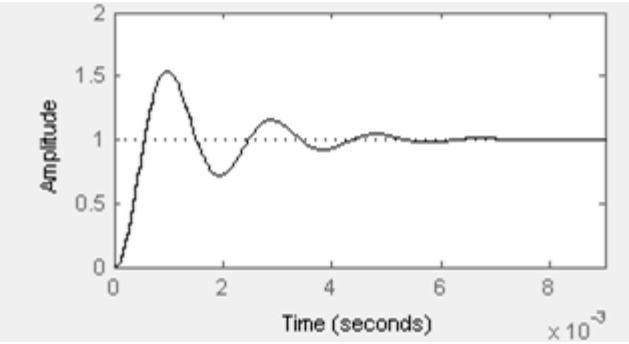


Figure 7.16: Discrete unit step response for the of DC-link voltage control

## 7.2 Final model

The controller parameters obtained from the SISOTOOL were used in the PMSG based WECS model in Simulink. The model is shown in the appendix section 12.1. The wind speed was varied in a step wise fashion: from 8, 10, 12, 10 and 8m/s in 10 seconds intervals. Figure 7.17 shows this input wind speed. The simulation is carried out over 50 seconds.

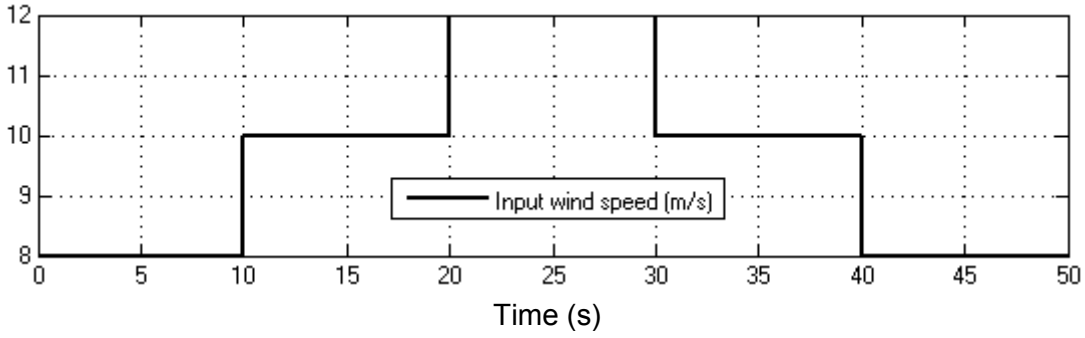


Figure 7.17: Input wind speed

### *7.2.1 Machine side model verification*

The angular speed of the PMSG is shown in Figure 7.18. The purple signal is the angular speed set point while the yellow signal is the output angular speed of the PMSG corresponding to the input wind speed in Figure 7.17. There is a small error between the angular speed set point and the output angular speed. The angular speed set point was determined using a 20 meters radius turbine with an 8.1 nominal tip-speed-ratio.

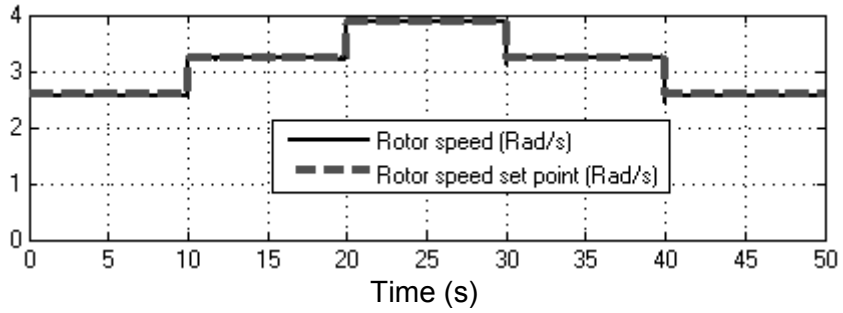


Figure 7.18: PMSG angular speed

The machine side d-axis current (Id) was set to zero to limit the machine side current. Figure 7.19 shows the Id current set point and the corresponding Id output current. The output Id current follows the set point with some transients corresponding to the step changes in input wind speed at the 10 seconds intervals.

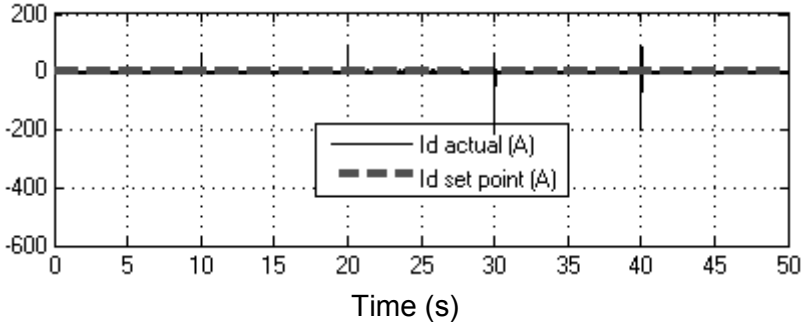


Figure 7.19: The machine side d-axis current

Figure 7.20 shows the machine side output q-axis current. The current increases with increase in input wind speed. It also corresponds with the electrical and mechanical torque. The mechanical and electrical torques are presented in Figure 7.21 and Figure 7.22 respectively.

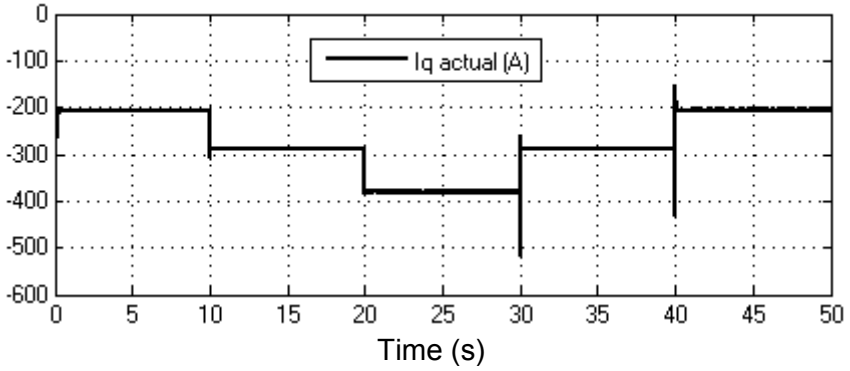


Figure 7.20: The machine side q-axis current

Figure 7.21 shows the input mechanical torque of the turbine corresponding to the step changes in input wind speed. The mechanical toque increases with increase in wind speed. The torque is less than zero so as to operate the PMSG in generator mode of operation.

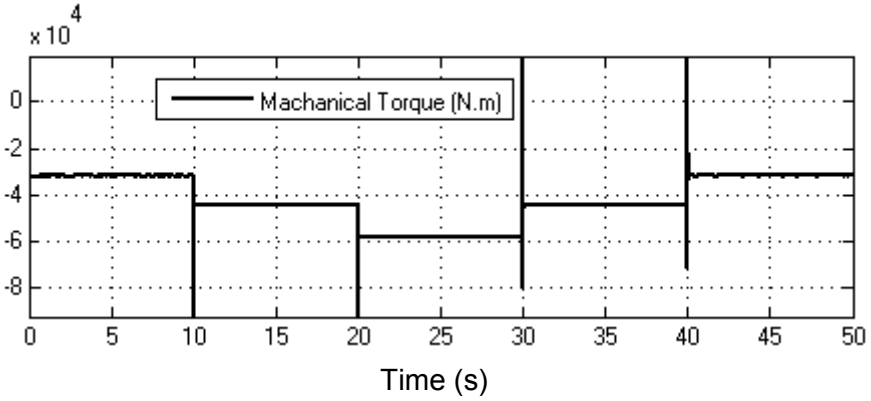


Figure 7.21: The mechanical torque

Figure 7.22 show the electrical torque of the PMSG. The electrical torque equals the mechanical torque so as to maintain a constant angular speed.

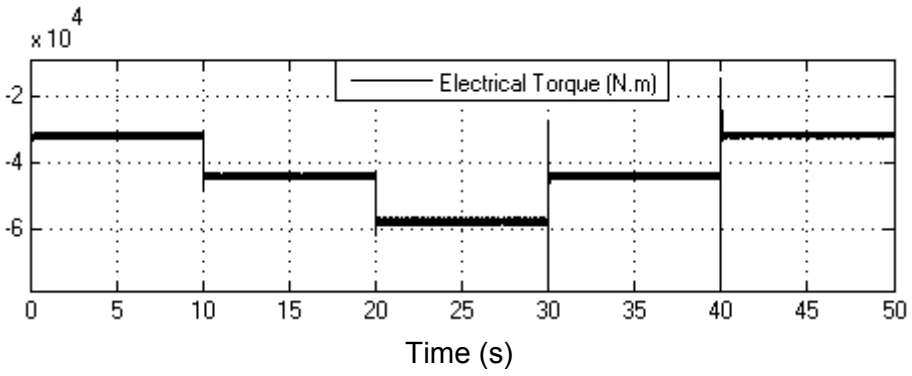


Figure 7.22: PMSG electrical torque

### *7.2.2 Grid side model verification*

The DC-link voltage is shown in Figure 7.3. The DC-link voltage set point is 600V. The DC-link output voltage increases with increase in wind speed and reduces with reduction in wind speed.

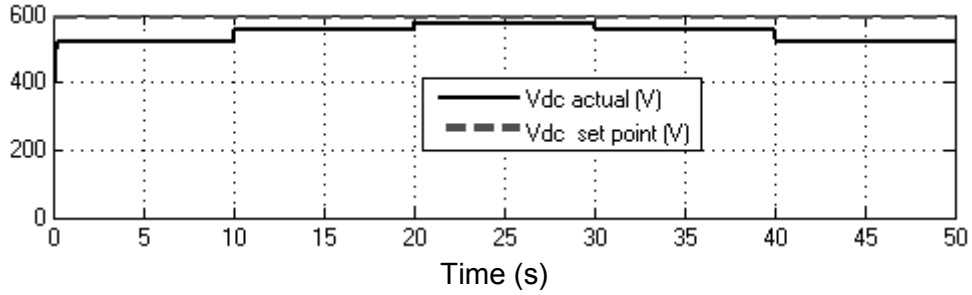


Figure 7.23: DC-link voltage

Figure 7.24 shows the grid side current in response to the wind speed step changes. The Io and $I_q$ currents equal to zero. $I_0$ is zero because of balance three-phase currents. $I_q$ is zero because the reactive power has been set to zero by setting the grid side q-axis current to zero to maintain a unity power factor. The $I_d$ current varies with input wind speed: it increases with increase input wind speed and decrease with decreased wind speed.

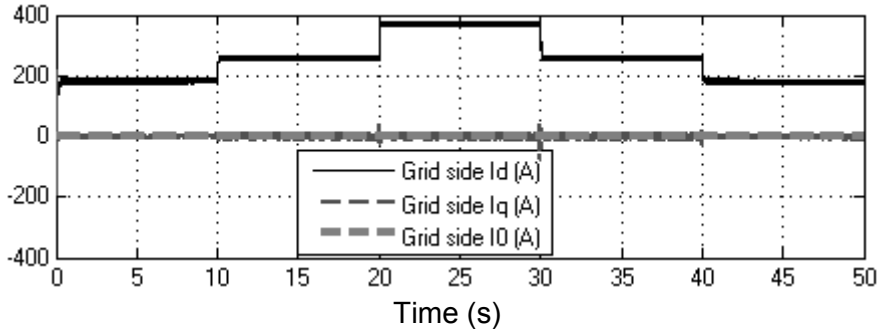


Figure 7.24: Grid side dq0 currents

The grid side voltages are shown in Figure 7.25. The Vo and Vq voltages remain zero. The Vd voltage is fixed at 555V. The Vo is zero because of balanced three-phase grid voltages. The Vq voltage is zero because it was set at zero so as to have independent control of the grid side reactive and active power as well as to have easy power measurements.

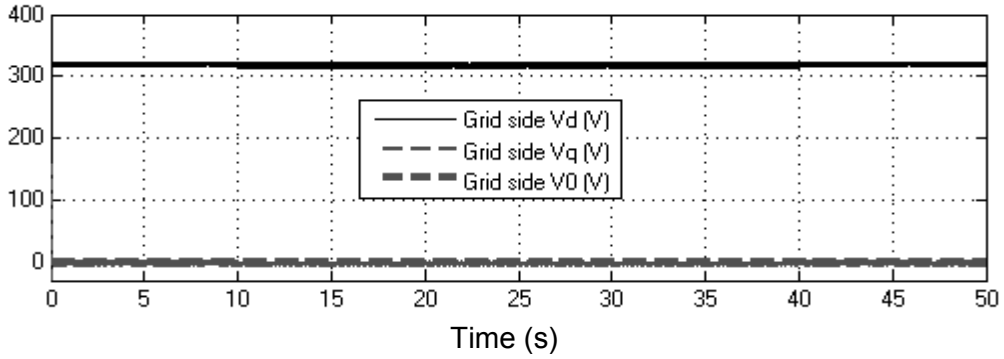


Figure 7.25: Grid side d-q axis voltages

Figure 7.26 shows the active power response of the system. The grid side active power closely matches the machine side active power. The difference between active power of the machine side and the grid side is caused by the losses. The losses increases with increase in current which is increased by increased input wind speed. The source of the losses on the grid side is the filter with a series resistance of one ohm. The losses on the grid side are therefore equal to the square of the current. The losses on the machine side are due to the resistance of the PMSG stator windings.

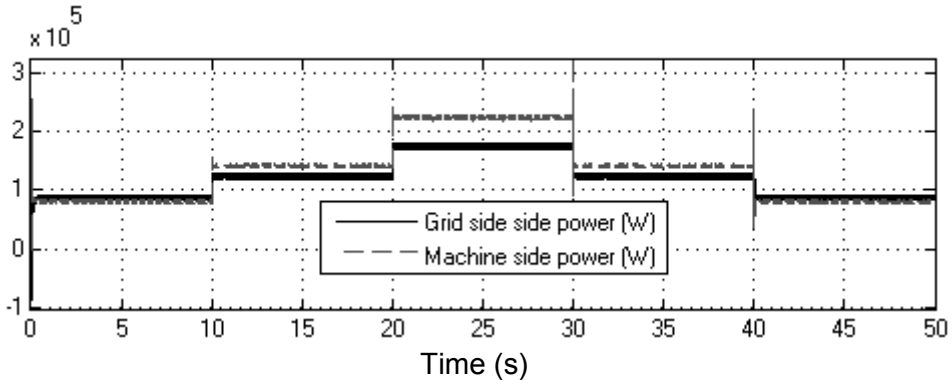


Figure 7.26: PMSG based WECS active power

Figure 7.27 shows the grid side reactive power. The reactive power remains zero and follows the set point. The reactive power was set to zero by setting the grid side q-axis current to zero.

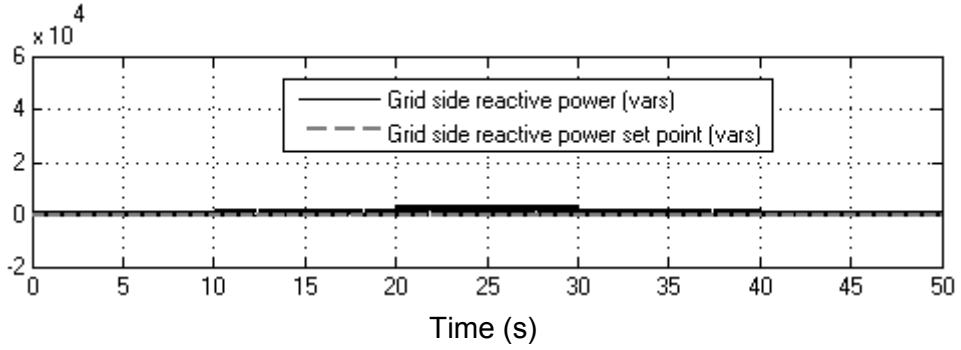


Figure 7.27: Grid side reactive power

# 8 Effect of PMSGs on power quality

This section takes a look at the impact of permanent magnet synchronous generators on power quality of the grid. The major problems looked at are flicker, harmonics and transient stability. A simple network was used in power factory to do the simulations.

## 8.1 System overview

The network used for simulations in power factory is shown in Figure 8.1. This is an eleven bus systems that has been set up to contain the network elements that are relevant to power quality and transient stability studies. The system has 10 sets of 5 PMSG wind turbines with active power ratings of 3 MW. The existing template in power factory was used to model the PMSGs. More details about the template can be found in the appendix. Other major elements in the network are the synchronous machine, the grid and three loads, Ld1 to Ld3. The synchronous machine represents a typical South African coal power station unit. Kusile coal power station generator 2 has an 810MVA apparent power rating. The mean length of the lines interconnecting the PMSGs is 1,36 km with a standard deviation of 0,38 km. The values of the elements used in the network are shown in table 8.1. The power quality indices were monitored at the PCC busbar.

.

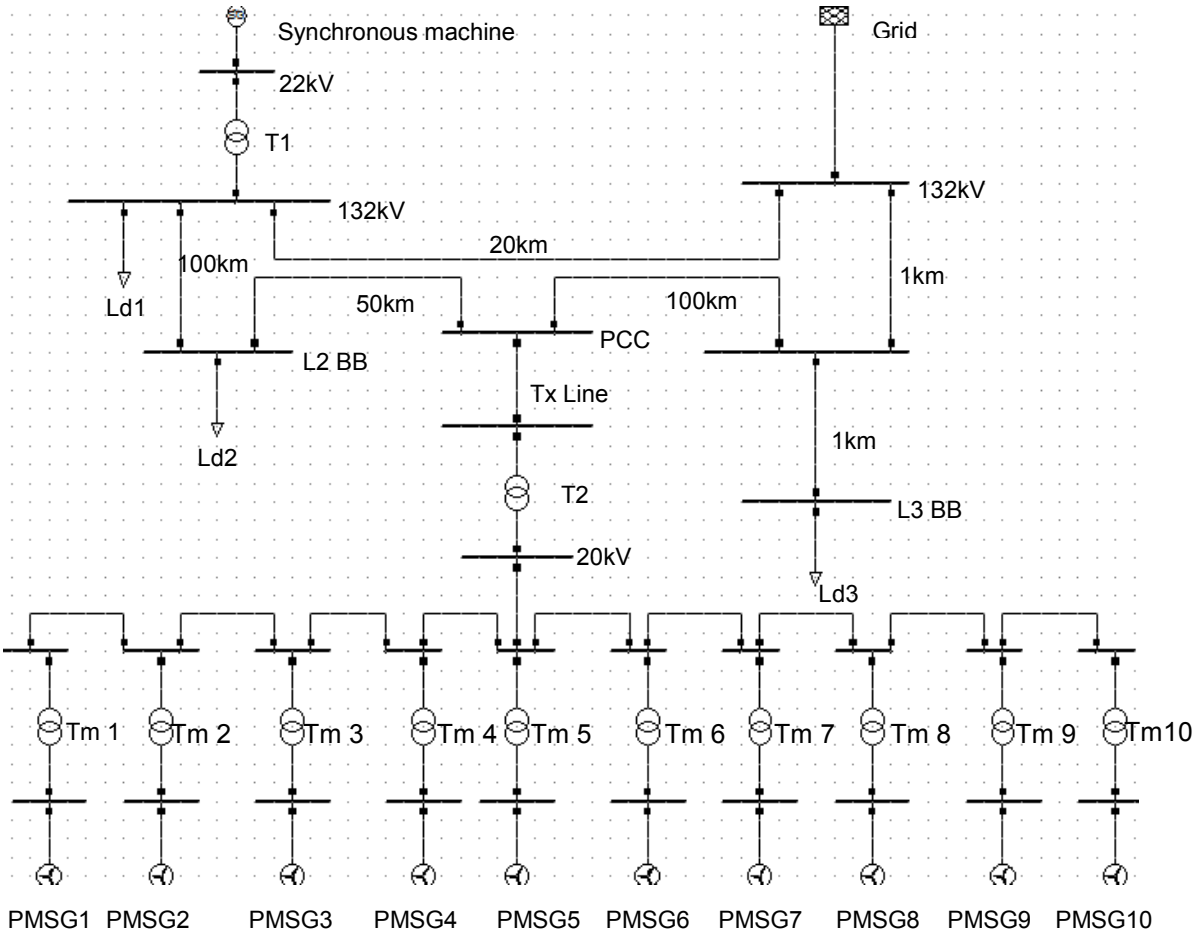


Figure 8.1: System overview

**Table 8.1: System elements and corresponding quantity**

| Element | Quantity |
|---|---|
| Synchronous machine | 810MVA |
| Ld1 | 300MW |
| Ld2 | 100MW |
| Ld3 | 100MW |
| PMSGs | 3MW x 50 units |

A small network was used to study the power quality and transient stability issues associated with WECSs. The outcome of the simulation is expected to be similar to the response of a larger system. The larger part of the system has been modelled by the external grid.

## 8.2 Effect of PMSG based WECS on voltage rise

PMSGs wind turbines cause voltage rise when they increase reactive power of production. To demonstrate this a case study is conducted where the reactive power of the PMSGs is increased in steps of 10MVar from 10MVar to 40MVar and the voltage at the PCC is monitored and plotted as a bar graph. The study is done under different grid strengths, different X/R ratios of the transmission line (Tx line), and different transmission line lengths.

### *8.2.1 Voltage rise and reactive power*

Figure 8.2 shows the voltage at the PCC in response to reactive power changes generated by the PMSG based WECSs. Reactive power generation is increased from 10MVars to 40MVars in steps of 10MVars while the active power is kept at 150MW. The voltage at the PCC increases with increase in reactive power production. This is because the voltage across the transmission line is a function of the active power and reactive power such that when the reactive power production increases, the voltage drop across the line is reduced and the PCC voltage increases. This corresponds to the findings in section 2.1.3. The voltage is below the 145kV voltage regulation upper limit and above the 118.8kV voltage regulation lower limit for a 132kV system [18].

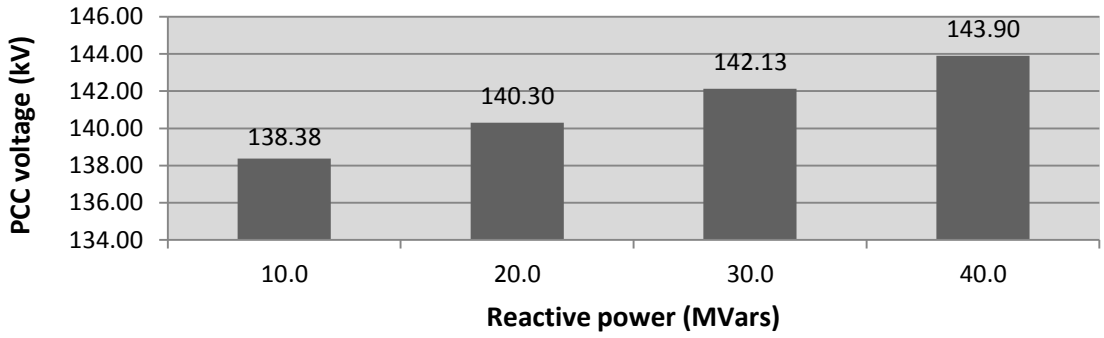


Figure 8.2: Effect of reactive power on voltage rise

### *8.2.2 Voltage rise and transmission line length*

Figure 8.3 shows the voltage at the PCC in response to increased transmission line (Tx line) length from 2km to 8km in 2km steps. The voltage at the PCC reduces with increase in transmission line length. The reason for this is that the voltage drop across the transmission line increases with increase in impedance of the line. The impedance of the line increases with increased line length. The voltage is below the 145kV voltage regulation upper limit and above the 118.8kV voltage regulation lower limit for a 132kV system [18].

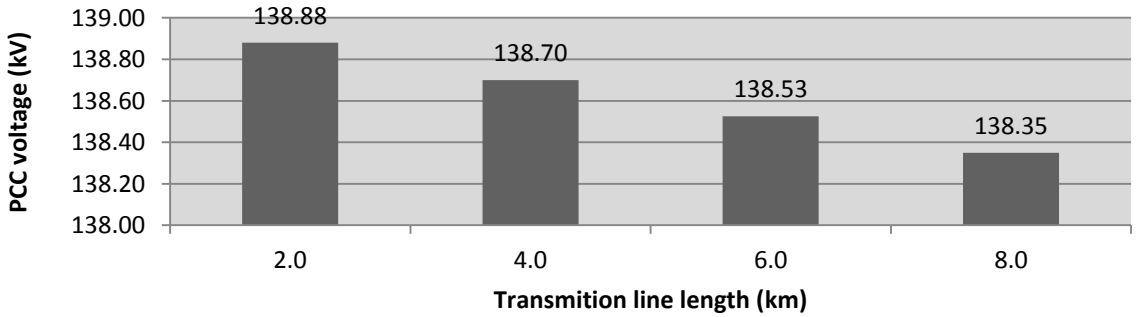


Figure 8.3: Effect of transmission line length on voltage rise

### *8.2.3 Voltage rise and X/R ratio*

Figure 8.4 shows the voltage at the PCC in response to different X/R ratios of the transmission line ( Tx line ). The X/R ratio was increased from 2 to 5 in steps of 1 while keeping the transmission line resistance fixed at 0.188 ohms. As the X/R ratio increases, the voltage at the PCC decreases. This is because the increased X/R ratio implies an increase in the reactance of the line. Increasing the reactance of the line increases reactive power demand of the line which then reduces the reactive power sent to the grid. Moreover, the increased reactance implies increased line impedance therefore increasing the voltage drop across the line. This then reduces the voltage at the PCC. The voltage is below the 145kV voltage regulation upper limit and above the 118.8kV voltage regulation lower limit for a 132kV system [18].

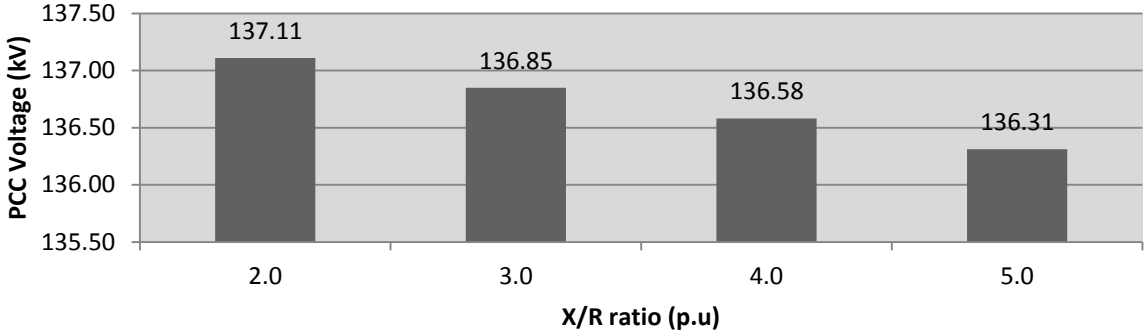


Figure 8.4: Effect of X/R ratio on voltage rise

## 8.3 Effect of PMSG based WECS on Flicker

PMSG based WECSs cause voltage flicker due to the stochastic nature of wind speed, wind shear and tower shadow effect. Varying wind speed causes proportional variation in generated active power which in turn causes PCC voltage fluctuations.

The effect of PMSG based WECSs was investigated using the DIgSILENT simulation language (DSL) focussing only on tower shadow effect as a source of flicker. The DSL code can be found in the appendix section 12.11. It was found in section 4.1 that flicker can be reduced by active power control as well as PCC voltage control methods. A PCC voltage control method is implemented in this section as a means to reduce the effect of flicker at the PCC.

A station controller is placed at the L2 BB busbar in Figure 8.1 to simulate a voltage controller. An input wind speed due to tower shadow effect was converted to corresponding active power shown in Figure 8.5. The active power is set at 150MW with 6.67% power dips every 0.06 seconds.

The short term flicker severity indices at the PCC for the cases with and without the station controller are compared for the same input wind speed.

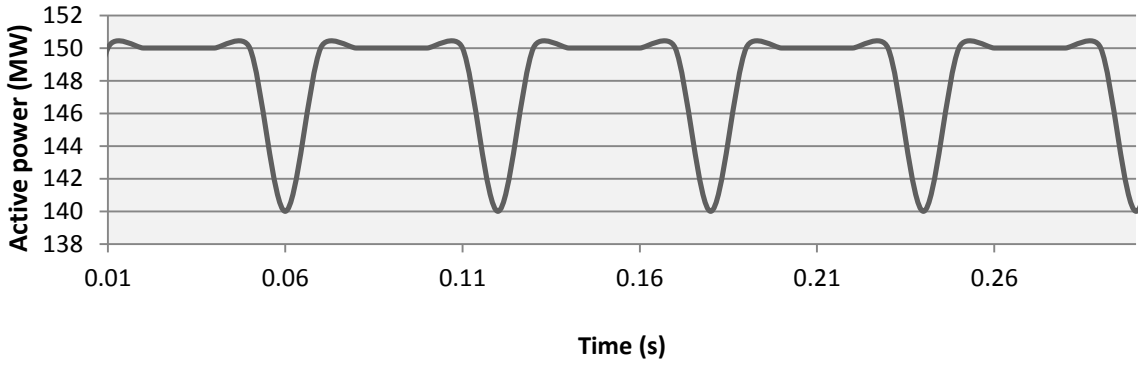


Figure 8.5: Active power due to tower shadow effect

### *8.3.1 Continuous operation flicker*

Figure 8.6 shows the PCC voltage for the case with and without the station controller installed. The PCC voltage has lower voltage dips compared to the case without the station controller. Figure 8.7 shows the short term flicker severity index for the case without the presence of a station controller and Figure 8.8 shows the short term flicker severity index for the case with the station controller installed at L2 BB busbar. The short term flicker severity index for the case without the station controller is 0.1634 while it is 0.1034 for the case with station controller connected. The station controller reduced the short term flicker severity index by 36.7%. The long term flicker severity index is less than 1 and the short term flicker severity index is less than 0.8. Thus the flicker produced does not violate the NRS048-2 flicker limits.

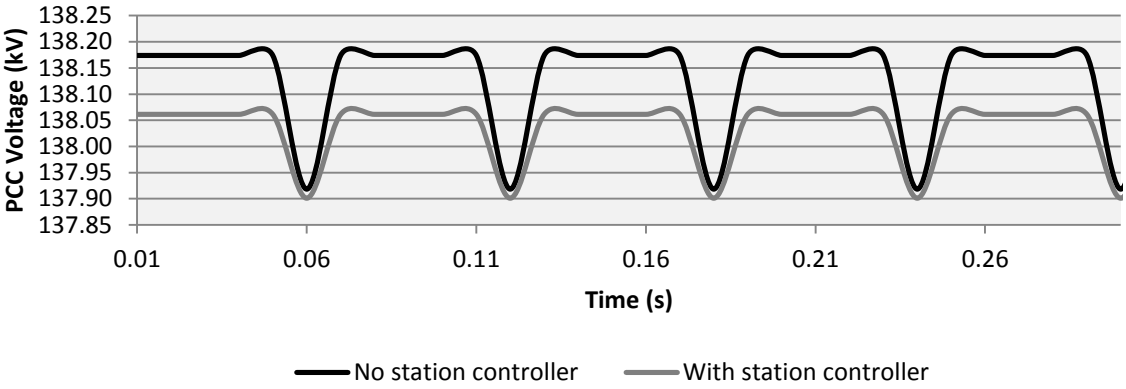


Figure 8.6: PCC voltage for case with and without a station controller

```
--------------------------------------------------------------------------------
|                                                    IEC-61000-4-15 Flickermeter
--------------------------------------------------------------------------------
| Signal:  y1     Time [s]:    [   5,0001 -  605,0000] Pst:     0,1634
|
--------------------------------------------------------------------------------
```

Figure 8.7: Pst value for case without station controller

```
--------------------------------------------------------------------------------
|                                                    IEC-61000-4-15 Flickermeter
--------------------------------------------------------------------------------
| Signal:  y1     Time [s]:    [   5,0001 -  605,0000] Pst:     0,1034
|
--------------------------------------------------------------------------------
```

Figure 8.8: Pst value for case with station controller

### *8.3.2 Switching operations and flicker*

The switching operations of PMSG wind turbines causes flicker at the PCC. The flicker short term and long term severity indices depends on the number of switching operations, grid strength as well as the step factor of the PMSG based WECSs. Both the step factor and the grid strength depend on the penetration level of the PMSG wind farm.

#### *i. Switching operations and grid strength*

Figure 8.9 shows the short and long term flicker severity indices at the PCC in response to different grid strengths. As the grid strength increases the flicker severity indices decrease. Increasing the grid strength implies an increase in fault level contribution from the grid as well as the synchronous machine. Thus the wind farm contribution to the fault level at the PCC is reduced which then reduces the flicker severity indices. The long term flicker severity

index is less than 1 and the short term flicker severity index is less than 0.8. Thus the flicker produced does not violate the NRS048-2 flicker limits.

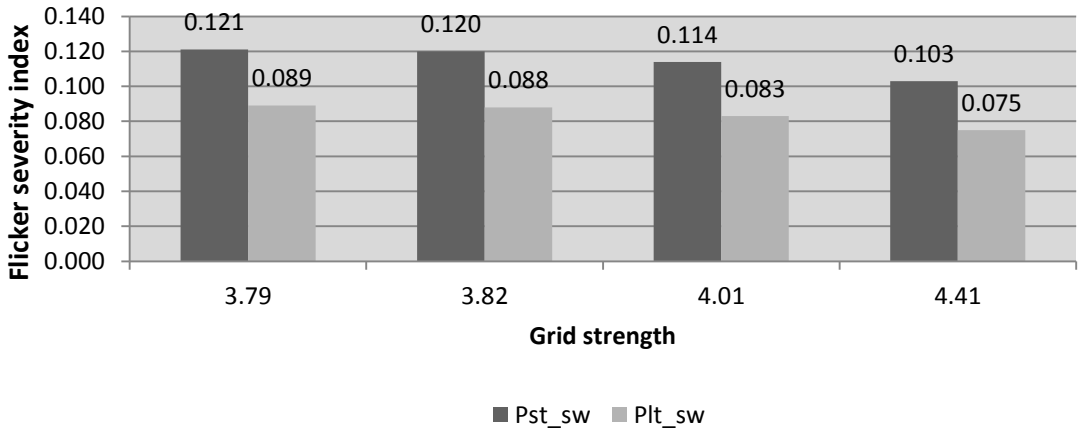


Figure 8.9: PCC flicker vs grid strength

### *ii. Effect of PMSG switching operations*

Figure 8.10 shows the flicker severity indices in response to different PMSGS turbine switching operations in the ten minutes (N10). N10 was increased from 1 to 4 in steps of 1. The short term flicker severity index increases with increased number of switching operations. The short term flicker severity index is less than 0.8. Thus the flicker produced does not violate the NRS048-2 flicker limits.

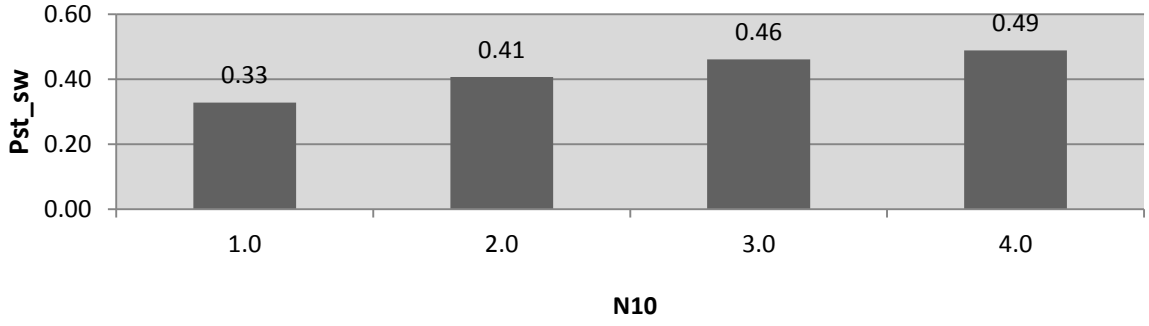


Figure 8.10: PCC flicker vs N10

Figure 8.11 shows the flicker severity indices in response to different PMSG turbine number of switching operation in 120 minutes (N120). N120 was increased from 4 to 10 in steps of 2. The long term flicker severity index increases with increase in the number of switching operations in an hour. The long term flicker severity index is less than 1. Thus the flicker produced does not violate the NRS048-2 flicker limits.

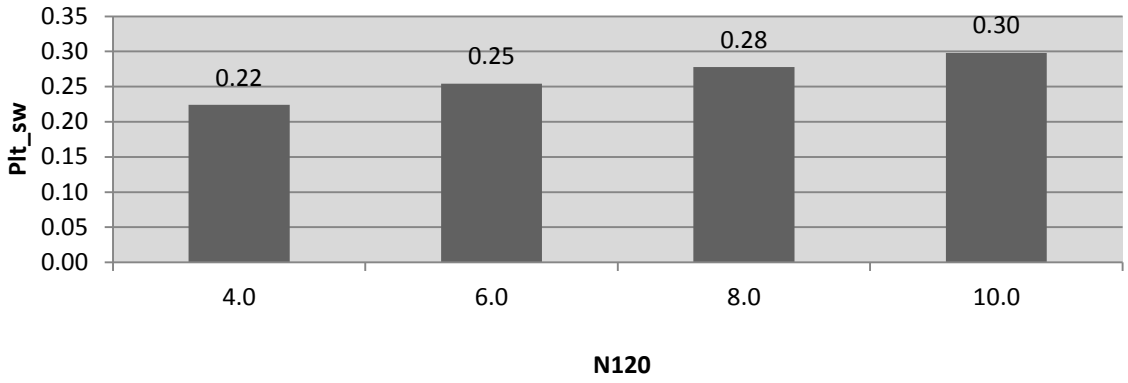


Figure 8.11: PCC flicker vs N120

### *iii. Flicker and step factor*

Figure 8.12 shows the PCC flicker severity indices in response to different PMSG turbine step factors. As the step factor increases the flicker severity indices increase. This is because increasing the step factor increases the contribution of the turbines to the fault level at the PCC. The long term flicker severity index is less than 1 and the short term flicker severity index is less than 0.8. Thus the flicker produced does not violate the NRS048-2 flicker limits.

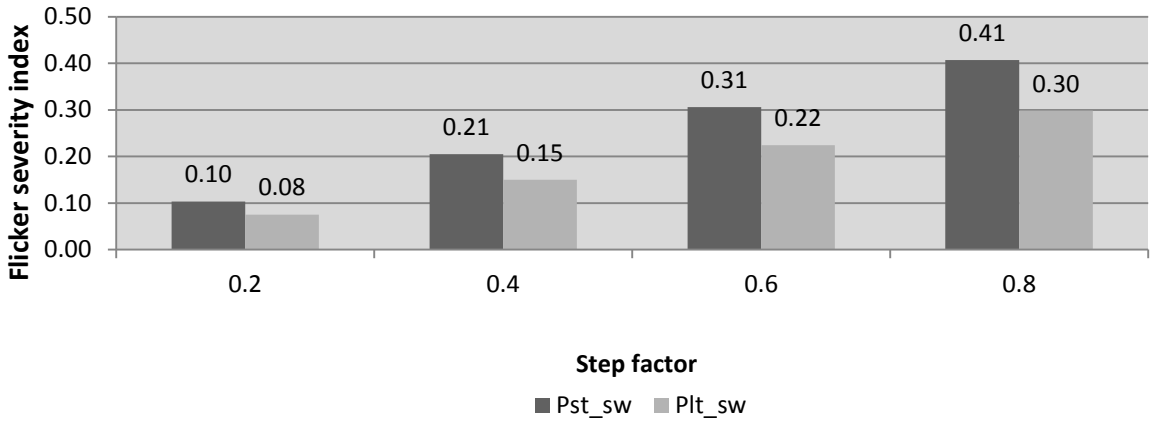


Figure 8.12: PCC flicker vs step factor

## 8.4 Effect of PMSG on harmonics

The harmonic model used to model the harmonics generated by the PMSG is shown in table 8.2. The model is based on the NRS 048:4 harmonic limits where a $5^{th}$ of each harmonic limit was taken to arrive at the model. The penetration level of the PMSGs was increased from 33% to 100% and the THD at the PCC was monitored.

**Table 8.2: THD model based on NRS 048:4 harmonic limits**

| h = 5 | h = 7 | h=11 | h= 13 | h = 17 | h = 19 | h = 23 | h = 25 | h = 29 | h = 31 | h = 35 |
|---|---|---|---|---|---|---|---|---|---|---|
| 1% | 0.8% | 0.6% | 0.5% | 0.32% | 0.32% | 0.32% | 0.32% | 0.092% | 0.088% | 0.83% |

### *8.4.1 THD and Penetration*

Figure 8.13 shows the PCC total harmonic distortion in response to different active power penetration of the PMSG based WECSs. As can be seen in the figure the THD increases with increase in active power penetration. This is because the amplitude of the harmonic content increases with increase in penetration. These findings differ from what was found in section 4.1 where the THD was observed to decrease with increase in penetration of the PMSG based WECSs. The apparent power rating of the PMSG based WECS based wind farm is 150MW. The penetration in Figure 8.13 has been expressed as the percentage of the apparent power rating of the wind farm. This is because the PMSG based WECS considered had a filter. Thus the increased penetration increased the fundamental with great margin compared to the harmonics as they were filtered out. In this case there is no applied filter to the model and hence the THD increases with increase in penetration. The THD is less than the 8% THD limit as set out in the NRS048-2 specification.

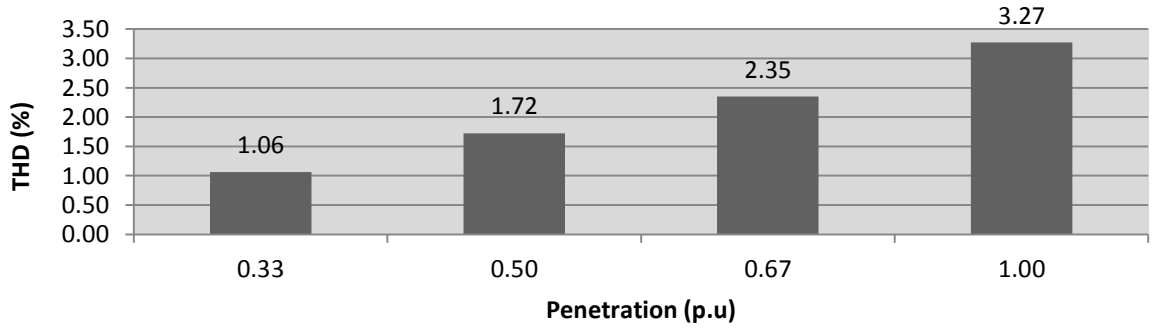


Figure 8.13: THD and penetration

## 8.5 Voltage sag and PMSG LVRT

The grid code requires wind turbines to remain connected to the grid even under low voltage conditions. WECS should produce reactive power to improve the low voltage condition in the network. Disconnecting wind turbines during low voltage is a treat to transient stability and has a potential to cause a blackout for the case of high penetration. This problem is demonstrated in this section. A three-phase to ground fault is applied to the L3 BB busbar in the network in Figure 8.1 and cleared after 100ms. This simulates a condition where the

protection at the busbar fails and the fault is cleared by back up protection schemes. This forms a point which lies in the area B South African grid code LVRT curve in Figure 3.6 in section 3.4.2. In this case the wind turbines are not expected to be disconnected.
The fault causes a low voltage condition at the PCC. A case where the PMSG based wind farm is disconnected (No LVRT) from the PCC is compared to the case where the farm remains connected (Yes LVRT). In both cases, the voltage at the PCC and the rotor angle of the synchronous machine are monitored.

### *8.5.1 LVRT of PMSG based WECS*

Figure 8.14 shows the PCC voltage for the case where the turbines remain connected (Yes LVRT) at the PCC and the case where the turbines are disconnected from the PCC (No LVRT) in response to a three-phase fault at the L3 BB busbar. The case where the turbines remain connected to the PCC has a better voltage response as the turbines produce reactive power to improve the low voltage condition. In both cases the voltage is below the 145kV voltage regulation upper limit and above the 118.8kV voltage regulation lower limit for a 132kV system [18].

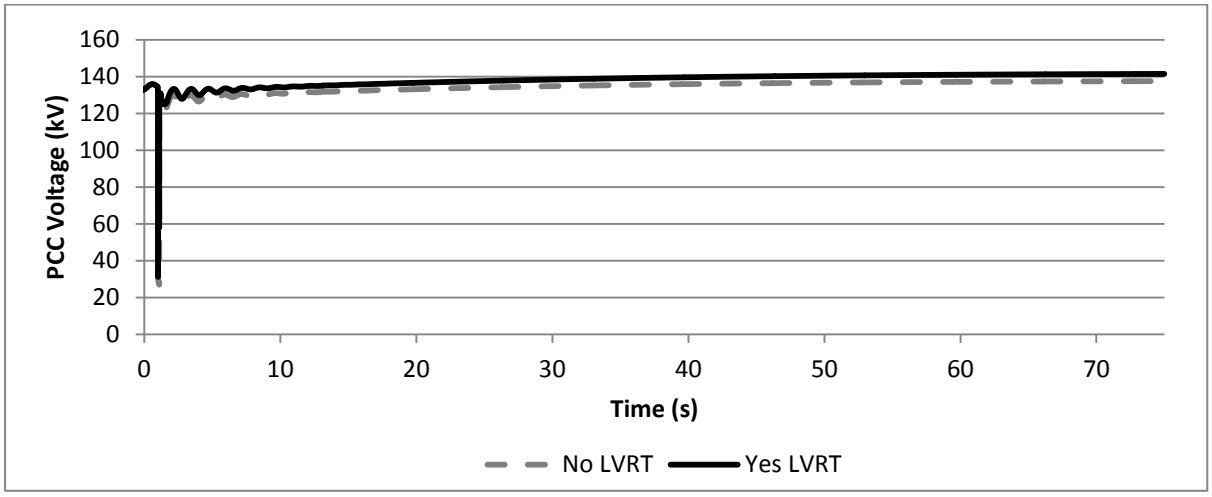


Figure 8.14: PCC voltage

Figure 8.15 shows the rotor angle of the synchronous machine for the Yes LVRT case and the No LVRT case. The system is transient stable in both cases. The rotor angle is more damped and has a short settling point in the Yes LVRT case than the No LVRT case. This is because the PMSG wind farm supplies some of the fault current required to supply the fault. This reduces the active power required from the synchronous generator to supply the fault and in turn reduces the rotor angle oscillations. Thus the LVRT capability of the turbine improves the transient stability of the grid.

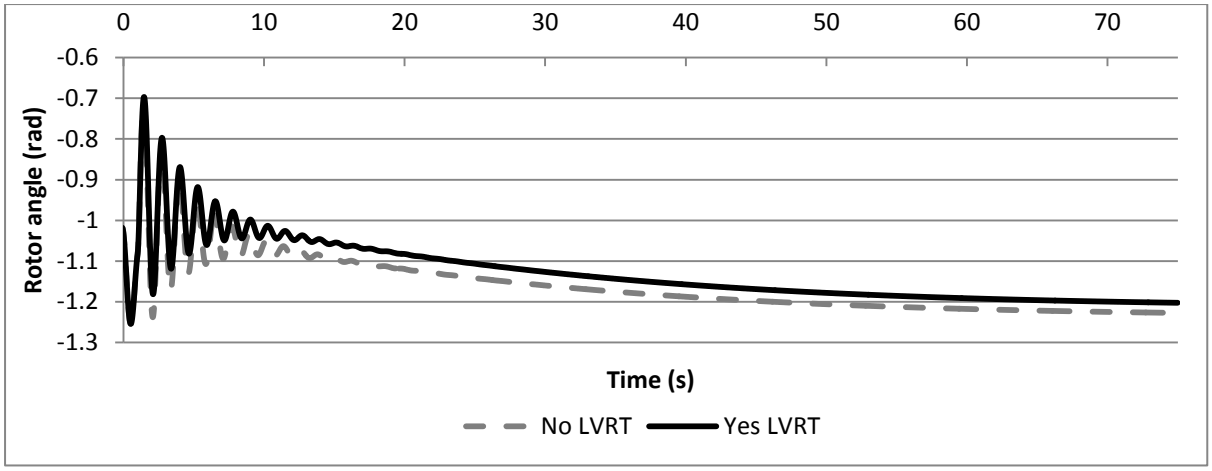


Figure 8.15: Synchronous machine rotor angle

# 9 Conclusions

## 9.1 Impact of WECS on power quality

In all the power quality studies conducted, the power quality indices were within limits. However, the power quality indices such as THD and flicker increases with increased penetration. Thus, as the wind power increases in the energy mix, the grid code has to be revised and new limits have to be set to meet the new generation.

The low voltage ride through permission curve for wind system will have to be revised to force wind system to remain connected to the grid as wind power increases in the energy mix. The system shown here was stable because the wind farm capacity was a small fraction of the synchronous machine. With increased wind power penetration, future wind farms might not be allowed to suddenly disconnect from the grid.

## 9.2 PMSG based WECS control

The electrical control of PMSG based WECSs is simplified by the use of the Park and Clarke transforms. The Park and Clarke transform make it possible to use simple control algorithms like the PI controllers.

## 9.3 The effect of PMSG turbine location

The voltage rise at the PCC is affected by the transmission line. The voltage at the PCC increases with decrease in transmission line length and X/R ratio.

## 9.4 Voltage improvement

PMSG based WECSs assist in voltage regulation by injecting reactive power when the PCC voltage is low and absorbing reactive power when the voltage is high so as to keep the voltage within grid code limits. There are three reactive power control methods that are commonly used to achieve this objective and these are constant reactive power, constant voltage and power factor control.

## 9.5 PMSG based WECSs improve transient stability

PMSG based WECSs improve the transient stability of the network by increasing or decreasing active power production during transient events. In the event where the active power is suddenly decreased, the PMSG based WECSs increases active power generation to meet the demand and thus the active power disturbance in the synchronous machines is reduced. This in turn improves transient stability.

## 9.6 Source of flicker

PMSG based WECSs produce flicker at the PCC due to varying wind speed which in turn varies the PCC voltage. Other sources of flicker are the tower shadow effect and wind shear effect as well as switching operations of wind turbines. The flicker severity indices at the PCC are proportional to the active power production. The degree of flicker is proportional to the grid strength because increased active power penetration of PMSG based WECS increases the fault level contribution at the PCC.

## 9.7 Source of harmonics

PMSG based WECSs achieve maximum power tracking under varying wind speed conditions by using power electronics devices. These devices produce harmonics. The THD decreases with increase in penetration in the presence of filter. However, if the filter is not used, the THD increases with increase in penetration. The THD at the PCC can be reduced through the use of multi-level converters as well as filtering.

## 9.8 Switching operations

The impact of switching operations can be reduced by reducing the step factor. This can be done by connecting the network in strong parts. Strong parts of the grid are parts where the fault levels are high relative to the fault level of the WECS.

# 10 Recommendations

## 10.1 Location of PMSG based WECSs

PMSG based WECSs should be installed closer (if possible) to the PCC so as to reduce the transmission line length. This reduces the power quality indices at the PCC. It is also advisable that the PCC chosen must have a high fault level so as to ensure high grid strengths and minimise the impact of the PMSGs impact on flicker severity indices.

## 10.2 LVRT of PMSG based WECSs

PMSG based WECSs must remain connected to the network even under low voltage conditions. This must be done so as to improve the voltage at the PCC. The PMSG based WECSs improves the transient stability of the grid if they remain connected to the PCC after a low voltage event.

## 10.3 Flicker reduction

The active power control methods should be used for decreasing the flicker severity indices at the PCC than the voltage control methods achieved by installing a voltage regulating device in the vicinity of the PCC. An additional device implies an additional cost of the PMSG based WECS which are higher than the cost of installing an active power controller.

## 10.4 PMSG based WECSs harmonics

Multi-level converter should be used instead of two-level converters. Multi-level converters reduce the THD at the PCC. A non-resistive filter should instead of a resistive one. The resistive element causes power losses and thus reduces the efficiency of the PMSG based WECS.

# 11 List of References


[1] “Department of Energy,” DoE, 1 June 2015. [Online]. Available: www.energy.gov.za/files/coal_frame.html. [Accessed 1 January 2016].

[2] A. Eberhard, J. Kolker and J. Leigland, “South Africa's Renewable Energy IPP Procurment Program: Success Factors and lessons,” 2014 Public-Private Infrastructure Advisory Facility, Washington, DC, 2014.

[3] L. McDaid, “Renewable Energy Independent Power Producer Procurement Programme Review 2014,” *Electricity Governance Initiative South Africa*, supported by World Resources Institute, 2014.

[4] J. G. Wright, T. Bischof-Niemz, J. Calitz, C. Mushwana, R. van Heerden and M. Senatla, “Formal comments on the Integrated Resource Plan (IRP) Update Assumptions, Base Case and Observations 2016,” *Council of Scientific and Industrial Research*, Pretoria, 2017.

[5] A. Betz, Introduction to the Theory of Flow Machines, Oxford: Pergamon Press, 1966.

[6] K. Han and Gz. Chen, “A Novel Control Strategy of Wind Turbine MPPT Implementation for Direct-drive PMSG Wind Generation Imitation Platform,” *Institute of Electrical and Electronics Engineers,* pp. 2255-2259, 2009.

[7] M. Yin, G. Li, M. Zhou and C. Zhao, “Modeling of the Wind Turbine with a Permanent Magnet Synchronous Generator for Integration,” *Institute of Electrical and Electronics Engineers,* vol. 6, no. 7, p. 2, 2007.

[8] T. Senjyu, R. Sakamoto, T. Kinjo, N. Urasaki, T. Funabashi, H. Fujita and H. Sekine, “Output Power Leveling of Wind Turbine Generator for All Operating Regions by Pitch Angle Control,” *Institute of Electrical and Electronics Engineers,* vol. 21, no. 2, p. 469, 2006.

[9] M. Sato, Y. Shima, H. Tkahashi and Y. Sanpei, “Inrush currents of induction generators due to abrupt connection to utility power networks,” *Electrical Engineering in Japan,* vol. 5, pp. 71-82, 1993.

[10] F. Gharedaghi, M. Deysi, H. Jamali and A. khalili, “Soft Starter Investigation on Grid Connection of Wind Turbines,” *Australian Journal of Basic and Applied Sciences,* vol. 5, no. 10, pp. 1146-1153, 2011.

[11] T. Petru, “Modeling of Wind Turbines for Power System Studies,” Chalmers University of Technology, Gothenburg, Sweden, 2003.

[12] M. Bello, “Network & Grid Planning Standard for Generation Grid Connection – Generators Technology Overview and Effects on Networks,” Eskom, Johannesburg, 2014.

[13]L. Xu and Y. Wang, “Dynamic Modeling and Control of DFIG-Based Wind Turbines Under Unbalanced Network Conditions,” *Institute of Electrical and Electronics Engineers,* vol. 22, no. 1, pp. 314-323, 2007.

[14] N. Mohan, T. M. Undeland and W. Robbins, Power Electronics Converters, Applications, and Design, Hoboken: Jolm Wiley & Sons, Inc, 2003.

[15] K.V. Kumar, P.A. Michael, J.P. John and S.S. Kumar, “Simulation and Comparison of SPWM And SVPWM Control for Three Phase Inverter,” *ARPN Journal of Engineering and Applied Sciences,* vol. 5, no. 7, pp. 61-74, 2010.

[16] A. Larsson, “The Power Quality of Wind Turbines,” Chalmers University of Technology, Göteborg, Sweden, 2000.

[17] T. Ise, Y. Hayashi and K. Tsuji, “Definitions of Power Quality Levels and the Simplest Approach for Unbundled Power Quality Services,” *Institute of Electrical and Electronics Engineers,* pp. 385 - 390, 2000.

[18] “Grid Connection Code for Renewable Power Plants (RPPs) Connected to the Electricity Transmission System (TS) or the Distribution System (DS) in South Africa,” *South African Bureau of Standards*, Pretoria, 2014.

[19] J.J. Gutierrez and J. Ruiz, A. Lazkano and L.A. Leturiondo, “Measurement of Voltage Flicker: Application to Grid-connected Wind Turbines,” in *Advances in Measurement Systems*, Shanghai, China, InTech, 2010, pp. 366 - 389.

[20] L.O. Tande, “Applying Power Quality Characteristics of Wind Turbines,” *Wind Energy*, Vol 5, no 1, pp 37-52, 2002.

[21] X. Hui, “Comparison of Two Calculation Methods of Flicker Caused by Wind Power,” *Institute of Electrical and Electronics Engineers,* pp. 1-4, 2011.

[22] H. Emanuel and M. Schellschmidt, “Power Quality Measurements of Wind Energy Converters with Full-Scale Converter according to IEC 61400-21,” *Institute of Electrical and Electronics Engineers,* pp. 1-7, 2009.

[23] G. Moschopoulos, R. Fadaeinedjad and M. Moallem, “Voltage sag impact on wind turbine tower vibration,” *Institute of Electrical and Electronics Engineers,* pp. 1-8, 2007.

[24] S. W. Mohod and M. V. Aware, “Power Quality and Grid Code Issues in Wind Energy Conversion System,” Intech, Rejika, 2013.

[25] RG. Coney, A. Booyzen, HO. Boshoff, RW. Curtis, AJ. Dold, W. Glynn, PA. Johnson, R. Koch, GR. Marloth, TO. Mould, M. Outram, AT. Smit, JS. van Heerden, D. Very, M. Wilson, “Electricity Supply — Quality Of Supply Part 4: Application guidelines for Utilities,” *South African Bureau of Standards*, Pretoria, South Africa, 1999.

[26] M. Bollen, “Definitions of Voltage Unbalance,” *Institute of Electrical and Electronics Engineers,* pp. 49-50, 2002.

[27] M. Manyage and P. Pillay, “Definitions of Voltage Unbalance,” *Institute of Electrical and Electronics Engineers,* pp. 50-51, 2001.

[28] J. Tan, W. Hu, X. Wang, Z. Chen, “Effect of Tower Shadow and Wind Shear in a Wind Farm on AC Tie-Line Power Oscillations of Interconnected Power Systems,” *energies,* pp. 6352-6372, 4 December 2013.

[29] W. Hu, C. Su and Z. Chen, “Impact of Wind Shear and Tower Shadow Effects on Power System with Large Scale Wind Power Penetration,” *Institute of Electrical and Electronics Engineers,* pp. 878-883, 2011.

[30] W. Hu, Z. Chen and Y. Wang, “Flicker Mitigation by Active Power Control of Variable-Speed Wind Turbines With Full-Scale Back-to-Back Power Converters,” *Institute of Electrical and Electronics Engineers,* vol. 24, no. 3, pp. 640 - 649, 2009.

[31] M. Seixas, R. Melício and V. Mendes, “Energy Conversion and Management,” *Elsevier,* p. 721–730, 2014.

[32] J. Conroy and R. Watson, “Low-voltage ride-through of a full converter wind turbine with permanent magnet generator,” *Institution of Engineering and Technology,* vol. 1, no. 3, pp. 182 - 189, 2007.

[33] X.P. Yang, X.F Duan and F. Feng, “Low Voltage Ride-through of Directly Driven Wind Turbine with Permanent Magnet Synchronous Generator,” *Institute of Electrical and Electronics Engineers,* pp. 1-5, 2009.

[34] D. Mehrzad, J. Luque and M. C. Cuenca, “Vector Control of Pmsg for Wind Turbine Applications,” The Institute of Energy Technology in Aalborg University, Aalborg, 2008.

[35] S. Samanvorakij and P. Kumkratug, “Modeling and Simulation PMSG based on Wind Energy Conversion System in MATLAB/SIMULINK,” *for an Energy Efficient Economy,* pp. 37 - 41, 2013.

[36] D. Sasi and J. Kuruvilla P, “Modelling and Simulation of SVPWM Inverter Fed Permanent Magnet Brushless DC Motor Drive,” *International Journal of Advanced Research in Electrical, Electronics and Instrumentation Engineering*, vol. 2, no. 5, pp. 1947 - 1955, 2013.

[37] N. Huang, “Simulation of Power Control of a Wind Turbine Permanent Magnet Synchronous Generator System,” Marquette University, Milwaukee, 2009.

[38] R. Park, “Two-reaction theory of synchronous machines, pt. I: Generalized method of analysis,” *American Institute of Electrical Engineers*, vol. 48, pp. 716 - 730, 1929.

[39] T.A. Haskew, S. Li, R.P. Swatloski and W. Gathings , “Optimal and Direct-Current Vector Control of Direct-Driven PMSG Wind Turbines,” Institute of Electrical and Electronics Engineers, vol. 27, no. 5, pp. 2326 - 2329, 2012.

[40] S. Sayeef, N. Mendis and K. Muttaqi, “Enhanced Reactive Power Support of a PMSG based Wind Turbine for a Remote Area Power System,” Research online, p. 3, 2010.

[41] A. Cimpoeru, “Encoderless Vector Control of PMSG for Wind Turbine Applications,” *Aalborg University*, Aalborg, 2010.

[42] A.H.K. Alaboudy, A.A. Daoud, S.S. Desouky and A.A. Salem, “Converter controls and flicker study of PMSG-based grid connected wind turbines,” *Ain Shams Engineering Journal,*vol. 4, no. 1, pp. 75-91, 2013.

[43] J. Glover, M.S. Sarma and T.J. Overbye, “Power System Analysis and Design”, *Stamford: Cengage Learning*, 2012.

[44] R.K. Soni, K. Aveent , R. Kumar and S.K. Singh, "Comparative Study on SVM and Hysteresis Control Strategies for Grid Side Converter of PMSG," Institute of Electrical and Electronics Engineers, 2014.

# 12 Appendices

## 12.1 PMSG control system in MATLAB Simulink

The control system is divided into machine side control and grid side control. Both Simulink block diagrams for machine and grid side are presented in this section. The PI controller parameters for the machine and grid side are listed in Figure 12.1.

**Table 12.1: The PI controller parameters**

| Description | P | I |
|---|---|---|
| **Machine side controllers** | | |
| Angular speed inner loop controller | 0.091 | 1 |
| Angular speed outer loop controller | 1 | 1 |
| Machine side d-axis current controller | 0.091 | 1 |
| **Grid side controllers** | | |
| Reactive power controller | 0.0052 | 1 |
| DC-link voltage inner loop controller | 0.0052 | 1 |
| DC-link voltage outer loop controller | 0.1 | 1 |

### *12.1.1 Machine side block*

The machine side model in MATLAB Simulink is shown in Figure 12.1. The model consists of a wind turbine, permanent magnet synchronous generator and the back-to-back converter. The back-to-back converter uses insulated gate bipolar transistor (IGBT) devices. The rest of the components are the measurement devices and conversion devices.

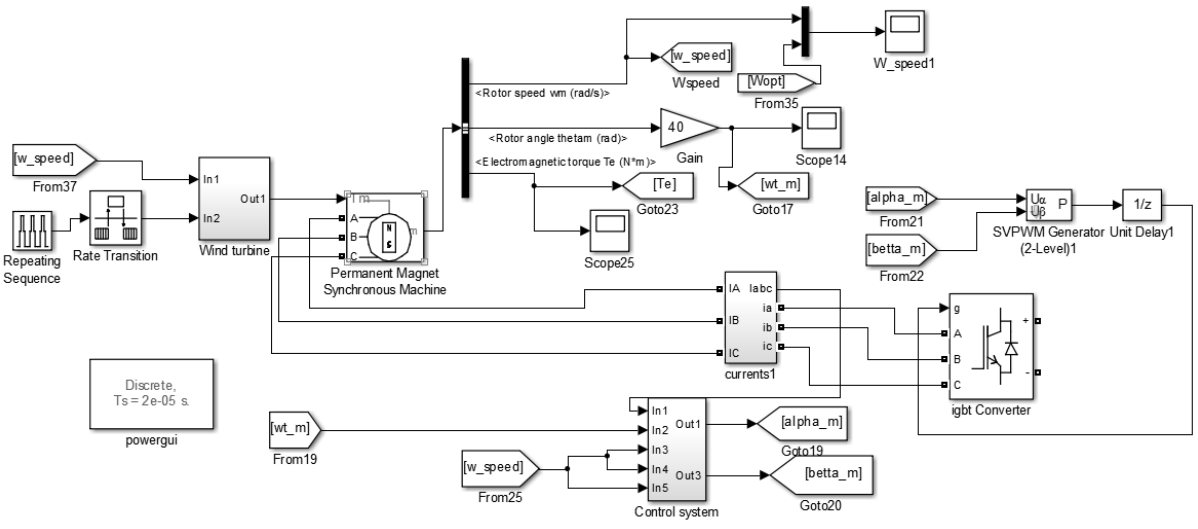


Figure 12.1: The machine side model in MATAB Simulink

### *i. Wind turbine*

The wind turbine model is shown in Figure 12.2. The input (in1) is the rotor angular speed of the PMSG. The pitch angle is set to zero so as to achieve maximum power. The turbine is operated in the maximum power point tracking region and the pitch controller is not included in the model. Input 2 (In2) is the wind speed in m/s. With these inputs, the turbine outputs a torque in p.u which is then scaled by the base torque and fed to the PMSG. Table 12.2 shows the turbine parameters.

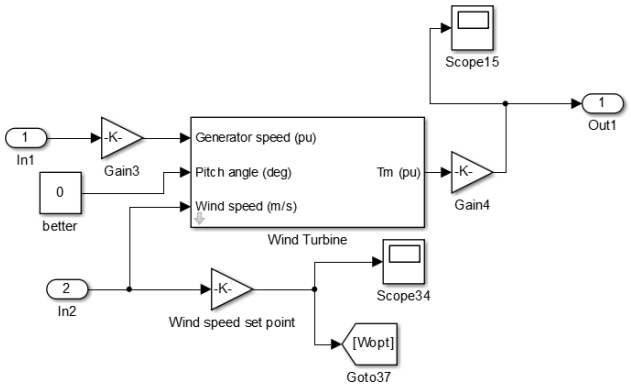


Figure 12.2: Wind turbine model

**Table 12.2: Wind turbine parameters**

| Turbine parameter | Value |
|---|---|
| C1 | 0.5176 |
| C2 | 116 |
| C3 | 0.4 |
| C4 | 5 |
| C5 | 21 |
| C6 | 0.006795 |
| Blade Diameter | 40m |
| Optimal tip-speed-ratio | 8.1 |

### *ii. Permanent magnet synchronous generator*

The permanent magnet synchronous generator used is surface mount PMSG to simplify the control system of the wind energy conversion system. The parameters for the permanent magnet synchronous generator used are given in table 12.3.

**Table 12.3: PMSG parameters**

| PMSG parameter | Value |
|---|---|
| R | 0.18 ohms |
| Lq | 0.0085 H |
| Ld | 0.0085 H |
| Flux | 4.5 Wb |
| Moment of inertia | 500 kg.m^2 |
| Rated power | 0.18 MW |

### *iii. Back-to-back converter*

The back-to-back converter used is based on IGBT devices. It is made up of 6 IGBTs that are each in parallel with a diode. The parameters of the IGBT based converters are listed in table 12.4.

**Table 12.4: IGBT converter parameters**

| IGBT parameter | Value |
|---|---|
| Snubber resistance | 100 000 ohms |
| Snubber capacitance | infinite |
| Forward voltages | 0V |

### *iv. Machine side Control system*

The machine side control system is shown in Figure 12.3. The control system consists of the speed and d-axis current control loops. The phase-locked loop (PLL) block measures the frequency and the angular position which are required for the Clarke and Park transforms.

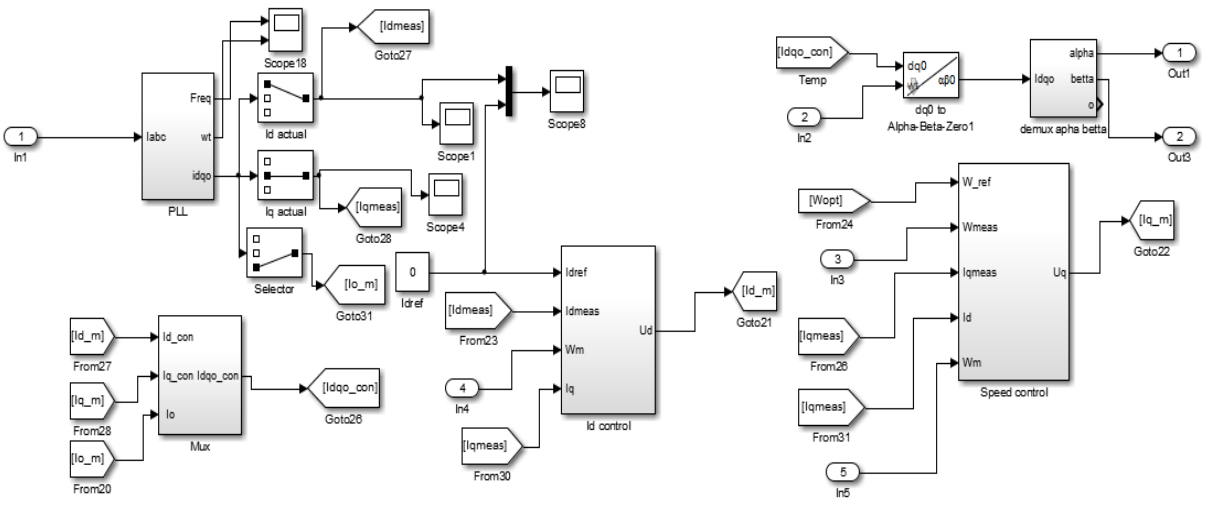


Figure 12.3: Simulink machine side control system

## 12.2 Phase-locked loop

The PLL block measures the phase and angular information required for Clarke and Park transform. The PLL block controller is shown in Figure 12.4. MATLAB Simulink has default settings for the PLL block. These settings are shown in table 12.5. The PLL block takes three-phase input currents or voltages and outputs phase angle and frequency. The block also has a Park transform block (the abc to dq block) which converts the three-phase currents to corresponding d-q axis currents. The Park transform block does this by making use of the angular information and applies the Park transform matrix on the three-phase quantities.

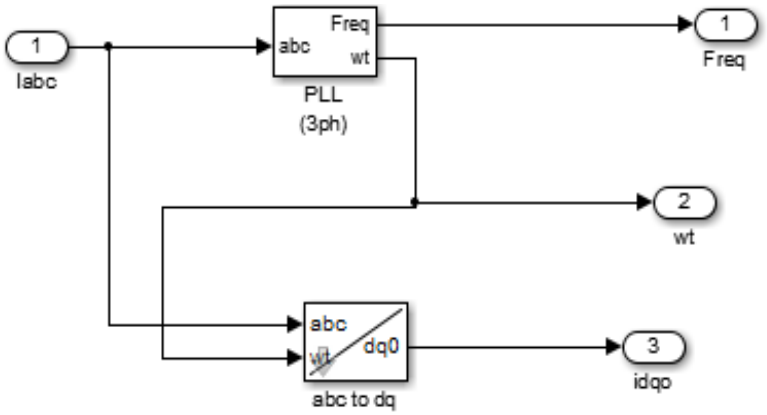


Figure 12.4: PLL block model

**Table 12.5: The PLL block parameters**

| Parameter | Value |
|---|---|
| Minimum frequency (Hz) | 2 |
| Initial input phase and frequency | 0 and 15 |
| Regulator gains [ Kp, Ki, Kd ] | [180, 3200, 1] |
| Time constant for derivative action (s) | $10^{-4}$ |
| Maximum rate of change of frequency (Hz/s) | 12 |
| Filter cut-off frequency for frequency measurement (Hz): | 30 |

## 12.3 MS d-axis current control

Figure 12.5 shows a detailed diagram of the PID controller for the MS d-axis current. The D parameter is set to zero. The I parameter is set to 1 and the P parameter is set to 0.091. The PI controller is in series with a 5 unit gain. The output is the d-axis voltage (Ud) which is then fed to the Clarke transform block to determine the space vector pulse width modulation (SVPWM) signal. This gain was determined using the root locus method. The inputs of the controller are the MS d-axis current set point (Idref), the measured MS d-axis current

(Idmeas ) and the MS q-axis current (Iq). The last input is the rotor angular speed (Wm). The inductance is represented by the Gain1 block which has a value of 8.5mH. The number of poles is represented by the Gain block which has a value of 40.

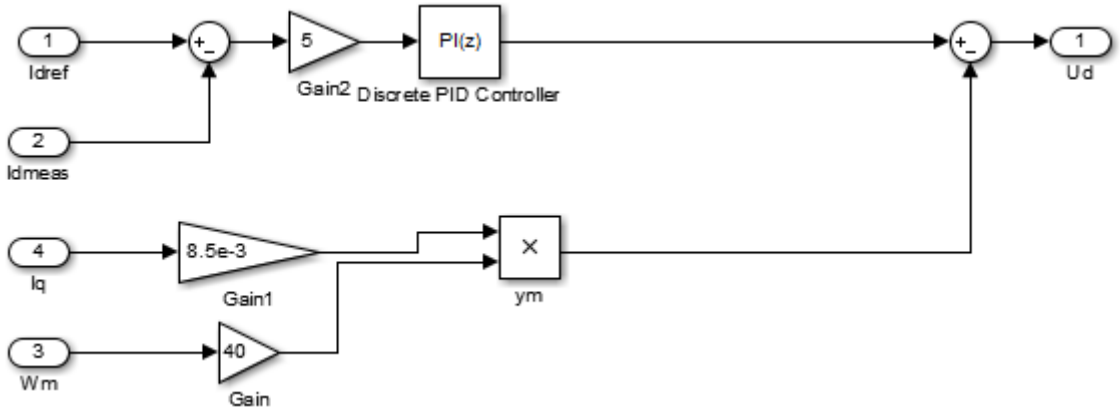


Figure 12.5: MS d-axis current control

## 12.4 Angular speed control

Figure 12.6 shows the speed controller. The speed controller has an inner and outer loop. The outer loop is the actual speed control while the inner loop is the MS q-axis current control loop. The inner loop is similar to the MS d-axis current control already discussed in the section above and the PI parameter are exactly the same. The speed controller has five inputs. The first input is the angular speed reference (W_ref). This is determined form maximum power point tracking methods where the optimal tip-speed-ratio and the radius of the turbine are used to determine the optimal angular speed required to extract maximum power from the wind. Other inputs include the measured angular speed (Wmeas and Wm), the MS d-axis current (Id) and the permanent magnet flux. The output of the speed controller is the q-axis voltage (Uq) which is fed to the Clarke transform block to determine the SVPWM signal.

The P and I parameters of the PI controller for the outer loop are each set to 1. The gain3 block in series with this controller has a value of 23600. This is a large gain and may prove to be impractical to implement in circuitry. The way around this problem is to use a PI anti-windup controller. What the anti-windup does is to reduce the requirement for a larger gain controller. However, the anti-windup controller is not implemented in this study because the controller will not be implemented in circuitry. This controller was done for model verification purposes and thus is sufficient for verifying the control philosophy of PMSG based WECS.

The Gain block represents the number of poles and has a value of 40 poles. The gain1 block represents the inductance of the PMSG and has an inductance value of 8.5mH.

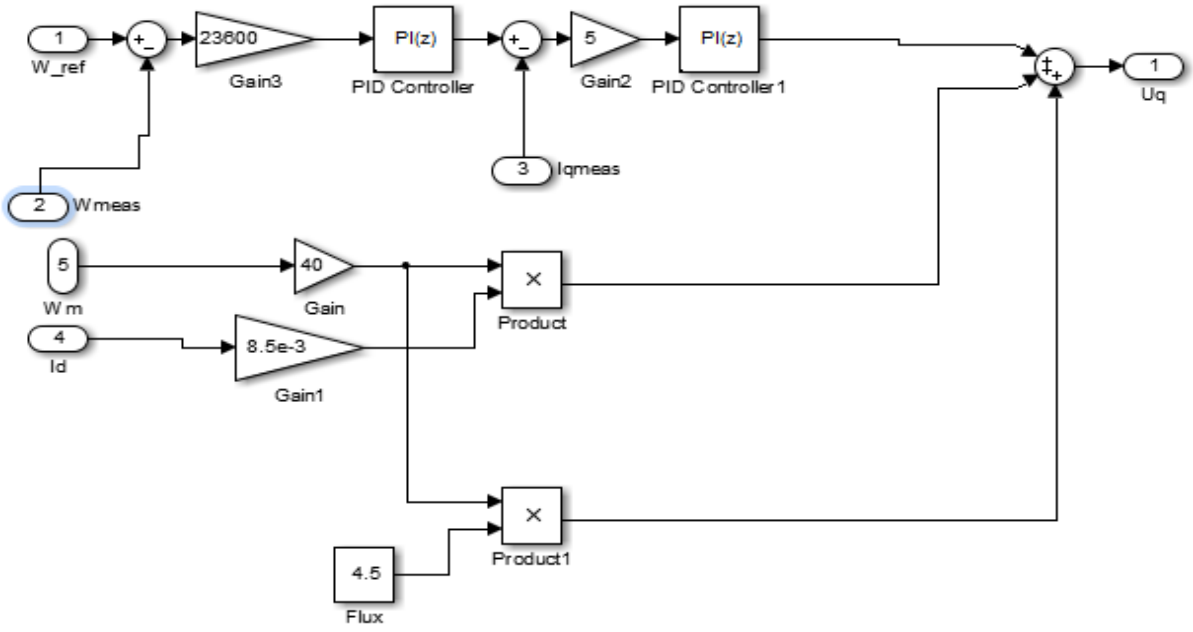


Figure 12.6: Angular speed control

## 12.5 Grid side block

The grid side block is responsible for controlling the DC-link voltage as well as reactive power sent to the grid. The block is shown if Figure 12.7. It consists of the DC-link capacitor, the back-to-back converter and an RL filter. Other components include the three-phase transformer and the grid. The rest of the elements are the Clarke transform blocks as well as measurement blocks. The parameters of the elements are shown in table 12.6. The parameters of the grid side converter are similar to those of the machine side converter.

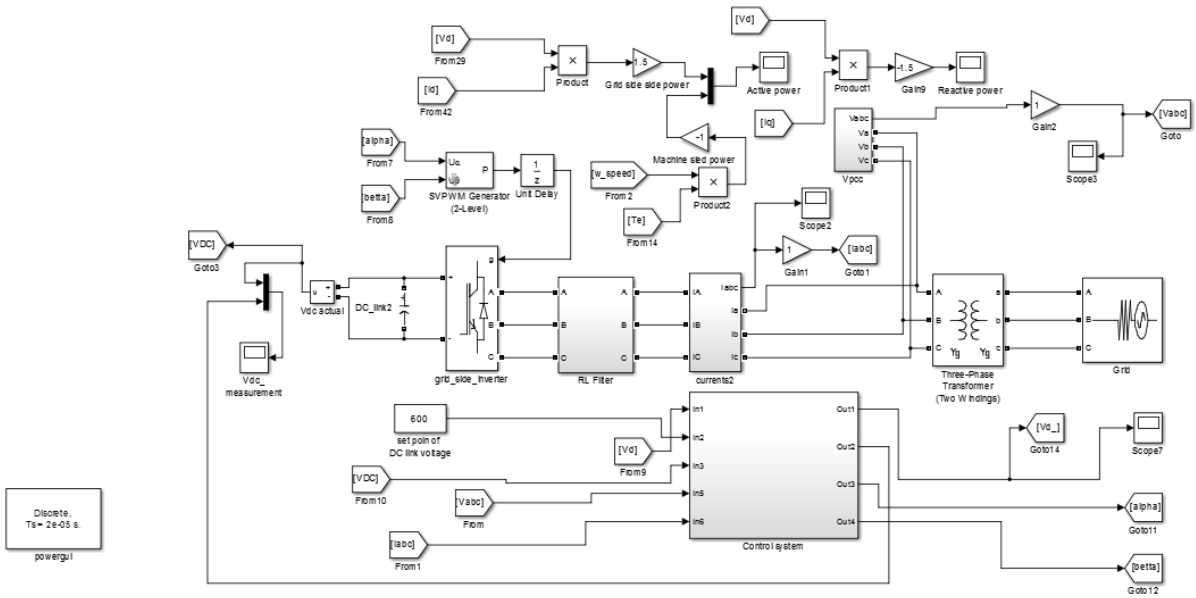


Figure 12.7: Grid side block in Simulink

**Table 12.6: Grid side elements parameters**

| Parameters | Value |
|---|---|
| DC-link capacitance | 65mF |
| Filter Resistance | 1 ohms |
| Filter inductance | 2.65 mH |

### *v. Control system*

A more detailed diagram of the control system is now shown in Figure 12.8. The reactive power control and DC-link voltage control are also shown in the Figure. The details of the DC-link and reactive power controls are given in the section 12.6 below.

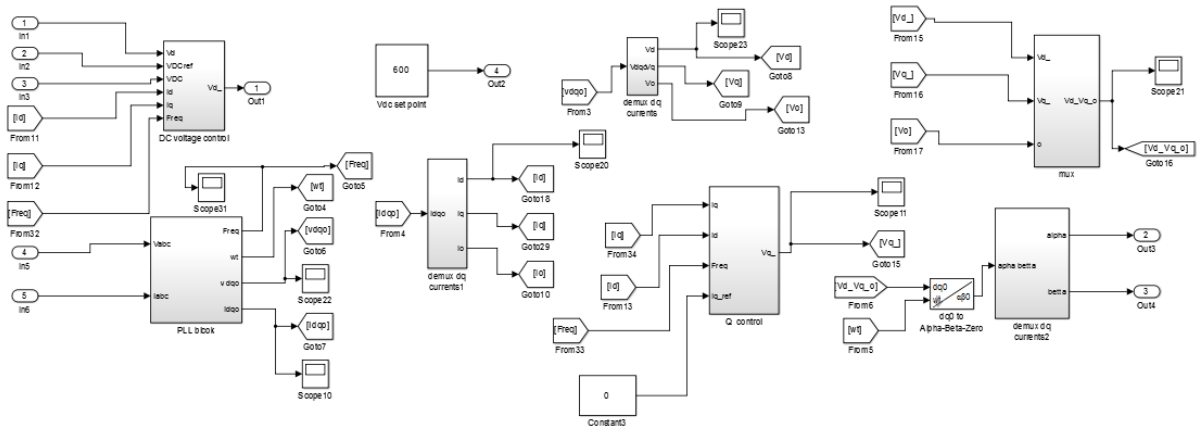


Figure 12.8: Grid side control system

## 12.6 Reactive power control

The reactive power controller is shown in Figure 12.9. The inputs to the reactive power controller are the reference q-axis current (Iq_ref) as well as its actual measurement (Iq), the measured d-axis current (Id) and the frequency (Freq). The output of the controller is the q-axis voltage which fed to the Clarke transform block to determine the SVPWM signal for switching the grid side back-to-back converter. The P parameter of the PID controller is set to 0.0052, the I parameter is set to 1 while the D parameter is set to zero. So the controller is a PI controller. The gain1 block represents the inductance of the filter times the grid side line angular frequency.

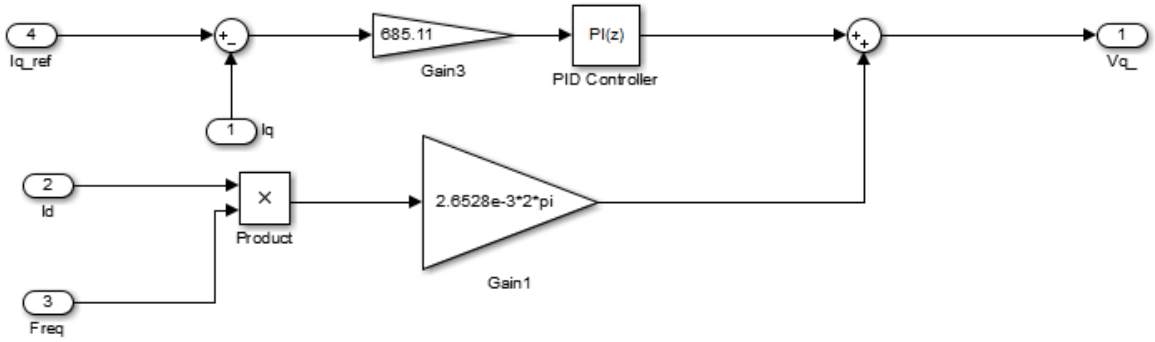


Figure 12.9: Reactive power control loop

## 12.7 D-link voltage control

The DC-link voltage controller has two loops which are the inner and outer loop. The inner loop is the d-axis current control while the outer loop is the DC-link voltage control. The inner loop is the same as the q-axis current control loop already discussed. The Simulink model of the DC-link voltage controller is shown in Figure 12.10. The inputs to the controller are the DC–link reference voltage and its measurement (VDCref and VDC respectively). Other inputs include the frequency (Freq), the q-axis current and the q-axis voltage (Vq). The output of the control is the d-axis voltage. The outer loop PID controller parameters are set as follows: the P parameter is 0.1, the I parameter is 1 and the D parameter is 0. So it is actually a PI controller. The Gain1 block has a value of 53,8. This was determined following the root locus method.

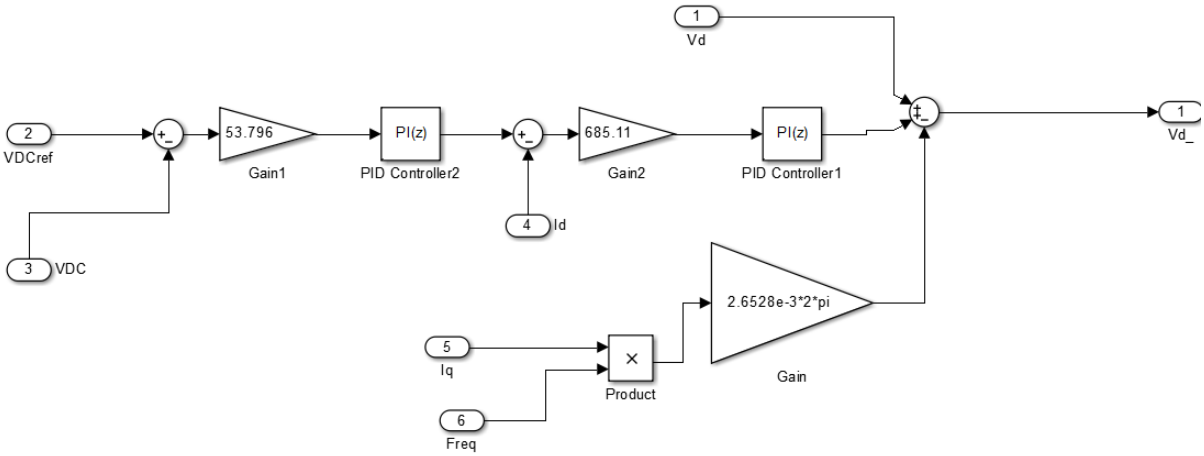


Figure 12.10: DC-link voltage controller

## 12.8 The phase-locked loop block

A detailed view of the grid side PLL block is shown in Figure 12.10. The parameters of the PLL block are shown in table 12.7. The PLL block has the PLL unit as well as the Park transform blocks for voltage and current. The inputs to the block are the three-phase currents and voltages. The outputs are the d-q axis voltages as well as currents, the frequency and the phase angle.

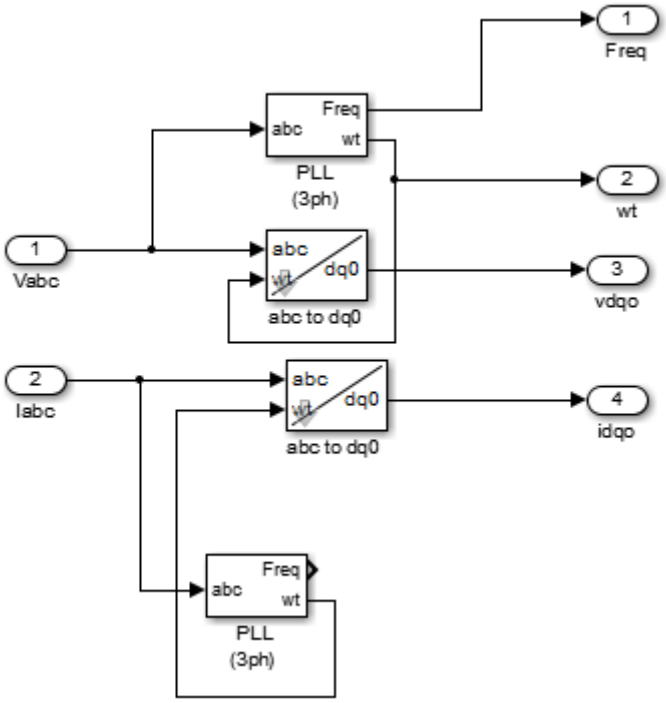


Figure 12.11: The Simulink PLL block

**Table 12.7: Grid side PLL parameters**

| Parameter | Value |
|---|---|
| Minimum frequency (Hz) | 45 |
| Initial input phase and frequency | 0 and 50 |
| Regulator gains [ Kp, Ki, Kd ] | [180, 3200, 1] |
| Time constant for derivative action (s) | $10^{-4}$ |
| Maximum rate of change of frequency (Hz/s) | 12 |
| Filter cut-off frequency for frequency measurement (Hz): | 60 |

## 12.9 Flicker model

Table 12.8 shows the flicker model used for switching operation studies done in power factory. In the model, the network impedance angle, power coefficient and voltage step factor are kept fixed. The step-factor, N10 and N120 are varied as per the associated case study.

**Table 12.8: Flicker model for switching operations**

| Network Angle, psi deg | Coefficient, C(psi) | Step Factor, kf(psi) | Voltage Change Factor, ku(psi) | N10 | N120 |
|---|---|---|---|---|---|
| 30 | 1 | Varied | 0.1 | varied | varied |

## 12.10 DSL code

The DSL code used to calculate voltage flicker is given in this section

```
!Code purpose: This programme exports the voltage at the PCC
!Date: 01/06/2016
!Author: Ntlahla Ntsadu
!Last reviewed: 17/01/2017

string sRes,rVal, str;
double d,Nvar,Nval;

double x, t, t1, t2, t3, time;
int n, ix,iy,inv,inv1;
double iRet;
double  sRe;

Reset.Execute();
Sim:tstop = 0.05;

fopen('C:\Users\LUCKY\Desktop\read_1.txt','w',0);

inv = 1;
time = 0;

while (time<=610){

      Reset.Execute();
```

```
 if (inv=1){
   WTG0:pgini=3;
   WTG1:pgini=3;
   WTG2:pgini=3;
   WTG3:pgini=3;
   WTG4:pgini=3;
   WTG5:pgini=3;
   WTG6:pgini=3;
   WTG7:pgini=3;
   WTG8:pgini=3;
   WTG9:pgini=3;inv1=0;

   Sim:tstop = 0.05;
   }
if (inv=0){
   WTG0:pgini=2.8;
   WTG1:pgini=2.8;
   WTG2:pgini=2.8;
   WTG3:pgini=2.8;
   WTG4:pgini=2.8;
   WTG5:pgini=2.8;
   WTG6:pgini=2.8;
   WTG7:pgini=2.8;
   WTG8:pgini=2.8;
   WTG9:pgini=2.8;

   Sim:tstop = 0.01;
   }

 if (inv=1){
   inv = 0;}
 else {inv=1;}

 Sim.Execute();
 LoadResData(Res);
 Nvar = ResNvars(Res);
 Nval = ResNval(Res,0);

 Reset.Execute();

 ix = 0;
 while (ix<Nval) {
 iy = 0;
 GetResData(x, Res, ix);  ! ix is the raw number, Res is the results
 str = sprintf('%f :', x); ! take the time
 t = x+time;                    !get the time value

 if(t>=0){
   while (iy<Nvar) {
   GetResData(x, Res,ix,iy);
   str = sprintf('%s %8.5f ', str, x);

      if (iy=0){t1 = x;}    !get the variable 1
      if (iy=1){t2 = x;}    !get the variable 2
      if (iy=2){t3 = x;}    !get the variable 3
```

```
        iy += 1;
      }


      fprintf(0,'%8.5f; %8.5f; %8.5f; %8.5f', t, t1, t2, t3);
      }
      ix += 1;
    }
ReleaseResData(Res); ! release the result file data from memory
time=t;

}

fclose(0);

WTG0:pgini=3;
WTG1:pgini=3;
WTG2:pgini=3;
WTG3:pgini=3;
WTG4:pgini=3;
WTG5:pgini=3;
WTG6:pgini=3;
WTG7:pgini=3;
WTG8:pgini=3;
WTG9:pgini=3;

!End of the programme
```